

The accuracy of cone beam computed tomography (CBCT) to determine newly formed bone within grafted maxillary sinus in sheep

David (Seung young) Ko

**UNIVERSITY
of
OTAGO**



Te Whare Wānanga o Otāgo

A thesis submitted in partial fulfilment of requirements
for the degree of Doctor of Clinical Dentistry
University of Otago, Dunedin, New Zealand

2015

Abstract

Grafting of the maxillary sinus floor has become a common surgical intervention to increase bone volume for implant placement (Wallace and Froum, 2003); the procedure can be performed either as an 1-stage procedure with simultaneous implant placement or as a 2-stage procedure before implant placement (Bruggenkate and Bergh, 1998). In a 2-stage procedure, the chosen graft material is placed into the sinus floor and the graft material is left to consolidate with newly formed bone. This consolidation should preferably occur before implant placement. However, currently there is no clinical tool to assess healing within the grafted sinus. A trephine bone biopsy can be harvested for histological assessment but this is invasive and not clinically useful. The current clinical guideline is to wait between six to twelve months after maxillary sinus grafting before implant placement (Rodriguez et al., 2003)

CBCT (Cone beam computed tomography) is a clinical 3-D (three-dimensional) radiographic tool for assessment of mineralised tissue (Ehrhart et al., 2008; Estrela et al., 2008) and may be used for assessment of graft healing within maxillary sinus. However, there are a limited number of studies looking at the use of CBCT in bone-density measurements (Benavides et al., 2012). Micro-computed tomography (μ CT) is a 3-D radiographic tool mainly used for in vitro studies. Specimens with a volume of approximately 5cm^3 can be scanned with up to a $1\mu\text{m}$ voxel resolution producing high-resolution radiographic images for mineralised tissues. There is growing evidence to suggest that μ CT can be used as a substitute method for histology to measure mineralised tissue, particularly trabecular bone (Thomsen et al., 2000; Thomsen et al., 2005).

With no clinical tool available for assessment of graft healing within the sinus, the purpose of this study was to assess whether CBCT can be used to measure the amount of newly formed bone in grafted maxillary sinus in sheep. To validate this, CBCT was compared with two reference standards; micro-computed tomography (μ CT) and histology.

Aim:

To assess the effectiveness of CBCT for quantifying newly formed bone within grafted sinus sites, using an animal model.

Method:

Maxillary sinus grafting in six sheep with bovine xenograft (Endobon[®]) was evaluated after a sixteen-week healing period. Specimens from each animal were analysed using three imaging techniques: CBCT, μ CT and resin-embedded histological sections. Two-dimensional "virtual" CBCT sections were matched with corresponding 2-D μ CT sections and digitised histological sections. μ CT and CBCT images were calibrated using known-density radiographic calibration standards. Using image analysis software (Image J, NIH, USA), % new bone (%NB), % residual graft (%RG), % mineralised tissue (%MT) were measured for matched regions of interest across each imaging technique and compared statistically ($p<0.05$).

Results:

CBCT measured %NB and %RG significantly higher than μ CT and histology. μ CT measured %NB significantly higher than histology. %RG measurements of μ CT and histology were not significantly different.

CBCT measured %MT significantly higher than both μ CT and histology. %MT measurements of μ CT and histology were statistically different but were very similar.

Conclusion:

Micro-computed tomography (μ CT) measurements of residual graft and new bone were affected as the radiodensities of residual graft (Endobon[®]) and new bone were similar. μ CT however appeared to be capable of measuring the combined area of graft and new bone (i.e., mineralised tissue) similar to histomorphometry.

Cone-beam computerised tomography (CBCT) markedly overestimated new bone, residual graft and the total mineralised tissue. CBCT lacks the resolution to accurately determine newly formed bone after maxillary sinus grafting, an important step before definitive implant placement.

Acknowledgements

I would like to acknowledge everyone who I have come to know and known better in the past three years. You are all part of this work, and only to some of you it is possible to give particular mention here.

I am deeply thankful to my principal supervisor, Professor Warwick Duncan, for his guidance, encouragement and continuous support throughout these three years., without whom I would not have completed this project.

I am also grateful to my co-supervisor, Dr Don Schwass, for his insightful comments and guidance throughout this entire process. I would like to thank Associate Professor Jonathan Leichter for his insightful comments in the preparation of this manuscript and conference presentations.

It would not have been possible to complete this research without help from people in the Department of Microscopy and Radiology. I would like to thank Diane Campbell for her help in preparing CBCT scans. I am also grateful for the technical help and tips I received from Andrew McNaughton, who contributed greatly to the analysis of the specimens.

Table of contents

Chapter 1	Introduction and literature review.....	1
1.1	Anatomy of human maxillary sinus.....	3
1.2	Changes in the alveolar bone and the maxillary sinus following tooth loss.....	5
1.2.1	<i>Alveolar ridge resorption</i>	5
1.2.2	<i>Sinus pneumatisation</i>	5
1.3	Maxillary sinus floor elevation.....	7
1.3.1	<i>Types of maxillary sinus elevation procedures.....</i>	7
1.4	Alternative to the sinus floor elevation – Short dental implant	9
1.5	Simultaneous or delayed implant placement with the sinus lift procedure	10
1.5.1	<i>One-stage versus two-stage implant placement</i>	10
1.5.3	<i>Delayed implant placement in grafted sinus (2-stage approach).....</i>	12
1.6	The influence of implant surface design on implant survival	13
1.7	The influence of pre-surgical height of bone on implant survival	14
1.8	The remodelling of graft material placed in the maxillary sinus.....	15
1.8.1	<i>Osteogenesis</i>	15
1.8.2	<i>Osteoinduction</i>	16
1.8.3	<i>Osteoconduction</i>	17
1.9	Sources of bone-graft/substitute materials	18
1.9.1	<i>Autograft</i>	18
1.9.2	<i>Allograft</i>	19
1.9.3	<i>Alloplast</i>	20
1.9.4	<i>Xenograft</i>	22
1.9.5	<i>The healing of different sources of graft materials placed in the Maxillary sinus....</i>	24
1.9.6	<i>Survival rates of implants placed in grafted sinus with different sources of graft materials</i>	25
1.10	Timing of implant placement	26
1.11	Cone beam computed tomography (CBCT)	29
1.12	Micro-CT (μCT)	33
1.12.1	<i>μCT versus histomorphometry.....</i>	33
1.12.2	<i>Sources of error in μCT</i>	35

1.12.3 <i>Skyscan 1172 Micro-CT Scanner</i>	37
1.13 Radiomorphometric analysis.....	38
1.13.1 <i>Grayscale calibration</i>	38
1.13.2 <i>Method of thresholding</i>	38
1.14 Histomorphometry	40
1.14.1 <i>Specimen embedding techniques</i>	40
1.14.2 <i>Limitation of histomorphometry with stereological analysis</i>	43
1.15 Morphometric analysis of grafted sinus with CBCT, μCT and histomorphometry..	44
.....	44
1.16 Animal models	45
1.16.1 <i>Sheep</i>	46
1.17 Aim.....	49
1.18 Objectives	49
1.19 Hypothesis	49
Chapter 2 Materials and methods	50
2.1 CBCT / μCT scan and histological preparation	50
2.1.1 <i>CBCT scan</i>	50
2.1.2 <i>μCT scan</i>	50
2.1.3 <i>Histological preparations</i>	56
2.2 Identifying 2-D virtual μCT and CBCT images corresponding to the histological images.....	64
2.2.1 <i>μCT</i>	64
2.2.2 <i>CBCT</i>	64
2.3 Image size calibration and selection of region of interest (ROI).....	67
2.3.1 <i>Image size calibration</i>	67
2.3.2 <i>Selection of a region of interest (ROI)</i>	67
2.4 Image analysis.....	71
2.4.1 <i>Histomorphometric analysis</i>	71
2.4.2 <i>Radiomorphometric analysis</i>	71
2.5 Statistical analysis	83
Chapter 3 Results.....	90

3.1 Post-operative recovery	90
3.2 Radiographic examinations of resin-embedded specimens	90
3.3 Descriptive analysis of matched images of CBCT, μCT, and histology	90
3.3.1 <i>Morphology of grafted sinus.....</i>	90
3.3.2 <i>Segmented image</i>	90
3.4 Quantitative analysis.....	95
3.4.1 Overall mean and individual mean for different tissues in CBCT, μ CT and histology	95
Chapter 4 Discussion	105
4.1 Introduction	105
4.2 CBCT	105
4.3 Micro-computed tomography (μCT)	108
4.3.1 <i>Morphometric analysis of grafted sinus</i>	111
4.4 Radiomorphometric analysis	114
4.4.1 <i>The use of radiographic standards</i>	114
4.4.2 <i>Global threshold and partial volume effect</i>	115
4.5 Parameters	117
4.6 Animal study	118
4.7 Influence of resin embedding on the quality of radiographic images	119
4.8 Histomorphometric analysis: methodology	120
4.9 Clinical implications.....	123
4.10 Confounding factors and other issues with the investigation.....	125
4.10.1 <i>Experimental design</i>	125
4.10.2 <i>Discarded animals</i>	125
4.10.3 <i>Examiner blindness and reproducibility of techniques</i>	126
4.10.4 <i>Lack of a control group</i>	127
4.10.5 <i>Samples from another experimental research</i>	127
4.10.6 <i>Image scale</i>	128
4.11 Recommendations for future research	128
4.11.1 <i>3-D analysis</i>	128
4.11.2 <i>Non-grafted sinus / use of other bone substitute</i>	128

4.11.3 <i>Investigation in other periodontal and peri-implant sites</i>	129
4.11.4 <i>Use of other imaging software</i>	129
Chapter 5 Conclusion	131
Chapter 6 Appendix.....	132
6.1 Appendix I: Ethical approval and sheep sinus surgery	132
6.1.1 <i>Ethical approval</i>	132
6.1.2 <i>Experimental animals</i>	132
6.1.3 <i>A choice of graft material</i>	132
6.1.4 <i>Surgical protocol</i>	132
6.1.5 <i>Postoperative pain and infection control</i>	134
6.1.6 <i>Euthanasia and perfusion protocol</i>	134
6.1.7 <i>Harvesting</i>	135
6.2 Appendix I.....	136
6.2.1 <i>Chemical reagents used</i>	136
6.2.2 <i>Equipment used</i>	136
6.3 Appendix III.....	139
6.3.1 <i>Ingredients for resin embedding</i>	139
6.3.2 <i>Resin embedding protocol</i>	140
6.3.3 <i>Staining with MacNeal's Tetrachrome/Toluidine Blue solution</i>	140
6.4 Appendix IV: Radiographic Calibration Standards (Phantoms) for Micro-CT (Schwass et al., 2009)	141

List of tables

Table 2.1 Micro-CT settings for all specimens.....	52
Table 3.1 Overall mean results and standard error for the area occupied by different tissues measured by CBCT, μ CT and histology.....	97
Table 3.2 Sample mean and standard deviation for each tissue measured by different techniques.	
.....	101
Table 6.1 Medications used during the sheep surgery.....	135
Table 6.2 Calibration standards densities.	143

List of figures

Figure 2.1 Maxilla blocks (Left and right) on a plastic platform in Galileos CBCT (Sirona Dental, USA).....	53
Figure 2.2 CBCT images of scanned maxilla in different viewing planes in Galaxis CBCT imaging software.....	54
Figure 2.3 4-0 Silk suture (Black braided silk, reverse cutting, Ethicon®).....	54
Figure 2.4 Trimmed specimen with a silk suture placed indicating the anteroventral position on the antral sinus wall (> 5cm ³)	55
Figure 2.5 The specimens wrapped in clear glad wrap positioned on µCT machine platform ...	55
Figure 2.6 The silk suture was replaced with an amalgam restoration.....	60
Figure 2.7 The specimen placed in a glass jar that has MMAIII pre-set base.....	60
Figure 2.8 Resin-embedded specimen, black line indicating the cutting direction that corresponds to the transverse plane of reconstructed µCT slices.	61
Figure 2.9 A radiographic scanned image of a resin-embedded specimen. Grafted sinus (Yellow arrow) and an amalgam marker are visible (Red arrow).	61
Figure 2.10 Struers Accustom-50 desktop cut-off machine. Specimen clamped on the platform and the wheel direction made parallel to the black line on the specimen block.....	62
Figure 2.11 Histological sections were glued onto an acrylic plastic slide using superglue (Cyanoacrylate). A custom-made hand press was used to press the sections onto the plastic slide for 60 seconds while the glue is set.....	62
Figure 2.12 Struers Tegra-Pol polishing machine with a speed adjustable turntable.....	63
Figure 2.13 Polished histological slide.....	63
Figure 2.14 In Image J, a stack of cross-sectional slices of µCT and a histological image of the same animal were opened. Using a horizontal scroll bar on the bottom of the window (yellow arrow), µCT slices were scrolled up and down until a radiographic image that closely resembles with the histological image was found.	65
Figure 2.15 3D CBCT Volume opened in Osirix. Using the 3D analysis, the volume was reoriented to match the plane of histological sections and then cropped vertically until the image that matches with the histology was found on its z-axis (Yellow arrow).	65
Figure 2.16 A raw 2-D CBCT image (top left) and an exported CBCT image from Osirix (bottom left) of the same specimen are shown. Comparing grayscale range demonstrated	

that two images have unequal grayscale range; the raw image shows gray value ranged between 10000~50000 whereas the modified image shows gray value ranged between 10-200. The changes in grayscale were due to the change in the format of image from 16-bit tiff file to RGB format that was inevitable as Osirix only allows exported dataset in RGB format.....	66
Figure 2.17 Matched section of histology (top), CBCT (middle) and μ CT (bottom). The images were scaled in millimetres (mm).....	68
Figure 2.18 Matched, scaled images of histology, μ CT and CBCT were superimposed to check if they are the same size. Superimposition: (a) between histology and CBCT. Notice difference in scale near the floor of the sinus. (b) between histology and μ CT. Notice unequal scale of hard tissue of sinus floor between two images (c) between μ CT and CBCT showing a good match in the scale. Yellow delineation refers to an area where two images failed to correspond. This was mainly due to tissue shrinkage and distortion in histological images.	69
Figure 2.19 A region of interest (grafted sinus) drawn on images of histology (top), CBCT(middle) and μ CT (bottom) with yellow outline.....	70
Figure 2.20 Colour thresholding of residual graft in a histological image. Hue, saturation and brightness bars in the threshold window were adjusted to select different tissues of interest (residual graft and new bone) within all histological images.	74
Figure 2.21 Any area that was not segmented using colour thresholding was manually selected using a wand (tracing) tool in Image J (shown in yellow outline).....	74
Figure 2.22 3x Hydroxyapatite radiographic standards (courtesy of Dr Schwass).	75
Figure 2.23 Radiographic standards of hydroxyapatite discs (x3) and an Endobon [®] sample mounted on platform (top), μ CT scan of the standards (bottom left), CBCT scan of the standards (bottom right).	75
Figure 2.24 Cross sectional μ CT images of HAp (hydroxyapatite) discs with ROI (yellow outline), (a) Low density HAp, (b) Medium density HAp and (c) High density HAp. ROI was drawn on one image every 50~60 images and the ROIs were interpolated vertically throughout images to produce a volume of interest (VOI) representing each disc and the mean grayscale of each disc was calculated.	76

Figure 2.25 Grayscale calibration of μ CT images using HAp discs. Mean grayscale of HAp discs obtained were correlated with corresponding total effective density (g/cm ³). A scatter plot shows a linear relationship between the grayscale (X-axis) and the density (Y-axis).....	77
Figure 2.26 Cross sectional μ CT images of HAp (hydroxyapatite) discs with ROI (yellow outline), (a) Low density HAp, (b) Medium density HAp and (c) High density HAp. ROI was drawn on one image every 50~60 images and the ROIs were interpolated vertically throughout images to produce a volume of interest (VOI) representing each disc and the mean grayscale of each disc was calculated.	78
Figure 2.27 Grayscale calibration of CBCT images using HAp discs. Mean grayscale of HAp discs were correlated with corresponding total effective density (g/cm ³). A scatter plot shows a linear relationship between the grayscale (X-axis) and the density (Y-axis).....	79
Figure 2.28 1x Prophylaxis paste container (11mm high x 20mm diameter), Emptied, cleaned with water/Alcohol 100%, dried. Filled with 1.8g Endobon® granules, packed and top sealed with 2 layers of adhesive tape	84
Figure 2.29 Reconstructed cross-sectional images of Endobon® in μ CT (Left) and CBCT (Right) scan.	84
Figure 2.30 To threshold new bone in grafted sinus, the antral cortical wall (asterisk) was used as a radiographic standard in both μ CT (Top) and CBCT (Bottom) images.	85
Figure 2.31 Thresholding residual graft using Endobon® scan (Upper right) as a standard (1.60- 2.71 gHAp/cm ³). This was applied to our μ CT image (Left) to measure residual graft ..	86
Figure 2.32 Thresholding new bone using the antral cortical bone as a standard (1.50-1.70 gHAp/cm ³)	86
Figure 2.33 Thresholding mineralised tissue (Residual graft + new bone) by combining the threshold range of residual graft and bone (1.50-2.71 gHAp/cm ³).....	87
Figure 2.34 Thresholding residual graft using Endobon® scan (Upper right) as a standard (1.37- 1.78 gHAp/cm ³). This was applied to our CBCT image (Left) to measure residual graft. ..	88
Figure 2.35 Thresholding new bone using the antral cortical bone as a standard (1.31-1.61 gHAp/cm ³).	88
Figure 2.36 Thresholding mineralised tissue (Residual graft + new bone) by combining the threshold range of residual graft and bone (1.31-1.78 gHAp/cm ³).....	89

Figure 3.1 Thresholded image of residual graft in histology (top), µCT (middle) and CBCT (bottom).....	92
Figure 3.2 Thresholded image of new bone in histology (top), µCT (middle) and CBCT (bottom).....	93
Figure 3.3 Thresholded image of mineralised tissue in histology (Top), µCT (middle) and CBCT (bottom).....	94
Figure 3.4 Overall mean of new bone in histology, µCT and CBCT with the standard error.....	98
Figure 3.5 Overall mean of residual graft in histology, µCT and CBCT with the standard error.	98
Figure 3.6 Overall mean of mineralised tissue (new bone + residual graft) in CBCT, µCT and histology with the standard error	99
Figure 3.7 Overall mean of connective tissue in CBCT, µCT and histology with the standard error.....	100
Figure 3.8 Mean % New bone measured by histology, µCT and CBCT in all six animals.	103
Figure 3.9 Mean % Residual graft measured by histology, µCT and CBCT in all six animals. 103	
Figure 3.10 Mean % Mineralised tissue (% residual graft + % new bone) measured by histology, µCT and CBCT from all six animals	104
Figure 3.11 Mean % Connective tissue measured by histology, µCT and CBCT from all six animals.	104
Figure 4.1 Thresholded µCT image of grafted sinus. Green colour indicates threshold area for new bone and residual graft is shown as red colour. Due to a considerable overlap in grayscale between bone and graft, complete separation of two tissues was not possible using thresholding. Note the antral sinus wall, which is composed of both red and green colours. Due to the overlap in the grayscale range between graft and bone, some areas of antral bone thresholded as residual graft in red colour. Likewise, within the grafted sinus, the periphery of each graft islet is thresholded as new bone in green colour due to its similar radiodensity to residual graft (red). The threshold histogram (right) shows how new bone and residual graft overlap in their grayscale range.....	113
Figure 6.1 The surgical site for maxillary sinus elevation in sheep.....	138
Figure 6.2 The steps in the surgical procedure: (a) the surgical site for maxillary sinus floor elevation in sheep, (b) Preparation of a circular osteotomy on cortical bone of sinus (c)	

Placement of bone graft following the elevation of sinus membrane (d) Placement of Endobon® (Smith, 2011).....	138
--	-----

List of abbreviations

CBCT	Computed cone beam tomography
μ CT	Micro-computed tomography
RG	Residual graft (mm^2)
NB	New bone (mm^2)
MT	Mineralised tissue (mm^2)
CT	Connective tissue (mm^2)
HAp	Hydroxyapatite
ROI	Region of interest
BMP	Bone morphogenic proteins
BV/TV	Trabecular bone volume
BS/TV	Bone-surface-to-volume
Tb.N	Trabecular number
Tb.Th	Trabecular thickness
Tb.Sp	Trabecular separation
CD	Connectivity density
2-D	Two-dimensional
3-D	Three-dimensional

SM	Schneiderian membrane
OPG	Orthopantomogram
DFDB	Demineralised freeze-dried bone
FDBA	Freeze-dried bone allograft
Runx2	Runt-related transcription factor-2
FGFs	Fibroblast growth factors
TGF- β	Transforming growth factor beta family
RANK	Receptor activator of nuclear factor kappa B
RANKL	RANK(Receptor activator of nuclear factor kappa B) ligand
OPG	Osteoprotegerin
OCIF	Osteoclastogenesis inhibitory factor
PDGF	Platelet-derived growth factor
TCP	Tri-calcium phosphate
RFA	Resonance frequency analysis
μ Sv	Micro-Sievert
PA	Periapical radiograph
gHAp cm^{-3}	The mass of hydroxyapatite (HAp) per unit volume
SNR	Signal-to-noise ratio

CCD	Charge-coupled device
MMA	Methylmethacrylate
BA	Bone area
BIC	Bone-to-implant contact
PC	Personal computer
NBF	Natural Buffered Formalin
EDTA	Ethylenediamine tetra-acetic acid
TV	Total volume of interest
VS	Volume of graft material
BV	Volume of bone
VS/[VS+BV]	Volume of graft material in relation to total mineralised tissue volume
TV	Total volume of interest

Chapter 1 Introduction and literature review

Since the introduction of endosseous dental implants, their use in dentistry has grown. Adequate bone quantity and quality are essential for implant placement. However, with a lack of bone as a result of the expansion of the maxillary sinus (pneumatisation) and residual alveolar bone resorption following tooth loss, placement of implants in the posterior maxilla is often difficult. Maxillary sinus grafting was therefore introduced to increase the bone volume at the sinus floor by elevating the sinus membrane and placing a choice of bone graft material. This procedure can be done as a one-stage procedure with simultaneous implant placement or as a two-stage approach where implant insertion is delayed until the graft material is consolidated with newly formed bone as the quantity and quality of bone will influence the implant success (Grunder, 2001; Jemt and Lekholm, 1994; Porter and von Fraunhofer, 2004; Rodriguez et al., 2003; Tinsley et al., 1999). Histomorphometry is the gold standard to assess bone healing in the grafted sinus. The composition of residual graft, new bone and soft tissue can be easily assessed; human and animal studies concerning the healing of graft materials within the maxillary sinus have been carried out using histomorphometric analysis to assess new bone (Alayan et al., 2015; Chaushu et al., 2010; Moy et al., 1993; Smith, 2011). However, this technique is not clinically useful since it requires a bone biopsy to be trephined from the grafted sinus, which results in considerable bone loss. At present, clinically, post-operative analysis of the sinus grafting is performed by two-dimensional (2-D) radiographs such as an orthopantomogram (OPG). However, lack of a three-dimensional (3-D) assessment and poor image resolution do not allow volumetric measurement and the measurements of newly formed bone around graft material (Feichtinger et al., 2007). Therefore, the optimal timing for implant insertion after the sinus grafting is determined based on our understanding of the nature of graft consolidation observed in animal and human studies (Alayan et al., 2015; Aparicio et al., 2001; Busenlechner et al., 2009; Chaushu et al., 2010; Moy et al., 1993; Smith, 2011), which is usually between six to twelve months after the grafting procedure (Jensen et al., 1997).

Cone Beam Computed Tomography (CBCT) is a non-invasive 3-D clinical radiographic tool that has demonstrated accuracy in both linear and volumetric measurements of bone and

other mineralised tissues (Benavides et al., 2012; Oberoi et al., 2009); CBCT is used to measure the volume of the grafted volume following the maxillary sinus grafting. However, there are no studies concerning its use to measure newly formed bone or residual graft within the grafted sinus after healing.

Micro Computed Tomography (μ CT) is a high-resolution research-use radiographic device for 3-D assessment of mineralised tissues. With a resolution of up to 1 micrometres (μm), μ CT has proven to be a valuable instrument in the analysis of trabecular bone structure. Feldkamp et al. (1989) first described the use of μ CT as a tool for 3-D analysis of trabecular bone structure. μ CT is well-suited for applications involving measurements of bone density (Kühl et al., 2010; Trisi et al., 2006) as well as determining changes in bone volume and microarchitecture (Thomsen et al., 2005; Uchiyama et al., 1997a). However, due to high radiation exposure, the use of this device is currently limited to post mortem mineralised tissue examination or in vivo small animal studies only.

Currently, there is a lack of studies comparing CBCT with histomorphometry or μ CT for analysis of bone formation within grafted maxillary sinuses. Only a couple of studies have compared μ CT and histology for morphometric analysis of the grafted sinus and found a strong correlation (Kühl et al., 2010; Trisi et al., 2006). Comparison of either histology or μ CT to the clinical tool CBCT does not appear to have been performed.

The aim of this study was therefore to compare measurements of histology and μ CT with CBCT in order to determine if CBCT could quantify newly formed bone in the grafted maxillary sinus. The samples will consist of a commercially available bone grafting material (Endobon[®] Biomet 3i, USA) placed into sheep maxillary sinus.

1.1 Anatomy of human maxillary sinus

The maxillary sinus is a pyramidal-shaped cavity within the maxilla. The average dimension of the maxillary sinus in adults is usually measured by 25-35mm mediolaterally, 36-45mm superoinferiorly, and 38-45mm anteroposteriorly. A cadaveric study by Gosau et al. (2009) has estimated the mean sinus volume of an adult sinus to be approximately 12.5ml.

The maxillary sinus is bordered by several anatomical structures. The posterior wall separates the sinus from the structures of the infratemporal and pterygomaxillary fossae, and the posterior superior alveolar nerve exists through this wall. The lateral wall is formed by the zygoma. The anterior wall extends to the canine fossa and contains the infraorbital foramen. The roof of the sinus forms the floor of the orbit and contains the infraorbital canal through which the maxillary nerve runs anteroposteriorly before exiting through the infraorbital foramen. The sinus also has a communication with the nose, found in the medial wall of the sinus, called the ostium. The average size of the ostium is 2.4mm in diameter, found in the middle meatus, space above the inferior concha (turbinate) and under the middle concha. In young children, the floor of the sinus is usually at the same level with the floor of the nose. However, there is often continued expansion during the third molar eruption, leading to its level one to 1.5cm inferior to the level of the floor of the nose in adults (Fonseca et al., 2013)

The sinus is lined with the Schneiderian membrane, made up of thin, ciliated respiratory epithelium, which is continuous with the membrane of the nose (Ritter, 1978). This membrane drains fluids such as pus and mucus to the nose via the ostium (Stamberger, 1986).

The arterial supply for the maxillary sinus is predominantly from the external carotid artery via branches of the maxillary artery. It is mainly from the infraorbital and the posterior superior alveolar arteries but also from branches originating from the posterior lateral nasal and sphenopalatine arteries, which may supply the middle portion of the sinus membrane (Bergh et al., 2000; Chanavaz, 1989). It is important to note that anastomosis may also form between the posterior superior alveolar artery and a terminal branch of the infraorbital artery.

The venous drainage of the sinus occurs via the facial vein, the sphenopalatine vein, and the pterygoid plexus of veins. These subsequently empty into the internal jugular vein. The lymphatic drainage of the sinus occurs via the infra-orbital foramen through the ostium and into the submandibular lymphatic system (Fonseca et al., 2013).

Nerve supply of the sinus involves the maxillary branch of the trigeminal nerve. The infraorbital nerve is subdivided into three branches before exiting through the infraorbital foramen: the posterior superior alveolar, the middle superior alveolar, and the anterior superior alveolar nerves. These nerve branches innervate not only the sinus but also the maxillary teeth and the buccal surfaces of the gingiva. The anterior superior alveolar wall is situated within the anterior wall of the maxillary sinus. The middle superior alveolar nerve travels through the roof of the maxillary sinus and then converges in the posterior superior alveolar nerve (Fonseca et al., 2013)

1.2 Changes in the alveolar bone and the maxillary sinus following tooth loss

1.2.1 Alveolar ridge resorption

Following tooth loss, the alveolar process undergoes a process of bone resorption and remodelling that results in overall loss in volume of the alveolar ridge (Araújo and Lindhe, 2005; Van der Weijden et al., 2009). While the empty tooth socket is filled with blood clot and subsequently converted into new bone, there is also concurrent resorption of the alveolar ridge. This process results in overall loss of alveolar ridge volume, which may limit available bone for implant placement. In the posterior maxilla, following tooth loss, there is greater resorption in the buccal alveolar plate than the palatal wall and also the loss of vertical height of buccal wall is more enhanced than the palatal wall. Concurrently, new bone replaces blood clot within the tooth socket. This three-dimensional change is also clinically identifiable by changes in the shape of the edentulous ridge. The edentulous ridge becomes thin and displaced more palatally from its original position due to greater buccal bone resorption (Pietrokovski and Massler, 1967). Complete denture wearers, following the extraction of teeth, demonstrate a rapid reduction in the alveolar bone ridge in the first year, followed by a gradual and continual reduction up to over 25 years, leading to a significant reduction in vertical height (Tallgren, 1972)

1.2.2 Sinus pneumatisation

The floor of the maxillary sinus is closely located to the posterior alveolar ridge in adults. The roots of the maxillary posterior teeth are often situated within the sinus surrounded by an undulating sinus membrane. Following tooth extraction, not only alveolar ridge resorption occurs but there is also an expansion of the sinus floor inferiorly towards the ridge by resorbing the alveolar bone. This expansion of the sinus is termed pneumatisation (Sharan and Madjar, 2008). The extent of sinus pneumatisation appears to increase as the duration of edentulism increases. The sinus may also expand to fill space previously occupied by teeth. Sinus pneumatisation was confirmed radiographically at sites where teeth are absent showing progressive expansion of the sinus over time in comparison to sites where teeth remain in situ, which show little or no difference (Sharan and Madjar, 2008). Along with the alveolar ridge resorption, the sinus

pneumatisation further decreases the available bone for implant placement in the posterior maxilla.

1.3 Maxillary sinus floor elevation

1.3.1 *Types of maxillary sinus elevation procedures*

1.3.1.1 Caldwell-Luc operation

The Caldwell-Luc operation was introduced in early 1970 as a surgical procedure to remove infection and diseased mucosa from the maxillary sinus while creating drainage via the inferior meatus into the nasal cavity (Macbeth, 1971). This technique was used vastly until the advent of endoscopic technique in the 1980s which promote physiological drainage of the sinus infection via the nasal ostium (Matheny and Duncavage, 2003). The operation begins by creating an osteotomy on the canine fossa intraorally. Through the prepared osteotomy, the infected Schneiderian membrane is dissected and the local anatomy is adjusted to create a direct drainage via the inferior meatus into the nasal cavity.

1.3.1.2 Lateral sinus lift

Individuals with long-term tooth loss in the posterior maxilla often present with inadequate bone for implant placement due to residual ridge resorption and pneumatisation of the maxillary sinus. The lateral sinus lift procedure has therefore been introduced in order to increase the height of bone (Tatum, 1977). The surgical approach is similar to Caldwell-Luc approach, except the Schneiderian membrane is preserved and elevated from the sinus floor and the resultant space is filled with a choice of graft material. This results in an increased height of bone for implant insertion.

The surgery is carried out intraorally and involves the following steps; a crestal incision with vertical releasing incisions is made and the lateral cortex of the maxilla is exposed. A bony window is made to provide access to the Schneiderian membrane. The membrane is then detached from the floor and elevated using various curettes. Once the membrane is elevated, the bony window is rotated medially and superiorly into the sinus. The resultant space is grafted with a choice of graft material. The flaps are repositioned and closed (BOYNE, 1980; Tatum Jr, 1986; Tatum, 1977).

1.3.1.3 Osteotome sinus floor elevation (Transcrestal sinus lift)

Osteotome sinus floor elevation is an intraoral sinus elevation technique introduced by Summers (1994) to elevate the sinus membrane at the time of implant placement (i.e., one-stage approach). This approach involves the elevation of the sinus membrane directly through the osteotomy prepared at the implant site. Through the use of a set of osteotomes inserted into the osteotomy, the soft trabecular bone overlying the sinus floor is condensed and displaced. This has been suggested to improve the quality of bone both lateral and superior to the site (Summers, 1994). A thin layer of alveolar bone that forms the sinus floor can also be fractured inward during this procedure and protruded upwards to elevate the sinus membrane, and the resultant space can be grafted with grafting material, increasing the height of bone available for implant placement. For this approach, however, a minimum pre-treatment bone height of approximately 4mm is suggested to achieve primary stability of the implant as grafting material does not provide any immediate implant support (Summers, 1994)

1.4 Alternative to the sinus floor elevation – Short dental implant

Short dental implants are an alternative approach to sinus floor elevation in an atrophied posterior maxilla (Misch et al., 2006; Morand and Irinakis, 2007). In sites with reduced bone height due to alveolar bone resorption and pneumatisation of the sinus, insertion of short dental implants can avoid the need for maxillary sinus floor elevation. In clinical studies, there is a lack of general consensus on the definition of what constitutes a short dental implant. Some studies consider implants less than 10mm in length as short dental implants (Annibali et al., 2012; Morand and Irinakis, 2007) whereas other clinical studies have defined short dental implants as implants that are $\leq 8.5\text{mm}$ (Anitua et al., 2008; Annibali et al., 2012; Morand and Irinakis, 2007; Nisand et al., 2015) or even 6mm (Srinivasan et al., 2014).

Since short dental implants can avoid the adjustment of the sinus position, it can eliminate the risk associated with Schneiderian membrane lift procedure, such as sinus perforation (Misch et al., 2006). In addition, it requires fewer visits and results in a lower treatment cost for the patient. A five-year, retrospective study looking at the survival rate of short dental implants ($\leq 8.5\text{mm}$) showed over 98% for the implants that were functional over five years following their placement (Anitua et al., 2008). A study by Misch et al. (2006) showed a 98.3% survival rate (one failed out of 22 placed) over a six-year period for short dental implants placed in the posterior maxilla. However, in these studies, due to a small number of subjects and the length of implants placed being an average of 9 mm, the significance of the findings are questionable when compared to the findings from standard implants that are 10mm or greater. A systematic review by Annibali et al. (2012) determined a 99.1% cumulative survival rate for short dental implants with a mean observational period of 3.2 ± 1.7 years. Griffin and Cheung (2004) demonstrated 168 hydroxyapatite (HAp) coated implants with the height of 6mm and the width of 6mm showed a success rate of 100% over the mean observational period of 34.9 ± 13.4 months. However, it is important to note these studies had a short-term follow-up, mostly less than a five-year observational period. In addition, it is important to note that 2mm bone loss around a 6mm, short dental implant installed due to peri-implantitis corresponds to a third of the entire implant length and should be viewed differently from implants that are 10mm or longer in length with the same height of bone loss, which will be a fifth of the implant length.

1.5 Simultaneous or delayed implant placement with the sinus lift procedure

1.5.1 One-stage versus two-stage implant placement

The sinus floor elevation procedure is referred to as a one-stage procedure, where the implant is placed simultaneously at the time of the procedure (with or without graft material) (Bruggenkate and Bergh, 1998). This differs from two-stage where the floor of the sinus is grafted with a choice of graft material and implant placement is delayed for several months to allow the graft to consolidate with new bone (Olson et al., 2000).

1.5.2 One-stage approach

In the one-stage approach, the original design of the lateral sinus lift introduced by Tatum (1977) involved insertion of a bone graft into the sinus floor. However, studies have confirmed bone regeneration in the sinus floor is possible with omission of a graft material as the implant apex placed at the time of sinus elevation can stretch out and lift the sinus membrane upwards as a “tent-pole” (Chen et al., 2007; Lundgren et al., 2004; Schmidlin et al., 2008). This allows blood clot formation within the resultant space between the sinus membrane, the implant, and the sinus floor (Chen et al., 2007). Subsequently, new bone will form in the space in accordance with the principles of guided bone regeneration (Lundgren et al., 2004).

This elevation approach without use of graft material can be performed in both lateral sinus lift and osteotome techniques. A study by Schmidlin et al. (2008) reported a 100% survival rate for implants that had been placed using the osteotome technique in a non-augmented sinus, after a mean period of 17.6 months. Pre-treatment residual bone height was approximately 5mm, and the implants were restored six months after their placement. Compared to the baseline radiographs, both mesial and distal aspects of the apex of the implants gained considerable amount of bone fill (>85%), indicating successful bone formation around implants without the use of graft material. Likewise, in a study by Chen et al. (2007), seventy-five implants were placed in 47 patients at the time of lateral sinus elevation without a graft material. The two-year survival rate was 100% and radiographic examination confirmed there is an increase in sinus bone height ranged from 3mm to 9mm with an average of 4.5mm (Chen et al., 2007). A clinical

study by (Sohn et al., 2008) observed bone formation around implants placed simultaneously with the lateral sinus elevation in the absence of a bone graft. A total of 21 implants were placed in ten patients in the posterior maxilla with a mean residual bone height of 5mm. Computed tomograms were taken before, and six months after surgery. A bone biopsy was also taken from the surgical site at six months following the surgery. Both the tomograms and histological analysis revealed a significant amount of bone formation around the apex of the implants, indicating the possibility of an adequate bone formation with the omission of bone grafts.

In animal studies, Palma et al. (2006) also observed successful bone fill and osseointegration of implants in non-augmented maxillary sinus sites. Four non-human primates underwent a bilateral sinus lift using the lateral sinus approach. On the right-hand side, the sinus was grafted with autogenous bone, and implants were placed simultaneously. On the left-hand side (test site), implants were placed, but grafting material was not used. After six months, the histological examination showed a similar amount of bone formation in both augmented and non-augmented sites and also in the amount of bone-to-implant (BIC) contact.

The one-stage approach of the sinus elevation with simultaneous implant placement allows space provision for blood clot on the sinus floor where new bone is formed and integrates with the implant, without having bone graft material. However, this one-stage approach is only possible if the implant primary stability can be achieved at the time of the surgery. Current guidelines suggest there should be at least 4mm of alveolar bone height where the coronal part of the implant should be engaged (Jensen et al., 1997). Without the implant stability, there will be micro-movement of the implant hindering blood clot stability and subsequently new bone formation. Fibrous encapsulation of the implant will be more likely to occur (Meredith, 1997; Sun et al., 2008). Therefore, in sites with inadequate residual bone (<4mm bone height), the two-stage approach where the sinus lift procedure is performed first and implant placement is delayed is recommended (Bruggenkate and Bergh, 1998). In the two-stage approach, the use of graft material is necessary in order to maintain the space on the sinus floor for bone regeneration. Implant placement should be delayed until good consolidation of the graft with new bone is occurred within the sinus which will provide the primary stability for implants that are placed later on.

1.5.3 Delayed implant placement in grafted sinus (2-stage approach)

The two-stage approach is indicated if there is a lack of residual bone height to achieve the primary stability of implants. Placement of a graft material on the floor of the sinus is necessary in the two-stage approach. Graft material holds the elevated membrane in position and maintains space below the sinus for bone formation. This formation of new bone around graft material is defined as consolidation. Consolidation increases the quantity of bone available to improve primary stability of implants placed in the future.

Different systematic reviews reported different results for the survival rates of implants placed via one-stage and two-stage procedures; In the report by Tolman (1994), the survival rates for delayed placement (i.e., two-stage) were lower than immediate implant placement (i.e., one-stage) in sinuses grafted with both block grafts (84% and 92%, respectively) and particulate grafts (91% and 100%) (Tolman, 1994). Conversely, Wallace and Froum (2003) reported the survival rates for delayed implant placement were similar to immediate implant placement (89.7% and 89.6%, respectively).

The reason for conflicting observations in these review papers appears to be due to the number of co-variables that were present in studies that were selected in the studies' meta-analysis (Wallace and Froum, 2003). These variables include machined versus rough implant surfaces and presurgical residual crestal bone height.

1.6 The influence of implant surface design on implant survival

The implant surface characteristics play a fundamental role in early bone healing and osseointegration of implants when the implants are placed (Albrektsson et al., 1986; Lundgren et al., 2004). Implants with various types of surface microtexture are available. Studies have reported that implants with rough surfaces showed increased bone apposition on their surfaces compared to machined ones (Del Fabbro et al., 2008; Lundgren et al., 2004; Palma et al., 2006; Wallace and Froum, 2003). For example, in a study by Palma et al. (2006), one implant with a machined surface and one with an oxidised surface (Mk III and Mk III TiUnite, respectively, Branemark system, Nobel Biocare) were placed immediately in the lifted-sinus space of the capuchin monkeys. Following six months of healing, the bone-implant contact (BIC) for the oxidised implants was greater than that of the machined implants, indicating that implant surface characteristics have a great influence on osseointegration. A systematic review by Del Fabbro et al. (2008) also observed greater survival rates for rough surface implants than machined ones. Regardless of the type of bone graft material placed in the sinus, an 86.3% survival rate was observed with machined implants (3,345 implants in 950 patients) while the rate for rough surface implants was 96.7% (8,303 implants in 2,544 patients).

Davies (1997); Davies (2003) explained the possible underlying mechanisms for this. He suggested that the rough implant surface improved the retention of the fibrin scaffold on which differentiated osteoblasts migrate and lay down new bone directly on the implant surface. The fibrin scaffold contracts as it matures and is replaced by bone. In machined surface implants, the fibrin is more likely to be detached from the implant surface as it contracts, interfering with the migration and direct contact of osteoblasts onto the implant surface and, hence, resulting in less bone-implant contact following healing.

1.7 The influence of pre-surgical height of bone on implant survival

For implant placement in the atrophied maxilla, residual alveolar bone height plays a critical role in the survival of implants. Residual bone height and bone quality (i.e., cortical versus trabecular) determines primary stability of implants. Without stability, micro-movement of the implant will hamper bone formation on the implant surface. Studies have shown an increase in failure rates of implants placed simultaneously in posterior maxillary sites with less than 2mm bone (Jensen et al., 1997). A recent animal study was carried out using a one-stage lateral sinus elevation in the maxilla of mini-pigs with different bone heights (2,4,6 and 8mm) (Fenner et al., 2009). The study showed all implants placed in 2mm residual bone failed. Bone-to-implant contact (BIC) was significantly higher in sites with 6mm bone than 2 or 4mm residual bone height and also crestal bone resorption was significantly lower for implants placed in 8mm residual bone compared to implants placed in 2 or 4mm of bone. These findings indicate that the osseointegration and survival rate of implants depends highly on the pre-surgical height of bone (Fenner et al., 2009). Some previous clinical studies, looking at survival rates implants placed in grafted sinus, however, did not report on the residual crestal bone height approach (Wallace and Froum, 2003). Also, the ranges of residual crestal bone height for both simultaneous and delayed placement overlap in a number of studies which may have resulted different implant survival rates in grafted sinus via both immediate or delayed approach (Wallace and Froum, 2003)

In two-stage sinus lift procedures, consolidation of graft material will increase the height of bone. Different grafting materials are available on the market and each graft material has different physical properties that will promote varying rate and degree of bone formation, which is an important step prior to implant placement (Busenlechner et al., 2009).

1.8 The remodelling of graft material placed in the maxillary sinus

Healing of bone/bone graft placed within the maxillary sinus shares a similar healing process to that of fractured bone or regeneration of bone defects (Hing et al., 2004; Lundgren et al., 2004). This healing process may slightly vary depending on individuals and the type of bone and bone graft placed. The next paragraph will provide a general overview of the healing process of bone/bone substitute placed in the maxillary sinus based on recent reviews and studies (Dimitriou et al., 2005; Einhorn, 1998).

The healing of graft material takes place via a complex process of haemorrhage/coagulation, inflammation, angiogenesis, mesenchymal cell differentiation, and bone deposition/absorption (bone remodelling). Following sinus floor elevation with graft material (either bone or bone substitute), a blood clot will form. This is followed by inflammation with migrating immune cells and fibroblasts to form an extracellular matrix and new blood vessels (angiogenesis). Via newly formed blood vessels, mesenchymal cells migrate and differentiate into osteoblasts and osteoclasts. These cells will initiate bone deposition and graft resorption (bone remodelling). Initially, woven bone is formed that will be remodelled into lamellar bone, which is more organised in structure. The rate of graft incorporation depends on the porosity of the graft material where greater macro- and microporosity leads to increased angiogenesis via the channels leading to faster graft incorporation (Aukhil, 2000; Dimitriou et al., 2005; Einhorn, 1998).

Graft material is categorised by difference in osteogenetic, osteoinductive, and osteoconductive characteristics.

1.8.1 Osteogenesis

Osteogenesis is defined as bone formation. To regenerate bone, the presence or recruitment of osteoblast precursors and growth factors at grafted sites is necessary. Osteoblast precursors can be provided by the recipient bed or by the graft material (cancellous autogenous grafts). Growth factors are sourced from the graft, recipient bed, and vasculature. It is believed that ‘intramarrow’ penetration increases both cellular and growth factor migration into the sites

where bone is regenerated, which is associated with up to 30% greater bone regeneration and higher bone density at grafted sites (Majzoub et al., 1999). Host mesenchymal stem cells infiltrate the grafted site within seven days. Surface osteocytes of cancellous autografts survive and are nourished by diffusion.

Bone regeneration is governed primarily by two basic multicellular units of osteoblasts (bone forming cells) and osteoclasts (bone resorbing cells). While these cells coordinate and function as one unit in remodelling bone, they originate from two separate embryonic lineages: osteoblasts are derived from mesenchymal cells (bone marrow stromal stem cells) whereas osteoclasts are derived from hematopoietic progenitors (monocyte lineage). Two transcriptional factors expressed by osteoblasts, Runt-related transcription factor-2 (Runx2) and Osterix/SP7, are necessary for the differentiation of mesenchymal cells into osteoblasts. Other key factors involved in osteoblast differentiation include vitamin D3, estrogen, parathyroid hormone, fibroblast growth factors (FGFs), and transforming growth factor beta family (TGF-beta). Osteoclast differentiation depends on the activation of colony-stimulating factor-1 receptor/macrophage, colony-stimulating factor/CD115, and receptor activator of nuclear factor kappa-B (RANK) receptors. Osteoblasts produce RANK ligand (RANKL) and its high-affinity decoy receptor, osteoprotegerin (OPG). The binding of OPG to RANKL blocks RANKL-RANK ligand interaction between osteoblast and osteoclast precursors, inhibiting the differentiation of the osteoclast precursor into an osteoclast. OPG is also known as the osteoclastogenesis inhibitory factor (OCIF).

1.8.2 *Osteoinduction*

Osteoinduction is a property of a graft material that can promote recruitment and differentiation of undifferentiated mesenchymal cells into mature osteoblasts (Albrektsson and Johansson, 2001). It is a basic mechanism underlying the fracture healing. An injury to bone marrow, cortical bone and surrounding soft tissues results in repair process where there are releases of growth factors that can help induce cell differentiation and mitogens (Albrektsson and Johansson, 2001). These growth factors not only act on bone forming cells but also affect other cells and tissue compartments such as fibroblast proliferation, extracellular matrix deposition,

mesenchymal cell differentiation, and vascular proliferation. Some growth factors may play roles during the early stage of bone induction; Platelet-derived growth factors (PDGF) and fibroblast growth factors (FGF) stimulate fibroblast and osteoblast proliferation. By contrast, other growth factors such as bone morphogenic proteins (BMPs) act on later stages of osteoinduction such as mesenchymal cell differentiation and vascular proliferation (Sheikh et al., 2015)

1.8.3 *Osteoconduction*

Osteoconduction is a property of graft material that provides a physical scaffold for the ingrowth of capillaries and the migration of osteoprogenitor cells. Biomaterials such as bone grafts and titanium implants feature this property. Certain materials such as copper and silver however are not osteoconductive. In regard to bone grafts, macroporosity and pore interconnection play an important role as these will determine the amount of capillary in-growth throughout the graft material and new bone deposition (Sheikh et al., 2015)

1.9 Sources of bone-graft/substitute materials

There are different sources of bone graft material available for maxillary sinus floor elevation. Different graft materials have different rate and pattern of consolidation with new bone during healing (Busenlechner et al., 2009). Autogenous bone, with its inherent characteristics of being osteoinductive and osteogenic, is recognised as the gold standard amongst graft materials (Jensen et al., 1997). Viable cells within the autogenous bone may improve consolidation of the graft with its host bone if they survive after implantation. However, the majority of viable cells are believed to necrose hence autogenous bone is mainly osteoinductive with limited osteogenic characteristic. In addition, due to the limited quantity of harvestable bone available from a secondary donor site with increased morbidity, the use of other sources of grafting materials may be preferred. Allografts (graft from a genetically non-identical donor of the same species) or xenografts (graft from a different species) may be used. To minimise immunogenic reactions due to the presence of viable cells, allografts are deep frozen or demineralised to remove viable cells and, hence, become less osteogenic and are mainly osteoinductive. Xenografts are commonly used as a bone substitute material in implant dentistry. Although xenograft is mainly osteoconductive, studies showed no significant difference in the survival rate of implants placed in xenograft compared to other sources of graft material, suggesting its use in the maxillary sinus grafting procedure (Hallman et al., 2002; Hising et al., 2000)

1.9.1 Autograft

Autograft refers to bone tissue harvested from the same individual, which is biocompatible with no risk of immunogenic rejection. This material combines an inorganic matrix of hydroxyapatite and organic components, e.g., osteoblasts, osteoclasts, osteocytes, osteogenic signalling proteins, and mesenchymal cells that promote osteogenesis (Misch and Dietsh, 1993). At present, autogenous bone is the only osteogenic material available and, thus, is recognized as the ‘gold standard’ for graft materials (Del Fabbro et al., 2005). With the presence of Bone Morphogenic Proteins (BMPs) readily available within the cortical bone, this material also has osteoinductive properties. Despite these benefits, due to the limited quantity of harvestable bone available from a secondary donor site with its increased risk of morbidity, the

use of other types of grafting materials may be indicated. Autogenous bone has been shown to resorb and remodel faster than other materials, which makes it unsuitable for use in sites requiring long term augmentation (Schlegel et al., 2002). Some studies suggest the possible benefits of using a combination of autograft and other types of graft material to increase the volume of the graft and minimise resorption during healing (Hallman et al., 2002). The differences in composition of autogenous bone harvested from various sites give rise to different rates of resorption. Dense cortical bone resorbs at a much slower rate than cancellous and marrow bone grafts. However, cancellous bone marrow is the primary source of stem cells for osteoblasts possibly giving the material its osteogenic properties. In contrast, cortical bone is known to carry bone morphogenic proteins (BMPs) and, thus, is osteoinductive (Cypher and Grossman, 1996)

1.9.2 *Allograft*

Allograft is a graft material that is derived from a genetically non-identical donor of the same species. Compared to an autograft, allograft does not require a secondary donor site and, thus, reduces surgical morbidity and shortens surgical time. However, allografts carry a risk of disease transmission. Therefore, the graft is often sterilised with irradiation or chemicals to remove any transmittable viruses or other types of microorganisms. Moreover, possible immunogenic rejection is another major concern with these materials. Various antigens, e.g., bone cells, cartilage, haematopoietic cells, vascular cells, and bone proteins, are recognizable by the host and may trigger an unfavourable immune response (Lei et al., 2008). The antigens within the allograft are eliminated via a "freeze-dried" or "demineralised freeze-dried" process. With allograft, cortical bone is often preferred over trabecular bone as it contains fewer antigenic substances. Cortical bone carries more bone matrix than trabecular bone and contains various types of proteins known to be osteoinductive (BMP). Freeze-dried and demineralized freeze dried bones are the main types of allografts used in contemporary dentistry.

1.9.2.1 Freeze-dried bone allograft (FDBA)

Freeze-drying is a process by which dehydration is achieved by removing water directly from frozen bone stored in liquid nitrogen. This results in more than 95% dehydration and

removes all cells, reducing its antigenicity while maintaining its mechanical properties. To minimize disease transmission, the material is additionally sterilized by irradiation and ethylene oxide. Although all cells are removed, cell proteins may still survive, which can be a target for host immune response resulting in graft rejection (Reikerås et al., 2008; Shegarfi and Reikeras, 2009)

1.9.2.2 Demineralised freeze dried bone allograft (DFDBA)

In addition to the freeze-dried process, bone is immersed in 0.6N of hydrochloric acid, which removes calcium (decalcification) and exposes osteoinductive proteins (BMP). However, due to the loss of calcium, the graft loses its mechanical strength.

1.9.3 *Alloplast*

Alloplasts are synthetic graft material that has osteoconductive properties. However, in orthopaedic research, some studies have suggested possible immunological reactions against this material, which may result in graft rejection and the resorption of the surrounding host bone (Bauer and Muschler, 2000). Depending on how these materials are processed and their composition, there are variances in their mechanical and chemical properties. Commonly used alloplastic materials include hydroxyapatite and tri-calcium phosphate (TCP).

1.9.3.1 Hydroxyapatite (HAp)

HAp is the principal inorganic component of human bone; mainly comprised of calcium and phosphorous. Due to its similar composition to biological bone mineral, it promotes host bone formation when placed. HAp materials are available with different physical properties including surface area (e.g., block vs particulate), porosity (dense, macro-porous, or micro-porous), and crystallinity (crystalline or amorphous) (Misch and Dietsh, 1993). Histological analysis demonstrated that the larger the material's particle size, the longer it takes to resorb due to a lesser surface area to volume ratio (Tofe et al., 1991). Likewise, porosity influences the resorption rate: HAp materials with greater porosity show greater resorption rates. Therefore, the physical properties of HAp should be considered when it is used for bone augmentation.

Bone material with larger particle size and dense HAp material will take longer time to resorb; hence, it is ideal for use in sites where a long-term matrix is desired (e.g., ridge augmentation for future implant placement). Conversely, HA material with smaller and more numerous particles and greater porosity is preferred in cases where faster consolidation is necessary for implant placement in the near future.

1.9.3.2 Beta Tri-calcium phosphate (β -TCP)

Similar to hydroxyapatite, β -TCP is also composed of calcium and phosphorous but in a different composition ratio. It is highly osteoconductive, providing the scaffold for bony ingrowth, and is often used as a composite graft with autogenous graft in sinus grafting. Suba et al. (2004) performed ridge preservation using β -TCP (Cerasorb, Curasan) and observed the formation of lamellar bone that replaced the graft material. Compared to the bovine xenograft, the β -TCP showed a greater reabsorption rate. In a study conducted by Artzi et al. (2003), β -TCP and bovine bone were used in critical defects in mongrel dog mandibles. The results showed excellent bone bridging with both of the materials, but the β -TCP had been completely reabsorbed by 24 months and replaced by lamellar bone (Artzi et al., 2003)

1.9.3.3 Bioactive glass

Bioactive glass is a biocompatible and osteoconductive material. It is composed of silicon dioxide containing calcium, phosphate, and sodium ions (Jensen et al., 2006). When bioactive glass comes in contact with fibrin scaffold, it results in the surface formation of hydroxyapatite, making it highly conducive for osteoblast attachment (Jensen et al., 2006). It is initially incorporated into the bone, and subsequently, via a remodeling process, it is reabsorbed and replaced by bone (Anderegg et al., 1999). Cancian et al. (1998); Cancian et al. (2003) compared the healing process involving HA with bioglass in monkey mandibular defects and has observed resorption and replacement of the bioactive glass material with new bone within 180 days, whereas adversely with HA, the formation of scar tissue development has been observed over the same period (Cancian et al., 1998; Cancian et al., 2003)

1.9.4 *Xenograft*

Xenografts are graft materials derived from natural bone from a different species, e.g., bovine. Xenograft is mainly osteoconductive. Organic components are removed in order to minimise the risk of disease transmission and immunogenic rejection while inorganic parts of the bone mineral and amorphous inorganic components of the trabecular bone are converted into a hydroxyapatite-maintaining bone scaffold. Lei et al. (2008) transplanted fresh pig bone and deproteinised pig bone into mice to assess the immunological response. The fresh bone elicited a specific IgG antibody response after a week of transplantation whereas the deproteinised bone resulted in a minimal T-cell immune response. At histological level, the fresh bone was present with a large concentration of lymphocytes while conversely, the deproteinised bone showed a minimal level or absence of lymphocytes, and there was a presence of fibroblasts and connective tissue in the gaps between graft particles, showing biocompatibility.

Bio-Oss® (Geistlich Pharma, USA) is one of the most commonly used xenograft materials in dentistry. Its use as a graft material for sinus grafting procedure has been demonstrated by several clinical studies (Martinez et al., 2010; Piattelli et al., 1999). Martinez et al. (2010) performed a histological analysis of Bio-Oss® grafted in the maxillary sinus for eight months. They observed the apposition of new bone on graft particle where the vital bone has ‘bridged’ the gaps between xenograft particles. The graft materials were neither encapsulated by any fibrotic tissues nor did they exhibit any chronic or acute cell infiltrations. Osteoblasts surrounded by extracellular matrix were frequently visible, indicating progressive mineralization where the quantitative results showed more than 30 percent volume of new bone created within the grafted site. Only 18.4 percent of the graft material was resorbed, leaving 81.6 percent of the graft remaining. These residual xenograft materials are accepted as a structural element in the bone-remodelling process and bone grows surrounding them (Martinez et al., 2010)

A large body of research on xenografts as a bone substitute for sinus augmentation has been documented and analysed. A systematic review by Wallace and Froum (2003) included a total of 5,267 implants that are placed in augmented sinus and followed up for a minimum of one year of functional loading. Eleven out of 34 included papers carried out the lateral sinus

elevation, either with the use of xenografts alone or in combination with autogenous bone, an allograft (demineralized freeze-dried bone graft), or mixed with platelet-rich plasma (PRP). The survival rate of implants placed in these sites showed no statistical difference compared to implants placed in autogenous bone alone (Wallace and Froum, 2003)

Interestingly, a study by Hising et al. (2000) reported significantly higher survival rates for implants placed in the sinus that were augmented with xenograft. In the study, 231 implants were placed in 92 sites that were augmented with either Bio-Oss® alone or in combination with autogenous bone. The survival rate for implants placed in xenograft alone was 92.2%, compared to 77.2% for implants placed using a composite of Bio-Oss® and autogenous bone.

Hallman et al. (2002) also reported a greater survival rate for implants placed in the sinus augmented with xenograft alone or in combination with autogenous bone, compared to those placed in sinus grafted with autogenous bone only. After one year of loading, the survival rates of implants placed in xenograft or in an 80:20 mixture of xenograft and autogenous bone were 94.4% and 96%, respectively. In contrast, the survival rate for implants placed in 100% autogenous bone was 82.4%.

In two-stage procedures where implant placement is delayed, studies reported no significant difference in the survival rate of implants when different graft materials were used (Olson et al., 2000). However, due to the less complicated procedure of using xenograft, the same predictability of success as autogenous bone has led to the use of xenograft alone or in combination with autogenous bone rather than the sole use of autogenous bone among clinicians today (Froum et al., 2006)

1.9.4.1 Endobon®

Endobon® (Biomet 3i, USA) is a biocompatible, synthetic, deproteinised, porous hydroxyapatite xenograft that is bovine-derived. It maintains the cancellous structure of bovine material, which allows rapid vascularisation and bony ingrowth. The material is manufactured from natural cancellous bone by removing organic components while preserving the trabecular

structure of the bone. It also transforms the mineral and inorganic bone components into hydroxyapatite (Hing et al., 1999). The macroporous structure of the material allows rapid vascularisation and bone apposition once it is placed (Hing et al., 2004).

A study conducted by Ramírez-Fernández et al. (2011) involved the use of Endobon® placed in rabbit tibia. The results of the study demonstrated similar histological findings to Bio-Oss®. An osseous defect made using a trephine bur was filled with Endobon® in a number of rabbits, and a histological sample was examined under a microscope at one, two, three, and four months following this procedure. The results demonstrated that, over time, the infiltrated area of granulation tissue was replaced by lamellar and trabecular bone, which also showed direct contact between the graft particles and the new bone. Between three to four months, there was a reduction in the size of graft particles, but it was minimal.

1.9.5 *The healing of different sources of graft materials placed in the Maxillary sinus*

Cellular events that occur during graft healing may vary depending on the type of graft material. In the case of an autograft, due to its osteoinductive and osteogenic properties, rapid graft consolidation will occur as long as the graft material is stable. De novo bone formation may occur within the graft material, as the material is osteogenic, containing viable osteogenic cells. Upon transplantation, the majority of viable cells within the graft material will undergo necrosis due to ischemia. Among these cells, the mesenchymal cells of the bone marrow are the most resistant, and they may even be stimulated to proliferate via changes in oxygen tension, pH, and the cytokine environment (Bauer and Muschler, 2000). Survival of these cells is believed to account for the greater efficacy of autogenous bone compared with other types of graft materials (Bauer and Muschler, 2000).

Many available allograft materials are demineralized, meaning that any viable cells that have the potential for immunogenic reactions are removed. These materials are mainly osteoinductive and osteoconductive. BMPs (bone morphogenetic proteins) are believed to be responsible for providing the osteoinductive properties of allografts. BMPs are a subgroup of a larger growth factor family of transforming growth factor (TGF) has osteoinductive

potential, which is responsible for the differentiation of osteogenic cells and bone formation (Celeste et al., 1990). When migrated mesenchymal stem cells make contact with BMP, the stem cells transform into osteoblasts and actively secrete down the bone. The formation of bone first initiates on the periphery and extends circumferentially around the sinus cavity to join the bone growth. As healing progresses, a doughnut effect mineralisation occurs that continues to advance inwardly until the central area is reached, and consolidation is completed (Busenlechner et al., 2009; Jensen et al., 1997).

1.9.6 Survival rates of implants placed in grafted sinus with different sources of graft materials

The survival rate of implants placed in sinuses with different sources of bone graft materials varied, but the differences were not significant. Beirne (2000) performed a meta-analysis of ten studies, which included 484 implants in 130 patients followed for six to 60 months. Implant survival rate was reported as follows: 90% for autogenous bone, 94% for hydroxyapatite (HA) + autogenous bone, 98% for demineralised freeze-dried bone (DFDB) + HA, and 87% for HA alone. There were no significant differences between the grafting materials. Aghaloo and Moy (2006) reported similar findings. From a total of 5128 implants placed in augmented sinus with follow-up periods of twelve to 102 months, autogenous grafts alone or autogenous with other graft mixtures showed 93.3% survival rate whereas the survival rates were 81% for alloplast and alloplast + xenograft, and 95.6% for xenograft alone.

It appears that the choice of graft material does not have any clinically significant impact on implant survival. However, it is true, histological analysis in animal studies observed different rate and extent of bone formation around different sources of graft materials within the sinus and also this was directly linked to bone-to-implant (BIC) contact for those implants placed either had simultaneous or delayed placement (Busenlechner et al., 2009; Rasmusson et al., 1999). Whether this different degree of BIC have any clinical influence on implant survival over long-term is questionable. As clinicians, an ideal graft material should be the one that quickly consolidates with new bone, which may reduce time interval between sinus grafting procedure and implant surgery and improve primary implant stability. In this regard, there are still growing numbers of different bone substitute materials with different properties introduced in the market today.

1.10 Timing of implant placement

In two-stage sinus elevation procedure, the probability of a successful implant treatment may be improved by allowing adequate healing of bone graft following its placement within the maxillary sinus. The ideal timing of implant surgery is when the graft is consolidated with new bone, hence achieving adequate mechanical properties to achieve implant's primary stability and osseointegration (Bauer and Muschler, 2000; Jensen et al., 1997; Kan et al., 2002; Ostman et al., 2005). Rasmusson et al. (1999) demonstrated that the delayed placement of implants in the maxillary sinus grafted with autogenous graft resulted in significantly greater stability for implants in comparison to simultaneously placed implants, as measured by resonance frequency analysis (RFA). Delayed implant placement also revealed a greater amount of newly formed bone trabeculae and interspersed bone marrow present at implant placement, which in turn resulted in a greater bone to implant contact compared with implants placed simultaneously.

The rate and extent of graft consolidation varies depending on the type of graft material, the tissues at the margin of the graft site, and the physiologic state of the host (Bauer and Muschler, 2000). Current clinical guidelines suggest waiting at least six months following sinus grafting procedure before implant placement (Jensen et al., 1997). This arbitrary timeline is based on the analysis of healing of different sources of graft materials in animal and human studies (Wallace and Froum, 2003). However, some studies reported that even after six months of the suggested healing period, the quality of bone was still poor and the initial implant stability was not achieved. In Lundgren et al. (1997), the overall success rate of implants placed in the sinus, six months after grafting was 80% indicating the definition of optimal healing period appears still inconclusive (Lundgren et al., 1997). A systematic review by Tolman (1994) showed that the survival rate of implants that are immediately placed into the sinus was significantly greater than implants had delayed placement which may indicate the grafted sinus of the delayed group did not show maturity in the quality and quantity of bone even after a given length of healing period (Tolman, 1994).

Histological analysis is the gold standard for assessment of graft consolidation. It visualises residual graft, new bone and connective tissue of the grafted sinus. Moreover, it can

also determine the type of bone (woven or lamellar) that has been formed. However, the technique is clinically not useful since it requires a bone biopsy from the grafted site. There is no clinical tool to analyse the amount of graft consolidation prior to implant insertion.

An extension of the healing period may increase the amount of consolidation. However, depending on the source of graft material (e.g., autogenous bone), a prolonged healing period may result in remodelling of bone grafts and subsequent reduction of the overall bone volume. A study by Widmark et al. (1997) observed extensive resorption of autogenous onlay graft in the buccopalatal direction up to 25% after four months past the grafting procedure. With other sources of graft materials (e.g., xenografts), grafts resorb minimally over time, but the quality bone that forms around graft material appears to decay over time. For example, in an animal study by Xu et al. (2005), deproteinised xenograft obtained from other rabbits were used with a sinus elevation procedure in 20 adult Japanese rabbits, and histomorphometry was performed at different time intervals. The results showed that the area occupied by new bone around the graft particles initially increased significantly up to sixteen weeks, but from sixteen to 64 weeks, it decreased significantly. Newly-formed, lamellar bone was replaced by large areas of bone marrow and adipose tissue over time, reducing the quality of bone within the grafted site. However, the area of residual graft did not change significantly, remaining the same over time.

Therefore, the timing of the implant placement should depend directly on the extent of graft consolidation with new bone in-growth, which is directly linked to the initial implant stability and the implant success. The rate of consolidation is different individually depending on the source of graft material used, the physiologic state of the host, and the type of procedure performed. An extended healing period may increase the extent of the consolidation. However, there is always an increased risk of the reduction in bone volume or bone quality. Also, there are a limited number of valid human and animal studies available to date to define the exact optimal healing period, which is as yet inconclusive. In clinical practice, this decision is made arbitrarily based on interpretation of radiographic images taken post sinus lifting, observations of the patient at various intervals after sinus grafting, and histological findings in other animal and human studies. Histological analysis of healing is the gold standard, but not clinically useful. A clinical tool that could be used for non-invasive evaluation of graft healing within the sinus is

needed. This can improve the clinical decision on the optimal timing of implant placement, which subsequently leads to increased implant success.

1.11 Cone beam computed tomography (CBCT)

Cone beam computed tomography (CBCT) was introduced in the late 1990s. In comparison to other types of tomographic imaging devices, e.g., medical computed tomography, CBCT quickly acquires a three-dimensional (3-D) volumetric image with shortened imaging time and less radiation (Lascala et al., 2014). CBCT has been widely accepted as a useful clinical tool for dental and maxillofacial imaging. In particular, it has been widely used in both pre-operative and post-operative assessment for surgical and/or prosthetic implant planning in the field of dentistry (Feldkamp et al., 1989; Hsieh, 2009).

The system works via a cone-shaped x-ray beam that passes through an object, which hits an x-ray detector (Scarfe et al., 2006). The x-ray source and the area detector synchronously move around the object at a 360-degree angle and scan 2D images at certain intervals, and each image is taken from a slightly different angle. The series of captured 2D images are reconstructed into 3D volumetric data by computer software programme. The resultant 3D volume data can be examined in three orthogonal planes (axial, sagittal, and coronal).

CBCT has several advantages compared to conventional medical CT. CBCT uses less radiation. By collimating the x-ray beam source, CBCT can limit irradiation to the region of interest, minimising the radiation dose. Most CBCT units can be adjusted to scan small regions for specific diagnostic tasks. The image resolution of CBCT is also higher than conventional CT. The volumetric data set consists of a 3D array of small cuboid structures known as voxels. The size of this voxel determines the resolution of the image. In conventional CT, the voxels are anisotropic – rectangular cubes where the longest dimension of the voxel is the axial slice thickness. Although the CT voxel could be as small as 0.625 mm^2 , depth is usually limited between 1 to 2 mm. In contrast, CBCT provides voxels that are isotropic, meaning all three dimensions are equal. Therefore, it can produce sub-millimetre resolution ranging from 0.4mm to as low as 0.080mm. CBCT also completes its scan in a single rotation, resulting in quick acquisition of the image. As a result, the radiation exposure time is minimised, and the risk of motion artefacts due to patient movement is also reduced. The average dose of radiation in CBCT ranges from 36.9 to 50.3 micro-Sievert (μSv), which is less than that of the conventional

fan-beam CT systems, ranging between 1,320-3,324 μ Sv and 1,031-1,420 μ Sv for mandible and maxilla, respectively. This reduces the effective patient dose down to levels similar to that of full-mouth periapical radiographs (13-100 μ Sv), or 4 to 15 times that of a single panoramic radiograph (2.9-11 μ Sv) (Scarfe et al., 2006).

CBCT is used across various dental fields, including oral maxillofacial dentistry (Gribel et al., 2011; Lascala et al., 2014), orthodontics (Holberg et al., 2005), endodontics (Tyndall and Rathore, 2008), periodontics (De Vos et al., 2009; Estrela et al., 2008), and all other fields of dentistry concerning dentoalveolar conditions (Tyndall and Rathore, 2008).

CBCT has demonstrated utility in both linear and volumetric measurement of mineralised tissues (Benavides et al., 2012; Feichtinger et al., 2007; Gribel et al., 2011). In a study by Feichtinger et al. (2007), the volume of bone gained following secondary grafting in cleft lip cases was assessed on the basis of three-dimensional (3D) radiography using CBCT. Compared to a conventional two-dimensional (2D) orthopantomogram, which produced significant underestimation of bone gain, CBCT demonstrated more accurate measurement of volume gained by the procedure. Gribel et al. (2011) conducted a study comparing CBCT against lateral cephalograms to ascertain how accurate and reliable CBCT is for craniometric measurements. The study found no statistically significant difference between the measurements acquired by CBCT and lateral cephalograms, suggesting that CBCT can be a substitute for lateral cephalograms, which also allow true 3D volumetric measurements. A recent systematic review by Benavides et al. (2012) reported that linear and volumetric measurement by CBCT is accurate and can be useful, particularly for dental implant planning.

There is scant evidence however supporting the use of CBCT for bone density measurements (Benavides et al., 2012). In a study by dos Santos Corpas et al. (2011), peri-implant bone density was measured using CBCT and compared against histology and two-dimensional intraoral periapical radiography. Eighty implants were placed in ten mini-pigs, and the animals were scarified after three months for analysis. The results showed that density measurement using CBCT was significantly different from histology, indicating that CBCT cannot accurately measure changes in bone density around an implant. In a study by Sohn et al.

(2010), CBCT was used to measure the density of alveolar bone at implant osteotomy sites. The study demonstrated a significant correlation between bone density measured by CBCT and primary implant stability. However, there was no parallel arm group (e.g., histomorphometry) to validate the density measurement by CBCT. Currently, there is no available research of CBCT in determining newly formed bone within healed grafted maxillary sinus based on density.

Another field where CBCT was studied vastly for density measurement is in the field of endodontics. Apical periodontitis, which is a pathological condition that results in considerable bone loss adjacent to the apex of teeth, can be examined by CBCT. In a study by Estrela et al. (2008), conventional periapical radiograph (PA), orthopantomogram (OPG) and CBCT were compared to ascertain how well CBCT could determine the presence of apical periodontitis. Compared to PA and OPG, CBCT detected more apical periodontitis than the others, indicating it is either the same or better at assessing apical periodontitis than conventional radiographs. Several other studies also reported on the efficacy of CBCT for determination of apical periodontitis; a study by Velvart et al. (2001) showed a greater accuracy of CT in detecting the presence of apical periodontitis than conventional periapical radiograph. Despite the use of medical CT instead of CBCT, the study confirmed that in all cases that required endodontic surgery, the signs of apical periodontitis were positively confirmed in the CT whereas in periapical radiographs, only 78% of the lesions were confirmed positively.

However, the superior accuracy of CBCT for detection of apical periodontitis may not be a result of its higher resolution than conventional radiographs; instead, three-dimensional (3-D) images in different planes made it possible to confirm the presence of apical lesions more easily than two-dimensional (2-D) conventional radiographs. Furthermore, apical periodontitis is a pathological condition in which there is a significant loss of mineral density in the bone adjacent to the apex of a tooth. Studies report that in order to detect apical periodontitis radiographically, more than 50% loss of mineral density must occur at the apex (Bender and Seltzer, 1961a; b; Estrela et al., 2008). To simulate the condition of apical periodontitis, Stavropoulos and Wenzel (2007) conducted an experiment using frozen pig mandibles, where they made either 1mm^3 or 2mm^3 bony defects beyond the apices of the extraction sockets. The teeth were reinserted, and the bone block was scanned using conventional periapical radiograph and CBCT. CBCT

consistently showed better sensitivity, positive predictive value, and negative predictive value than the intraoral periapical radiograph with respect to the detection of the defect. However, since the defect itself was a result of physical removal rather than the pathological resorption of normal bone, the mineral density within the site was zero, providing significant contrast of the defect with neighbouring mineralised tissues resulting in easy detection of the defect by CBCT. So far, there are lack of studies validating the accuracy of CBCT for determination of density changes, which may be able to be particularly useful to distinguish between graft and new bone in grafted sinus.

1.12 Micro-CT (μ CT)

μ CT offers a non-destructive 3D radiographic image of mineralised tissue structures. It provides a high level of resolution, up to $1\mu\text{m}$, at which trabecular bone architecture of both human and animals can be visualised (Bouxsein et al., 2010). As a trade-off for high resolution, μ CT generates a high level of radiation which limits its application to in vitro human and animal tissue studies (Hildebrand et al., 1999; Müller et al., 1996) or partly small animal in vivo animal studies (Postnov et al., 2003)

Quantitative and qualitative morphometric analysis of bone structure was traditionally done by histomorphometry. However, histological preparation is destructive, resulting in a significant loss of volume by the thickness of the cutting blade. For the 3-D measurement, series of 2-D histological sections are indirectly measured by stereology based on an assumption of a fixed structural model but this could potentially lead to unpredictable errors, as trabecular bone may change its structural type continually in three dimensions (i.e. anisotropic) (Feldkamp et al., 1989; Hildebrand et al., 1999). Also, depending on the type of tissue embedding medium for histological preparation, tissue shrinkage can result in distortion of the tissue dimension. With the advent of μ CT, the direct measurement of 3-D trabecular structure without destructive preparation and tissue distortion is now possible.

1.12.1 μ CT versus histomorphometry

Previous studies reported a moderate to high correlation between 3-D μ CT and histomorphometry for the assessment of trabecular bone architecture (Chappard et al., 2005; Thomsen et al., 2005; Uchiyama et al., 1997b). Thomsen et al. (2005) analysed the trabecular structure of human tibia biopsies using histomorphometry and μ CT. They found a strong correlation ($r = 0.95$) between the two techniques for bone volume (BV/TV) and connectivity density (CD). Regression analysis for BV/TV demonstrated y-axis intercept was not significantly different from 0 indicating BV/TV measurements between the two techniques were similar. Their study concluded that μ CT can be used as a substitute for conventional histomorphometry for morphometric analysis of bone. In a study by (Chappard et al., 2005) a morphometric analysis of trabecular bone in human iliac bone biopsies was performed in parallel to 3-D μ CT

and histomorphometry. They found a strong correlation for bone volume (BV/TV) between the two techniques ($r = 0.937$), although μ CT slightly overestimated the results compared to histomorphometry (bias +2.8%). Correlations for trabecular thickness (Tb.Th), trabecular separation (Tb.Sp) values obtained between μ CT and histomorphometry were low. Uchiyama et al. (1997a) performed quantitative morphometric analysis on trabecular bone architecture of iliac biopsies obtained from 15 patients using μ CT and histomorphometry, similar to other studies mentioned earlier. The results showed strong correlations between the two techniques for all parameters including BV/TV ($r = 0.949$), Tb.Th ($r = 0.907$), and Tb. Sp ($r = 0.930$). Despite other parameters including Tb.Th, Tb.Sp and Tb.N demonstrated variable results in different studies, there was moderate to good correlation demonstrated between μ CT and histomorphometry for bone volume (BV/TV).

While the majority of published μ CT studies assessed trabecular bone architecture, some studies have attempted to utilise μ CT to determine bone quality around dental implants. In a paper by Park et al. (2005), peri-implant bone contact was analysed by 3-D μ CT to determine how accurate μ CT is in comparison to conventional histomorphometry. Twenty-four titanium implants placed in the tibia of New Zealand white rabbits were assessed after three months. Although the mean bone-to-implant contact in μ CT was significantly different from the result obtained from histomorphometry, histomorphometric data and μ CT data appeared to be linearly correlated. Vandeweghe et al. (2013) placed two implant materials (Titanium [Ti] and hydroxyapatite [HAp]) in both the tibia and the femur of lop-eared rabbits. The samples were examined after two and four weeks using 3-D μ CT and histomorphometry. Bone area (BA) and bone-to-implant contact (BIC) were measured at 0.75mm from the zone around each implant. It was observed that the measurements made using μ CT were not significantly different to those from histology, suggesting that μ CT can replace histomorphometry where direct, non-invasive, three-dimensional analysis of bone architecture is indicated. However, the findings of these studies must be interpreted with caution. Park et al. (2010) commented that beam-hardening effect near metal objects impairs the image quality of μ CT, particularly of sites near dental implants. This finding was confirmed by Schouten et al. (2009), who found that histomorphometry obtained superior results for peri-implant bone volume and bone-to-

implant contact measurements compared to μ CT due to the beam-hardening effect in μ CT images near the metal implant surface (Schouten et al., 2009).

As μ CT has proven to be useful for morphometric analysis of trabecular bone, μ CT is now widely used in medical research as a radiographic tool to analyse the 3D changes in trabecular bone pattern in bone metabolic diseases such as osteoporosis (Müller et al., 1998; Thomsen et al., 2005; Uchiyama et al., 1997b).

1.12.2 *Sources of error in μ CT*

1.12.2.1 Beam hardening

X-ray sources in μ CT are polychromatic (polyenergetic), meaning there is a spectrum of X-rays (photons) with different energy levels (Van de Casteele et al., 2004). Beam hardening is a process by which, in the polychromatic X-rays, photons with low energy are selectively absorbed and removed from the X-ray beam as the beam passes through the object. As more low energy X-rays are removed, the beam becomes progressively harder. In other words, the X-rays with higher energies are less attenuated (Bouxsein et al., 2010). The amount of beam hardening is dependent on the initial X-ray spectrum and the density of the object that the X-ray penetrates into. It is important to note that where the spectrum of the initial X-ray is narrower, there is less beam hardening. Beam hardening causes a non-linear relationship between the recorded signal (grayscale) and the density of the object. As a result, the outer surface of the sample appears relatively denser than it really is while the central part of the sample appears lighter. This results in the contrast of the projection image not being quite proportional to the object thickness, which causes pronounced edges, streaks, and artefacts in the reconstructed image, significantly affecting the quantitative measurement in μ CT (Postnov et al., 2003).

The beam hardening effect can be corrected by hardware filtering (Van de Casteele et al., 2004). When placing a filter between the x-ray source and the object, such as an aluminium plate, low energy x-rays are resorbed before the beam reaches the object (Chueh et al., 2006). The main disadvantage of this method is the decrease in x-ray intensity, which results in a decrease of the signal-to-noise ratio (SNR). The hardware filtering method only provides a

reduction in the beam hardening effect and does not entirely eliminate beam hardening. The beam hardening phenomenon becomes prominent with scanning of dense metal material such as dental implants. The hardware filtering cannot correct beam hardening phenomenon effectively, and it still may obscure the actual changes in bone density measured by μ CT (Park et al., 2010)

1.12.2.2 Ring Artifacts

Ring artefacts are resultant phenomena on μ CT images due to defective or uncalibrated x-ray detector elements. These appear as concentric circles superimposed on the reconstructed μ CT image. The presence of these artefacts could significantly hamper the post-imaging analysis. Ring artefacts may become more prominent as the resolution of the scan is enhanced, where recalibrating the detector may eliminate the artefacts.

1.12.2.3 Scatter (Compton Scattering)

Scattering is caused when a photon of X-ray source is deflected or reflected from its original path. This results in more photons being detected in an area of x-ray detecting panel that otherwise would have very few photons (Fleischmann and Boas, 2011). This effect commonly occurs with the presence of very dense materials, such as metals that have higher atomic numbers. Photons of X-rays are more likely to collide against the electrons occupying such metals, resulting in a deviation of its traverse path and leading to the image of scattering. Radiopaque streaks will appear superimposed on the images that are adjacent to the hard tissues; this scattering may be eliminated by minimising the presence of any metal parts during the scan. Alternatively increasing the level of kV results in a harder X-ray beam and, thus, a lesser scattering effect. The metal becomes more transparent on the scanned image as higher energy X-rays are more likely to traverse the metal block. However, as the level of x-ray energy increases, it results in less contrast between mineralised and soft tissues.

1.12.3 *Skyscan 1172 Micro-CT Scanner*

The Skyscan 1172 micro-CT scanner (Bruker Corporation, Germany) is a high-resolution desktop μ CT scanner, capable of dynamic variable acquisition geometry, allowing for faster scans at a high resolution, up to $0.5\mu\text{m}$. The scanner operates with a connected computer running either 32-bit or 64-bit Windows XP or by connecting to a group of computers, which enhances its performance, particularly during reconstruction. The x-ray tube produces x-rays with cone-beam geometry. An x-ray spot size of $< 8\mu\text{m}$ at 8W can be generated with 20-80kV energy. The x-rays that have traversed the object are detected by a charge-coupled device (CCD) detector and are converted into digital data. Subsequent volumetric reconstruction of raw data involves a Feldkamp algorithm for beam hardening correction. The Skyscan 1172 has a three-camera resolution system, which presents the possibility of scanning to a high resolution of $5.7\mu\text{m}$, a medium resolution of $11.5\mu\text{m}$, and a low of $22.9\mu\text{m}$ voxels. The medium resolution of the Skyscan 1172 produces reconstructed images at $17.34997\mu\text{m}$ in voxel size. The maximum object height for scanning at medium resolution is 22mm, although oversized objects up to 50mm high can be scanned, with a selectable option of double scanning. The platform on which the object is scanned is adjustable in height, allowing position of the object on the path of x-ray beam source. At its highest resolution, the Skyscan 1172 can produce details up to $0.5\mu\text{m}$ using a 12-bit 10 megapixel (4000 x 2300) CCD camera. At this resolution, the Skyscan 1172 scans objects up to 35mm diameter or up to 68mm diameter with camera offset. The medium resolution configuration also uses the same camera. Alternately, a second, 1.3 megapixel (1280 x 1024), 12-bit, cooled CCD camera offers lower resolution to about $2.0\mu\text{m}$, standard scans up to 20 mm diameter or up to 37 mm diameter with camera offset.

1.13 Radiomorphometric analysis

Radiomorphometry is defined as the quantitative analysis of structures shown on radiographic images in grayscale. In order to quantify different tissue parameters within radiographic images, thresholding technique is used to segment different tissue compartments based on their differences in grayscale. In the medical and dental research, the utility of digital radiography as a clinical tool is growing. For example, the dual energy x-ray absorptiometry is already widely used clinical radiographic tool to measure bone density (Mazess et al., 1990).

1.13.1 Grayscale calibration

μ CT produces radiographic images in grayscale. Instead of reporting grayscale values, transforming these into mineral density gHAp cm^{-3} [the mass of hydroxyapatite (HAp) per unit volume] is always preferable (Zou et al., 2011). With a series of radiographic (calibration) standards made out of hydroxyapatite at known density, grayscale can be calibrated into the mineral density (gHAp cm^{-3}), allowing quantitative analysis with μ CT. This has been demonstrated to be useful for determining the mineral density of dentine in dental caries research (Schwass et al., 2009)

1.13.2 Method of thresholding

Thresholding produces a binary image of foreground tissues of interest and background tissue, which is an important step prior to quantitative measurement of mineralised tissues in radiographic images of μ CT. Inappropriate thresholding will reduce the potential power of μ CT (and also CBCT) and may introduce systemic bias in the measurements; hence, proper thresholding of the structure is an important step.

A commonly used technique for segmentation is the global threshold; a single threshold will be chosen, above which all grayscale will be marked as tissue of interest and below which all remaining grayscale will be marked as background tissue. This can be performed by histogram analysis, where the starting point of the gradient in grayscale representing the tissue of interest is identified. Previous studies that used the global threshold method to segment the area

occupied by trabecular bone in μ CT found a moderate to good correlation with histomorphometry for trabecular bone morphometric analysis (Chappard et al., 2005; Thomsen et al., 2005; Uchiyama et al., 1997b).

Despite such ease of use, the quality of segmented images by global thresholding can be reduced by problems such as beam hardening and noise. The effect of beam hardening can be minimised through placement of a filter in front of the x-ray beam during the scan. Noise can be reduced by increasing the length of the scan or by filtering the image (e.g. 3-D Gaussian smoothing), with appropriate algorithms during reconstruction. However, this smoothing algorithm reduces image noise in exchange for image resolution; hence, the appropriate amount of smoothing is necessary.

In addition, the quality of segmented images by global thresholding may be impeded by the partial volume effect. The partial volume effect is defined as the loss of intensity or grayscale of regions due to the resolution of the imaging system. In CBCT and μ CT images, this could refer to a voxel that contains both mineralised and non-mineralised tissues, which will have lower mean grayscale than an image with mineralised tissue only but will have higher grayscale than non-mineralised tissue sites. This lowered grayscale will produce a ‘smear-out’ appearance around the true boundary of mineralised tissue in the reconstructed image. Trabecular bone that is particularly thin will be more prone to this smear-out effect and does not reach grayscale that would represent its apparent density. This partial volume effect will cause the optimal threshold for one area to be different from the optimal value in other parts; hence, the global threshold in general will result in undersize in thin trabeculae and oversize of thick trabeculae.

1.14 Histomorphometry

Histomorphometry is defined as the quantitative study of the microscopic organization and structure of a tissue (e.g., bone) especially by computer-assisted analysis of images formed by a microscope (Van Oosterwyck et al., 2000). The preparation of a specimen for histomorphometric analysis requires sectioning of a specimen, which is irreversible and destructive (Van Oosterwyck et al., 2000). In clinical practice, histology is not a practical method to assess bone. However, some previous studies obtained a bone biopsy from implant osteotomy site for histological analysis (Cordaro et al., 2008; Zijderveld et al., 2004), which allows the analysis of bone microarchitecture. For grafted sinus, this bone biopsy method provides information on the quantity of newly formed bone along with the amount of residual graft following a healing period. Because of the destructive nature of this procedure, many previous studies only obtained bone biopsy during implant placement, which means histological analysis of bone cannot be performed prior to implant placement. Alternatively, in vitro animal studies allow histomorphometric analysis of the whole grafted area. However, this only allows clinicians to ascertain how well each different graft material resorbs and is replaced by new bone within a given animal, and there are always limitations on extrapolating these findings to clinical trials in humans.

1.14.1 Specimen embedding techniques

Depending on the type of analysis, there are many histological methods available, each having advantages and disadvantages. The well-known techniques that are frequently used are frozen/cryo-embedding, paraffin embedding, and plastic embedding.

The gold standard for experimental verification of sinus graft healing is the analysis of resin-embedded, undemineralised sections using histomorphometry to determine the amount of mineralised trabecular structures, bone vitality (expressed by number of osteocytes with recognisable nuclei), and the number of osteoblasts and blood vessels in the stroma (Dalle Carbonare et al., 2005).

1.14.1.1 Cryo-embedding

The cryo-embedding method involves an immediate freeze of tissue, which preserves almost the near-natural state of cellular and protein integrity. This makes the tissue sensitive enough for protein detection by immunohistochemistry. However, due to its freezing process, severe distortion of the tissue morphology occurs, making the method undesirable for morphometric assessments. The freezing of the biopsy sample does not require fixation prior to embedding, so the sections can be quickly prepared (Hernandez-Verdun et al., 1991)

1.14.1.2 Paraffin embedding

Paraffin embedding requires fixation prior to the embedding procedure, and more processing time and steps are required. However, the tissue morphology is better preserved than with cryo-embedding (Sullivan-Brown et al., 2011). Paraffin embedding can produce sections that maintain proteins, DNA, and RNA, making it ideal for immunohistochemistry (Wright and Manos, 1990). While embedding and sectioning in paraffin provide reasonably good results, the artifacts produced in wax can limit any improvement in cellular resolution that thinner sectioning would provide.

When paraffin embedding is used for assessment of hard tissue such as bone or teeth, decalcification must be performed to remove calcium ions from these hard tissues. Calcium is stored in a form of hydroxyapatite in both bone and bone substitute materials. The removal of calcium by decalcification makes the bone flexible for cutting and pathological investigation for paraffin embedded tissues. This process of decalcification takes time, as bone specimens have to be left in decalcifying agents for several days or weeks prior to paraffin embedding. Depending on the type of decalcifying agents and their concentration, bone tissue deterioration also may occur. In the worst case, hard tissue such as tooth enamel may be completely eliminated, making it unsuitable for hard tissue assessment.

1.14.1.3 Resin embedding

The main advantage of embedding in plastic resins is the ability to produce ultra-thin sections for mineralised bone specimens. The resin embedding method is not always accompanied by the decalcification (demineralisation) process, and hence hard tissue integrity can be maintained. Many of the current studies handling hard tissues, such as bone and teeth, use the resin-embedding method, where specimens can be sectioned using a high-speed saw.

The advantage of this method is to be able to differentiate unmineralised osteoid and trabecular bone structures. It also provides ease of storage and superior preservation of cytological detail. However, resin embedding also carries disadvantages. One of the main disadvantages of resin embedding is the loss of sections of the specimens due to the thickness of the cutting blade. Although the use of the automatic microtome with special tungsten carbide blade may preserve the entire volume of the specimens during section (Uchiyama et al., 1997a), the use of a cutting wheel for resin embedding specimens is common.

Even with the same MMA embedding procedure, different amounts of shrinkage may occur depending on the method of cutting: microtome or cutting wheel. In a study by Uchiyama et al. (1997a), the shrinkage of MMA embedded tissue before and after cutting with a microtome was examined. Up to 17% of specimen shrinkage occurred on the side of the tissue surface perpendicular to the microtome knife whereas the width of the tissue parallel to the side of the knife during cutting remained intact.

This research required an embedding technique that allows the preservation of the morphology of bone structure for quantitative bone histomorphometry as the study focused on looking at residual graft and new bone within the grafted sinus. Resin embedding of undecalcified bone specimens suits best for this purpose (Erben, 1997; Mawhinney and Ellis, 1983; Wolf et al., 1992) and reportedly was used in various bone research, including studies of bone metabolic disorders (Chappard et al., 2005; Mawhinney and Ellis, 1983; Thomsen et al., 2005) and bone remodelling (Löe, 1959).

A tetrachrome solution is useful in staining bone biopsy. It is primarily for use as an aid in the diagnosis of metabolic bone disease. The stain demonstrates and differentiates several types of lamellar osteons, cellular features, and complex structures of the zone of demarcation of osteoid seams initially described by Löe (1959).

1.14.2 *Limitation of histomorphometry with stereological analysis*

In histomorphometry, trabecular number (Tb.N), trabecular thickness (Tb.Th), and trabecular separation (Tb.Sp) are parameters that are indirectly measured based on assumption that trabecular structure is a fixed-structure model such as a rod-like or plate-like structure. However, the distribution of trabecular bone is heterogenous; its architecture is a mixture of both rods and plates. Therefore, these parameters measured based on the assumption will carry a degree of errors which will be different from measurements obtained directly from 3D μ CT (Bouxsein et al., 2010).

1.15 Morphometric analysis of grafted sinus with CBCT, μ CT and histomorphometry

Morphometric analysis of grafted maxillary sinus using CBCT does not appear to have been performed. There are a limited number of studies that performed morphometric analysis of grafted maxillary sinus using μ CT (Kühl et al., 2010; Trisi et al., 2006). Kühl et al. (2010) carried out μ CT analysis of bone biopsy of grafted sinus to assess the amount of residual graft and new bone. The biopsy was obtained from five patients who received different mixtures of autogenous bone and bone substitute with different healing periods. The results demonstrated good separation and segmentation of bone and residual graft by thresholding method, indicating μ CT can be a reliable radiographic tool for analysis of bone remodelling within grafted sinus. However, the finding of this study was limited by the lack of control (e.g., histology) to validate the accuracy of the μ CT measurements.

Similarly, Trisi et al. (2006) carried out in vitro examination of biopsy of grafted sinus using μ CT and histomorphometry. Three sinuses, grafted with a mixture of autogenous bone and bone substitute (Biogran[®]), were biopsied after 5, 6 and 15 months. The samples were analysed by μ CT and histomorphometry to determine total volume/total bone volume (TV/TBV4, which represents the total volume of bone plus residual graft in the matrix), bone volume/total volume (BV/TV, which represents the total volume of bone in the matrix), and graft volume/total volume (GV/TV, which represents the total volume of graft in the matrix). μ CT measurements were calculated from 400 reconstructed sections, while histomorphometry was performed from three sections per sample. The results showed that the volume of the bone + graft (total mineralized tissue) measured by μ CT and histomorphometry were similar.

1.16 Animal models

For animal research concerning testing of novel surgical techniques or materials (e.g., osteogenic potential of graft material), selection of an animal that has similar anatomical, physiological and biological features to humans is crucial. The findings of the animal research should be extrapolated to clinical studies.

However, in research comparing different techniques for morphometric analysis of a tissue, the animal choice may be of a little significance. The animal selection should be related to the tissue that is going to be assessed by the different techniques. The objective of this study was to determine how effective CBCT is to measure the healing of grafted maxillary sinus by comparing CBCT with μ CT and histomorphometry. Previously, studies assessing the healing of grafted sinus using histomorphometry or μ CT utilised human bone biopsy taken from the grafted sinus using a trephine bur (Kühl et al., 2010; Trisi et al., 2006). Although the utility of human biopsies is justifiable, the technique is invasive and the number of samples to harvest can be limited. Also, the size of the sample will be restricted to only a portion of the entire grafted sinus. For these reasons, utilising an animal model appears more practical to compare different techniques for bone morphometric analysis.

This study utilised samples of grafted sheep sinuses from another animal study where they assess the healing of different sources of graft material placed in maxillary sinus in a sheep model (Unpublished data).

As for maxillary sinus elevation, larger animals generally appear to be more desirable on the basis of their similar anatomical size to humans. Apart from the non-human primates, sheep demonstrates a similar anatomy and histology of the sinus to the human sinus. In addition, surgical access is simpler compared to other animals, such as mini-pigs or dogs (Haas et al., 1998). The sheep is a widely available animal in New Zealand as homogenous flocks, and there is also a growing body of research reporting on the use of sheep as an animal model in dental implant research (Duncan et al., 2008; Smith, 2011).

1.16.1 *Sheep*

Sheep show more promise as animal models, as they have a similar body-to-weight ratio as humans and are more socially accepted as a commercially utilised animal (Pearce et al., 2007). As such, the use of sheep models in orthopaedic research is increasing (Martini et al., 2001). However, on the histological level, sheep have a different bone composition than humans. Sheep bone is predominantly comprised of primary bone structures, where the osteons are less than 100 μm in diameter and contain at least two central blood vessels and the absence of cemental lines. In comparison, human bone is mainly composed of secondary structures (Pearce et al., 2007). Sheep bone shows higher density and, thus, greater strength. The apparent density of sheep trabecular bone from the proximal tibia was 0.61g/cm³, with an apparent ash density of 0.41g/cm³ (Nafei et al., 2000). This is higher than the reported bone density of the human femoral trabecular bone, which has an apparent density of 0.43g/cm³ and 0.26g/cm³, respectively. However, the bone density may vary depending on location and age. Sheep and humans have similar patterns of bone remodelling and turnover (Pearce et al., 2007; Willie et al., 2004). A histological study of bone healing around porous implants placed in the distal femur under load showed humans and sheep have similar patterns and rate of bony in-growth over time (Willie et al., 2004). Estaca et al. (2008) found sheep are an ideal model for sinus floor elevation. They compared sheep, goats, and pigs to identify which animal is the most ideal to simulate the sinus elevation procedure in humans. The results showed that sheep and goats had thin cortical bones and enough consistency of the sinus membrane that is similar to that in humans. Also, sheep have a similar topography of the sinus to humans. However, the floor of the sinus in these animals is located distantly from the buccal vestibule. The intraoral approach would involve a wide opening of the vestibule caudally and dorsally. This can pose a problem for the animals when eating, drinking, and chewing. Therefore, the intraoral approach for sinus floor elevation is avoided in these animals for their survival and general wellbeing during the postoperative period (Valbonetti et al., 2015). The extraoral approach is a more generally accepted protocol for sinus floor elevation in sheep (Alayan et al., 2015; Duncan, 2005; Haas et al., 2008).

1.16.1.1 The anatomy of sheep sinus

The anatomy of sheep sinus was described (Estaca et al., 2008; Masoudifard et al., 2008; Valbonetti et al., 2015), using both three-dimensional radiography and histology. The sheep sinus is located between the maxilla, the zygomatic bone, and the lacrimal bone. It extends anteroposteriorly from the third premolar tooth to a position past the third molar tooth. The maxillary sinus communicates with the palatine sinus through a wide opening, dorsal to the infraorbital canal (Valbonetti et al., 2015). These two sinuses also communicate directly with the nasal cavity through the nasomaxillary aperture (Schummer et al., 1979). The sheep sinus consists of a small mediodorsal part and a large ventrolateral part, partially separated by the infraorbital canal. The dorsal part is small and extends to the rostral end of the sinus. Caudally, the sinus increases in size and is connected to the palatinus, placed on the medial side of the infraorbital canal. The ventral part extends from the orbit to the facial tuber. Rostrally, it extends to a point midway between the facial tuber and the infraorbital foramen (Estaca et al., 2008). Compared with the human maxillary sinus, the sheep sinus is narrower and more elongated. Although the calculated volume of the sinuses is quite similar in both species, the vertical height is narrower, and the anteroposterior length is wider in sheep compared to humans (Valbonetti et al., 2015).

1.16.1.2 Histology of Sheep Sinus Membrane

A histological assessment of maxillary sheep sinus demonstrated that the epithelial layer is made up of pseudostratified columnar ciliated epithelial cells and scattered goblet cells facing towards the sinus cavity. Lamina propria is divided into two sub-layers: a vascular layer of loose connective tissue containing a blood vessel network situated immediately underneath the epithelial mucosa and a deep layer of dense connective tissue containing the mucosal glands. The lamina propria acts as the periosteum-like connective tissue adjacent to the bone of the maxillary sinus, and it lacks any evidence of bone foci. The thickness of the sinus membrane varies in sheep, with the average thickness being $0.850 \pm 0.52\text{mm}$ (Valbonetti et al., 2015).

1.16.1.3 Remodelling Pattern of Bone/Bone Substitute Placed in Sheep Maxillary Sinus

The remodelling of bone grafts placed in sheep maxillary sinuses has been histologically examined (Alayan et al., 2015; Duncan, 2005; Haas et al., 1998). Variations in the pattern of remodelling have been observed depending on the type of graft material placed and the healing period. Alayan et al. (2015) examined remodelling of two different types of graft material including a mixture of iliac graft and Bio-Oss® (50:50 ratio) and Bioactive glass at 8, 12 and 16 weeks following sinus floor elevation. Histological analysis showed the amount of new bone formation is proportional to the length of the healing period. The in-growth pattern of new bone was examined. New bone was migrated from bony walls of sinus including lateral, medial and floor of the sinus; however, no bone in-growth was observed near the elevated Schneiderian membrane. The authors concluded the sinus membrane lacks osteogenic potential, and new bone is mainly originated from bony walls of the sinus. This finding is in agreement with the findings of Haas et al. (1998), where new bone formation observed from the buccal wall of the sinus too. Interestingly, it has been demonstrated the Schneiderian membrane in human subjects has osteogenic potential that can play the important role in the augmentation procedure (Srouji et al., 2009).

1.17 Aim

To determine the efficacy of CBCT for quantification of newly-formed bone within grafted maxillary sinus

1.18 Objectives

To perform morphometric analysis of grafted sheep maxillary sinus using CBCT and compare the results against two reference techniques of histology and μ CT. Parameters including % new bone, % residual graft, % mineralised tissue will be assessed to compare the results between the techniques.

1.19 Hypothesis

CBCT can accurately quantify newly-formed bone and residual graft in grafted maxillary sinus.

Chapter 2 Materials and methods

The specimens for this study came from another large study investigating healing of different grafting materials in sheep sinus. Ten, healthy, two-year-old ewes received lateral sinus elevation on one side of the sinuses (random allocation) using xenograft material, Endobon® (Biomet 3i, USA). Two animals were killed immediately after the surgery (baseline, zero-week healing group) whereas the remaining eight animals were euthanized after 16 weeks (16-week healing group). Following euthanasia, the maxilla was harvested from each animal and stored separately in plastic containers containing 20% ethanol. A specimen code was written with a black permanent marker pen on each plastic container. The details on ethical approval and how the sheep sinus surgery was performed are described in Appendix I.

2.1 CBCT / μ CT scan and histological preparation

2.1.1 *CBCT scan*

The maxillary blocks were scanned with a cone-beam computed tomography (CBCT) (Galileos X-ray system, Sirona Dental, USA). The specimens stored in 20% ethanol were taken out and placed on a flat plastic specimen platform (Figure 2.1). Each specimen was scanned individually using the Galileos preset settings for “child”. The parameters for this were: Radiation Time 2000ms, Tube current 5mA, Tube voltage 85kV, full field of view (FOV). After the scan, the specimens were placed back into their plastic containers in 20% ethanol. Each scan produced a dataset size of 1024 x 1024 x 16 bit, stored as a DICOM file. The raw CBCT volume was viewed in the Galaxis CBCT imaging software that comes with the Galileos CBCT machine (Sirona, USA) (Figure 2.2)

2.1.2 *μ CT scan*

Following the CBCT scan, the specimens were scanned using a desktop micro-computed tomography (μ CT) machine (Skyscan 1172 X-ray Micro tomograph, Antwerp, Belgium). To start with, the specimens were cut into a smaller volume ($< 5\text{cm}^3$) to fit within the μ CT scanning platform. External soft and hard tissues including teeth were removed to generate specimens

consisting of the grafted sinus with surrounding bony walls. A 4-0 silk suture (Black braided silk, reverse cutting, Ethicon[®]) (Figure 2.3) was placed on the lower front side (i.e. anteroventral) of the antral wall to keep a record of its anatomical orientation (Figure 2.4).

Each specimen was wrapped in a clear glad wrap to minimise dehydration during scanning and placed on the μ CT stage using plasticine (Figure 2.5). A preview image was displayed on a computer screen using the connected PC-based Skyscan software. The platform was adjusted until the entire specimen was within the field of view. A double layer scan was performed for specimens that were higher than 50mm in height. All specimens were scanned using the following settings which were determined by a previous experiment work of using this machine (Park et al., 2010):

Table 2.1 Micro-CT settings for all specimens.

Parameter	Setting
Voltage	80 kV
Current	125 μ A
Filters	Al 0.5mm
Exposure	1180ms
Camera Pixel Size	11.57 μ m
Frame averaging	Level 4
Geometrical correction	On
Flat field correction	On
Ring artefact correction	10
Random movements	Level 20
Median filtering	On
Smoothing	None
Beam hardening correction	50 %
Rotation	180°
Rotation step	0.4°
Image pixel size	17.35 μ m

The scanning of each specimen took approximately three hours. The raw data was saved in tiff format on a dedicated personal computer (PC) that is hardwired to the Skyscan 1172.

The Skyscan NRecon software was used to reconstruct the raw μ CT data into a stack of cross-sectional (transverse) slices. The Skyscan NRecon program utilised the Feldkamp algorithm to reconstruct the raw data into a series of 2000 x 2000 pixel image slices in tiff format, parallel to the direction of μ CT x-ray beam. At the completion of the scan, the specimens were stored back in their plastic container with 20% ethanol.



Figure 2.1 Maxilla blocks (Left and right) on a plastic platform in Galileos CBCT (Sirona Dental, USA).

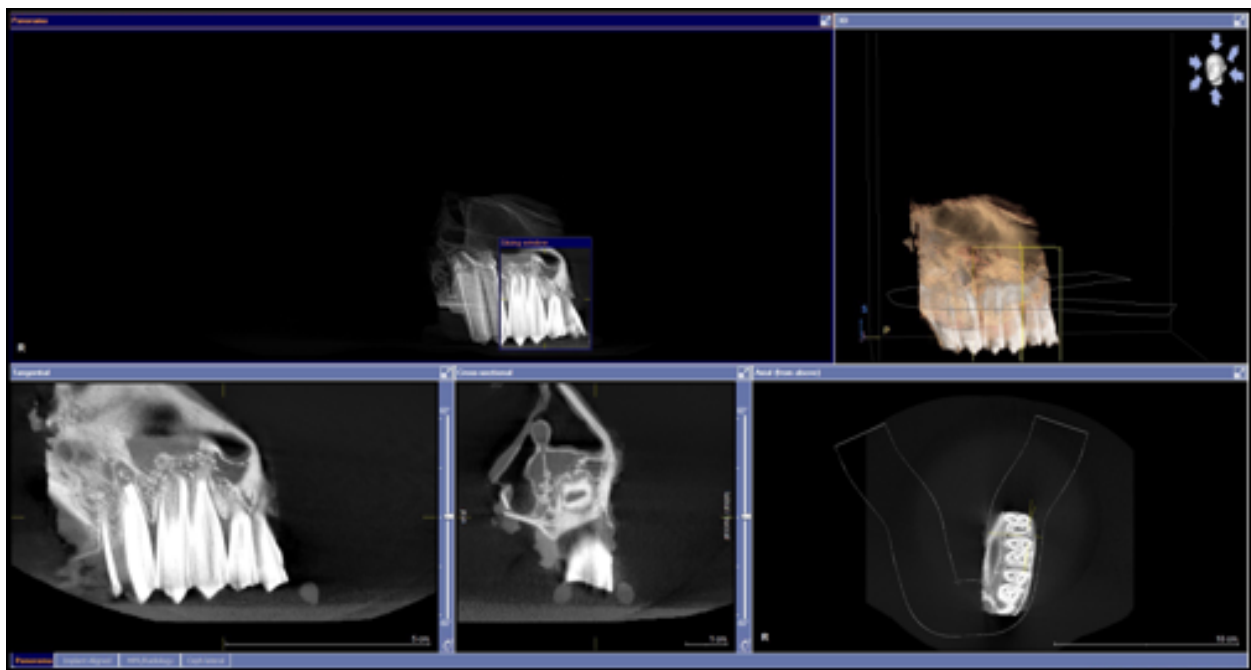


Figure 2.2 CBCT images of scanned maxilla in different viewing planes in Galaxis CBCT imaging software.



Figure 2.3 4-0 Silk suture (Black braided silk, reverse cutting, Ethicon®).



Figure 2.4 Trimmed specimen with a silk suture placed indicating the anteroventral position on the antral sinus wall ($> 5\text{cm}^3$).



Figure 2.5 The specimens wrapped in clear glad wrap positioned on μCT machine platform.

2.1.3 Histological preparations

2.1.3.1 Resin-embedding protocol

Following CBCT and μ CT scan, the specimens were resin-embedded using the protocol described by Duncan (2005), which is summarised in Appendix III. Mixtures of methyl methacrylate (MMA) (Sigma-Aldrich, USA), MMA I, MMA II, and MMA III were made according to the above protocol.

The silk suture on the antral wall of the specimens were removed and replaced with an amalgam restoration (Figure 2.6) to help identifying specimen orientation with radiographs later on. A small cavity was made where the suture was using a slow speed dental handpiece with a #5 round bur (1.60mm in diameter) and was filled with dental amalgam.

The specimens were dehydrated in increasing concentrations of ethanol solutions: 20% ethanol (2 days), 40% ethanol (2 days), 70% ethanol (2 days), 95% ethanol (2 days), 100% ethanol (repeated twice within a day). Dehydrated specimens were transferred to xylene (Ajax Finechem Pty Ltd, New Zealand) for four days, with two changes of xylene during this time period, on a rotating platform in a fume hood. The specimens were washed with methyl methacrylate (MMA) monomer and placed in MMA I and MMA II for two days each.

Each dehydrated specimen was placed into a glass jar that had a pre-set base of MMA III (Figure 2.7). The glass jars were prepared one week prior to the time required, by filling with MMA III to a one-third depth of approximately 8mm. Once the specimens were transferred, the remaining space within the jar was filled with MMA III to immerse the specimens in MMA III and sealed with a screw top metal lid and allowed to set in the dark surrounded by water to dissipate heat and hasten polymerisation (Bell, 1939). Following the polymerisation, the embedded specimens were retrieved by breaking the glass jars. Excess resin was trimmed off, and the surfaces of the specimens were polished with Tegra-Pol polishing machine (Struers, Ballerup, Denmark) (Figure 2.12), that was fitted with a silicon carbide paper grade #1000 (Struers, Ballerup, Denmark).

The embedded specimens (Figure 2.8) were radiographed to identify the location of the grafted sinus (Figure 2.9). The specimens were laid with the antral wall facing upwards on a Kodak X-omatic® cassette fitted with a Lanex® fine screen intensifier and filled with Kodak T-mat G/RA film. The cassette was positioned beneath a Rotanode™ (Toshiba, Japan) tube-head attached to a Schonander (Stockholm, Sweden) Skull Unit radiography machine. The film was exposed for 0.08 seconds at 50mA / 50kVp and processed in an automatic processing machine. Once radiographed, the location of the sinus was drawn with a black permanent marker on the embedded specimens.

2.1.3.2 Cutting of the resin-embedded specimens

In order to produce histological sections that matches closely to 2-D µCT digital sections, an attempt to cut the resin-embedded specimens at parallel to µCT cross-sectional images was made. The 3-D µCT data was assessed in Image J software (the National Institute of Health, USA). Identifiable anatomical landmarks in µCT and the resin blocks were compared and the direction of the cut was outlined on the embedded specimens with a permanent marker pen (Figure 2.8). This manual approach did not result in the accurate match of the plane between µCT and histological sections; however, it allowed approximate match between the two techniques.

The blocks were sliced into a series of histological sections using the Struers Accustom-50 precision desktop cut-off machine fitted with a diamond cutting wheel (MOD 13 127 x 0.4 x 12.7mm) (Struers, GmbH, Switzerland). The specimens were clamped onto the metal platform. The wheel was set parallel to the pen-marked line (Figure 2.10) and was positioned to initiate at two millimetres (mm) outside the one-end of the grafted sinus and continued to make cuts until the other end of the grafted sinus was reached. The following settings were used: Cut interval 450µm, Rotation off, H2O on, 3200 RPM, F value: High, 0.070mm/s.

During the cut, the blade travelled on the y-axis through the specimens whereas between each cut, the specimen moved on the x-axis by 450µm. This process produced twelve to fourteen

sections per specimen depending on the size of the grafted sinus, with a section interval of 850 μ m (450 μ m of set interval plus 400 μ m of the thickness of the wheel blade).

The sections were glued with superglue (Cyanoacrylate) on an opaque, square plastic slide. A custom-made hand press was used to press the sections on the plastic slide for 60 seconds until the cyanoacrylate glue was set (Figure 2.11). The slide number was engraved on the reverse side of the slide using a slow-speed dental drill with a round bur. The number consisted of the specimen code and a prefix number. The prefix numbers started at “1” and proceeded in increments of 1 (so that 1 indicated the first histological slide, and so on). All histological slides were then manually polished down to a final thickness of approximately 100 μ m using a TegraPol machine (Struers, Ballerup, Denmark) (Figure 2.12), fitted with silicon carbide sandpapers of different grit grades. The machine was set to 120 RPM with ongoing water irrigation. A gentle finger pressure was applied to push the slides against the sandpaper. The slides were initially trimmed with #300 and #500 grit paper until the thickness became approximately 100 μ m which was confirmed with a digital micrometre. Once 100 μ m was reached, #1200, #2400, and #4000 grit papers were used to polish the slide (figure 2.13). Six consecutive serial slides per animal, near the midpoint of the grafted site, were selected and used for subsequent staining and analysis.

2.1.3.3 Staining of the histological slides

The slides were etched and decalcified by immersing in 40% ethanol, followed by 1% formic acid in an ultrasonic bath, and then was stained with MacNeal’s tetrachrome (methylene blue, azur II, and methyl violet). The staining protocol is attached in Appendix III.

2.1.3.4 Digitisation of the histological slides

The histological slides were digitised via a light microscope (Olympus AX70, Olympus Optical Co. Ltd, Japan) connected to a computer imaging system (Micropublisher 5.0 RTV, Qimaging) at 4x magnification. Using an imaging software Volocity 5.2.0 (Improvision, MA, USA), a series of point images were captured from a single histological slide. An overlay

covering the histological section was made. Points were created within the overlay where a series of images are captured. The resultant set of digital images were then exported in TIFF format and imported into Autopano Pro 2.5.2 (Kolor, USA), where they were digitally combined together (i.e., montaged) to produce a continuous, large-scale digital histological image.

2.1.3.5 *Number of samples for statistical analysis*

A total of ten animals (including two animals at baseline and eight animals at 16 weeks of healing) were processed for μ CT, CBCT, and resin embedding for histology. Each animal produced ten to fourteen histological slides depending on the width of the grafted sinus. Six consecutive histological slides that were close to the midpoint of the grafted sinus were used for analysis.

Four animals (two at baseline and two from the 16-week healing group) were discarded, as there were voids in μ CT images due to procedural error. From the remaining six animals (all 16-week healing group) with a total of 36 histological slides, four histological slides were discarded, as there were streaks and voids in the sections due to excessive polishing. Finally, a total of 32 histological sections were analysed and compared with matched 2-D digital sections of CBCT, μ CT.



Figure 2.6 The silk suture was replaced with an amalgam restoration.



Figure 2.7 The specimen placed in a glass jar that has MMAIII pre-set base.



Figure 2.8 Resin-embedded specimen, black line indicating the cutting direction that corresponds to the transverse plane of reconstructed μ CT slices.

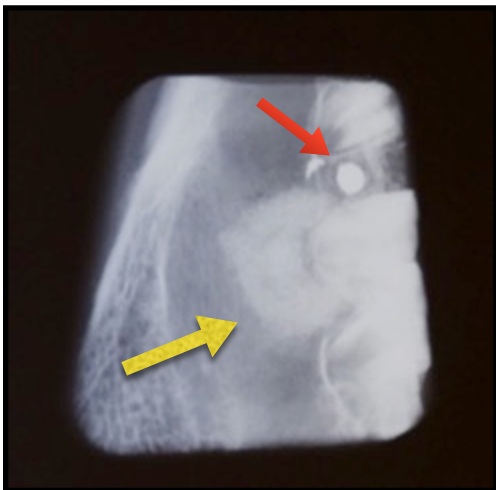


Figure 2.9 A radiographic scanned image of a resin-embedded specimen. Grafted sinus (Yellow arrow) and an amalgam marker are visible (Red arrow).



Figure 2.10 Struers Accustom-50 desktop cut-off machine. Specimen clamped on the platform and the wheel direction made parallel to the black line on the specimen block.



Figure 2.11 Histological sections were glued onto an acrylic plastic slide using superglue (Cyanoacrylate). A custom-made hand press was used to press the sections onto the plastic slide for 60 seconds while the glue is set.



Figure 2.12 Struers Tegra-Pol polishing machine with a speed adjustable turntable.



Figure 2.13 Polished histological slide.

2.2 Identifying 2-D virtual μ CT and CBCT images corresponding to the histological images

Using histological images as the reference, 2-D μ CT and CBCT images that closely correspond to the histological images were generated in each animal sample.

2.2.1 μ CT

Reconstructed cross-sectional sections of μ CT and a histological image of the same animal were opened in Image J (NIH, USA). With the histological image as a reference, a stack of transverse μ CT sections were scrolled up and down until an image that has the most similar appearance to the histological image was found. The topography of hard tissues such as the floor of the sinus, the antral wall, and the grafted sinus between two images were compared to help identifying most closely matched images (Figure 2.14).

2.2.2 CBCT

2-D CBCT images that match histological images were identified using a DICOM viewing software, Osirix (32-bit version, Pixmeo, Switzerland), which allowed the re-slicing of CBCT volume into a different orientation. Firstly, the CBCT raw data was exported from Galaxis (Sirona Dental, USA) in DICOM format with following settings: highly dynamic (16-bit), 0.1mm resolution voxel size. The exported data was opened in Osirix as a 3D volume. CBCT volume was reoriented in the x- and y-axes to match the plane to the histological images. Then, using a crop tool, the newly oriented volume was assessed on its z-axis (transverse plane) to identify a CBCT image that closely matched the histological image (Figure 2.15). The identified CBCT section was then exported with a thickness of 100 μ m to match to the thickness of the histological image. The exported data was in RGB format, as a result of this, the image resolution was affected. The software did not allow exporting data into raw images. Compared to the raw images in tiff format, the RGB images showed the reduction in grayscale ranges indicating the reduction in image resolution (Figure 2.16).

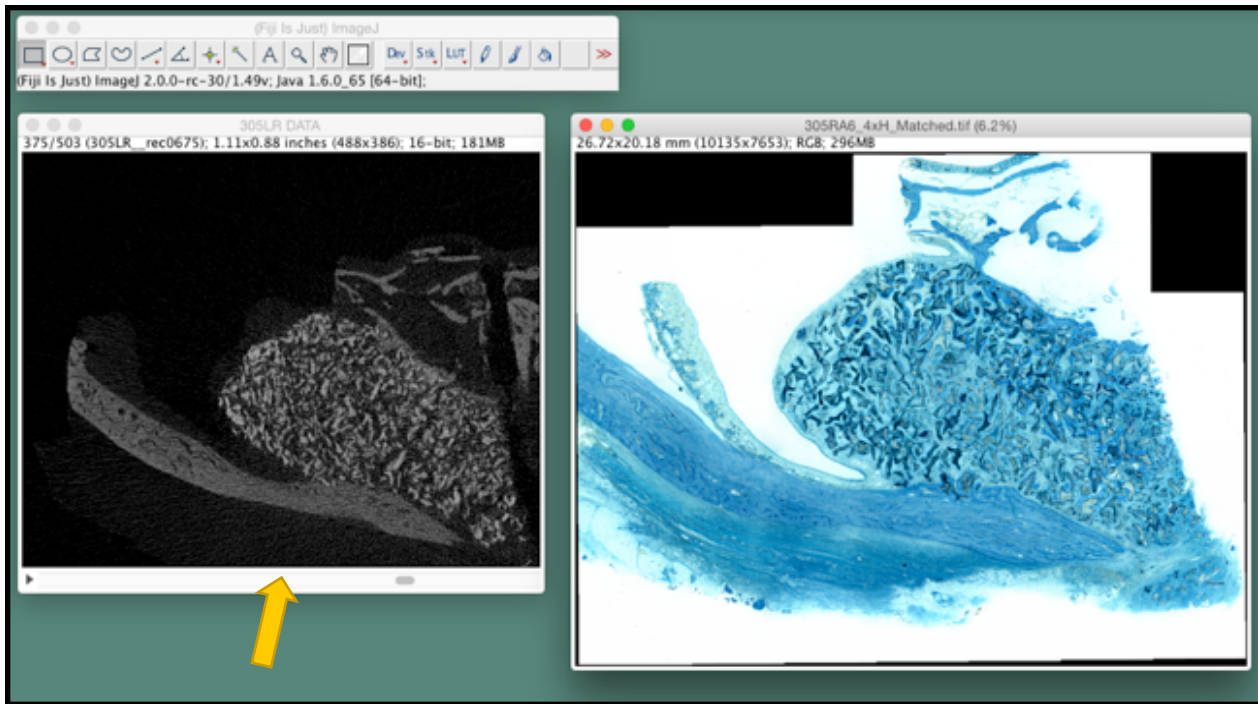


Figure 2.14 In Image J, a stack of cross-sectional slices of μ CT and a histological image of the same animal were opened. Using a horizontal scroll bar on the bottom of the window (yellow arrow), μ CT slices were scrolled up and down until a radiographic image that closely resembles with the histological image was found.

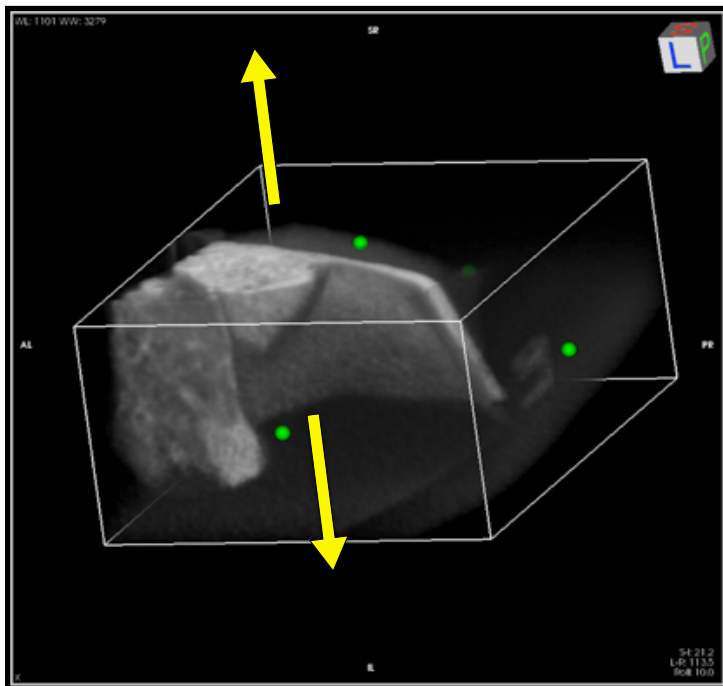


Figure 2.15 3D CBCT Volume opened in Osirix. Using the 3D analysis, the volume was reoriented to match the plane of histological sections and then cropped vertically until the image that matches with the histology was found on its z-axis (Yellow arrow).

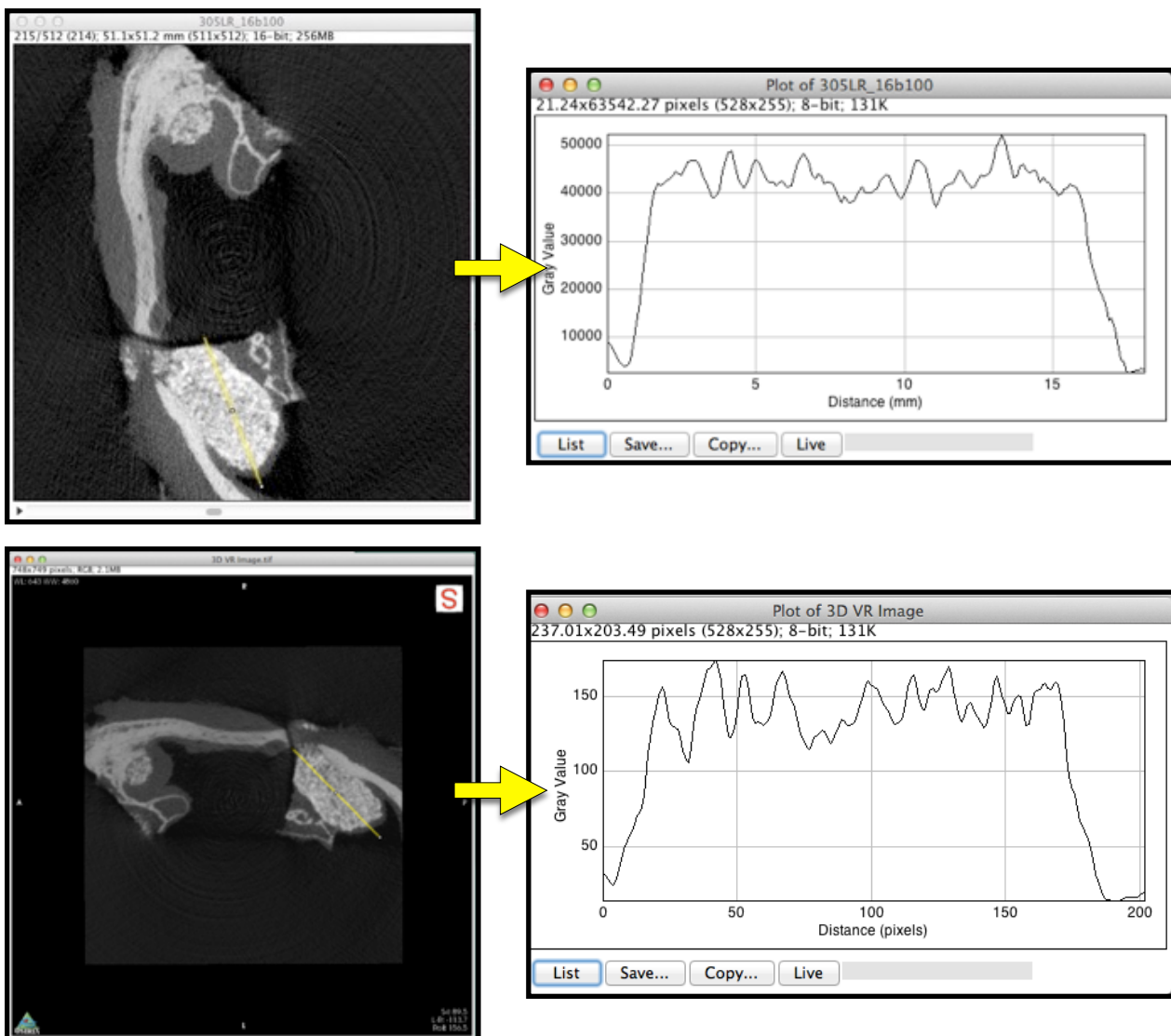


Figure 2.16 A raw 2-D CBCT image (top left) and an exported CBCT image from Osirix (bottom left) of the same specimen are shown. Comparing grayscale range demonstrated that two images have unequal grayscale range; the raw image shows gray value ranged between 10000~50000 whereas the modified image shows gray value ranged between 10-200. The changes in grayscale were due to the change in the format of image from 16-bit tiff file to RGB format that was inevitable as Osirix only allows exported dataset in RGB format.

2.3 Image size calibration and selection of region of interest (ROI)

The closely matched 2D images of CBCT, μ CT, and histology were analysed using Image J (Version 1.49, Wayne Rasband, National Institute of Health, USA). We performed radiomorphometric analysis in CBCT and μ CT images whereas histomorphometric analysis was performed for histological images. Parameters including the percentage area of residual graft (%RG), new bone (%NB) and mineralised tissue (residual graft + new bone, %MT) were assessed in each technique and compared.

2.3.1 Image size calibration

The matched images of CBCT, μ CT, and histology were firstly scaled to match their dimensions. The histological images were calibrated in millimetres (mm) by taking the actual dimensions (mm) of the histological slides. The dimensions of the CBCT and μ CT images were then adjusted according to the histological images. All three images were compared side-by-side to confirm their dimensions relative to each other (Figure 2.17). The dimensions of μ CT and CBCT were almost equal whereas the histological images showed slight difference in its dimensions compared to the radiographic images as the tissues were shrunk and distorted from the resin-embedding procedure (Figure 2.18).

2.3.2 Selection of a region of interest (ROI)

The grafted sinus was chosen as a region of interest (ROI). In histological images, a polygon selection tool was used to outline ROI. The same method was used to delineate ROI in μ CT images. The ROI in μ CT was then duplicated and applied to CBCT images to produce the same ROI. ROI between μ CT and CBCT showed a good agreement in outlining the grafted sinus (Figure 2.19).

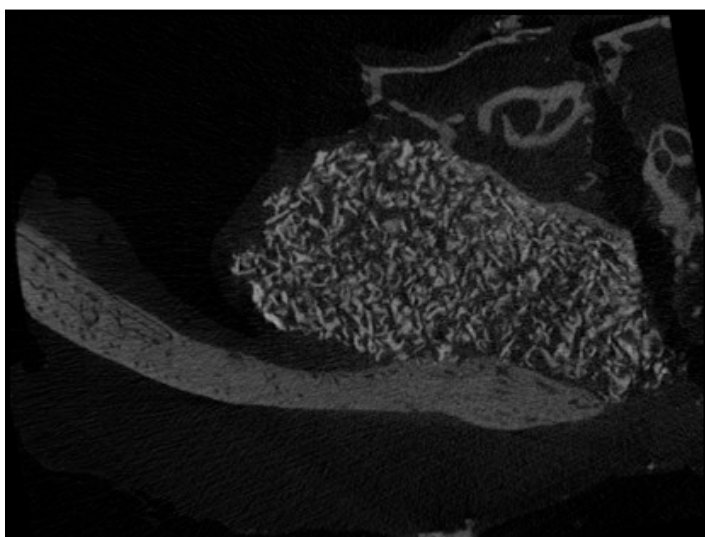
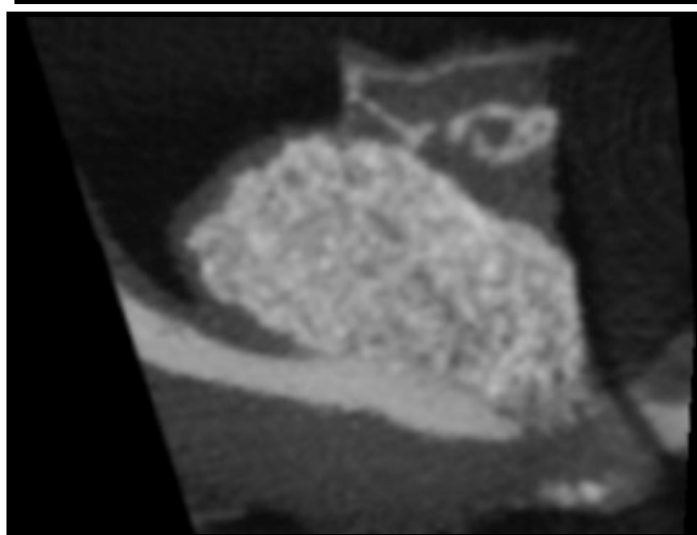
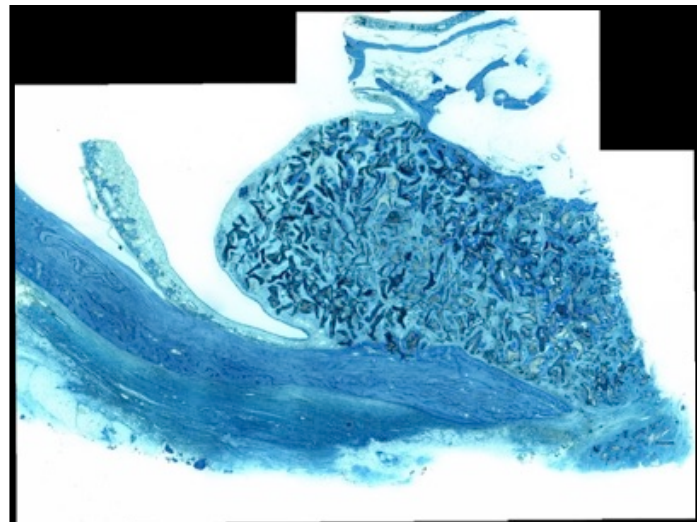


Figure 2.17 Matched section of histology (top), CBCT (middle) and μ CT (bottom). The images were scaled in millimetres (mm).

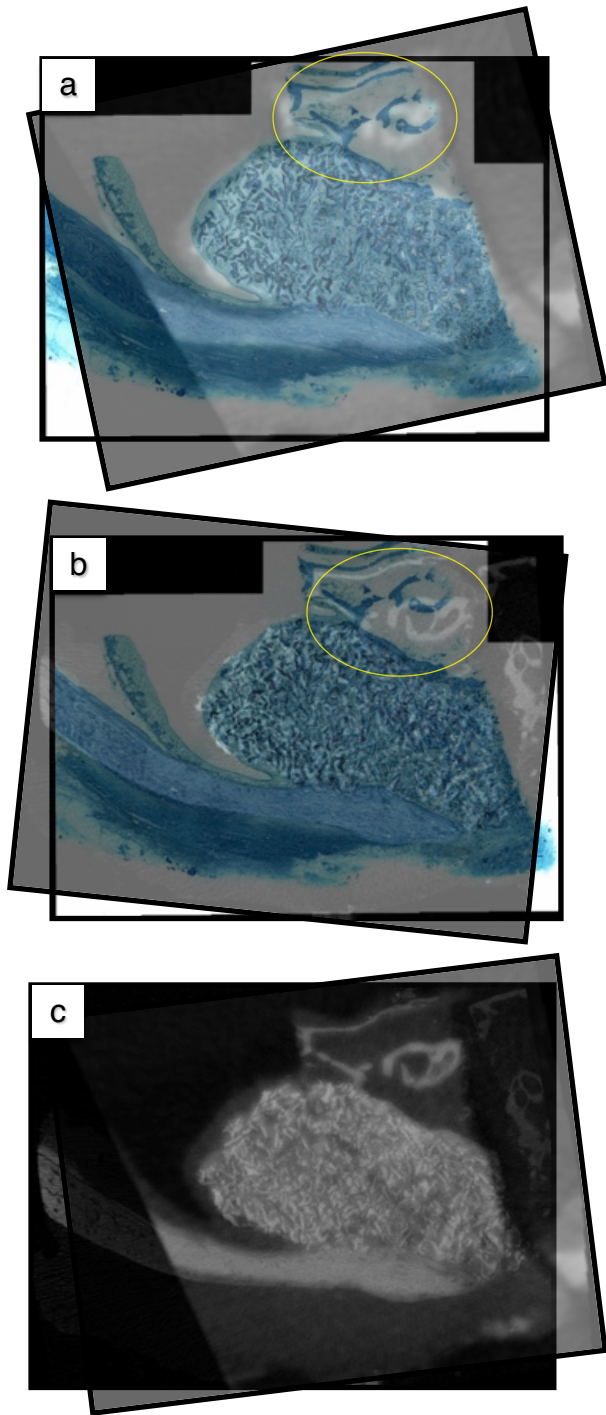


Figure 2.18 Matched, scaled images of histology, μ CT and CBCT were superimposed to check if they are the same size. Superimposition: (a) between histology and CBCT. Notice difference in scale near the floor of the sinus. (b) between histology and μ CT. Notice unequal scale of hard tissue of sinus floor between two images (c) between μ CT and CBCT showing a good match in the scale. Yellow delineation refers to an area where two images failed to correspond. This was mainly due to tissue shrinkage and distortion in histological images.

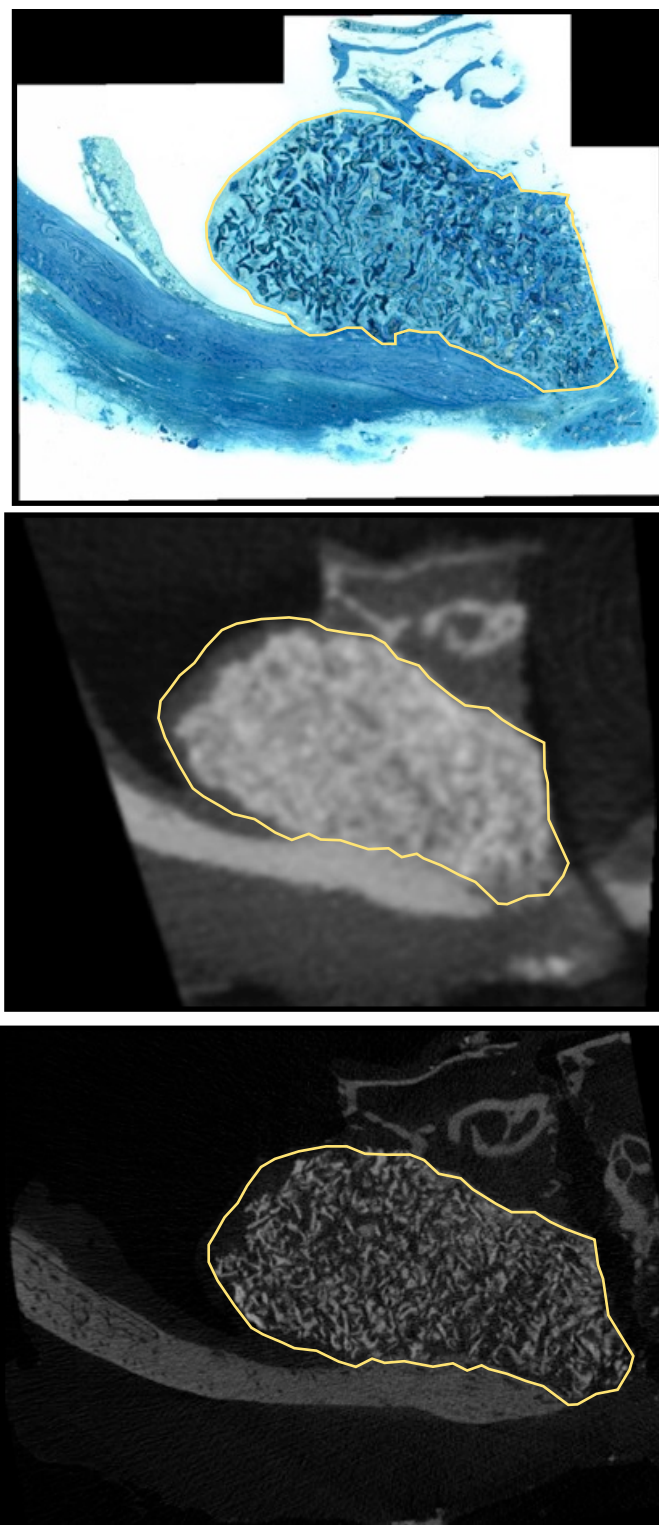


Figure 2.19 A region of interest (grafted sinus) drawn on images of histology (top), CBCT(middle) and μ CT (bottom) with yellow outline.

2.4 Image analysis

2.4.1 *Histomorphometric analysis*

Colour thresholding was carried out to identify area of residual graft (RG) and new bone (NB) within the region of interest (ROI) in the histological images. As different tissues were stained at different intensity, this allowed separation one tissue over another using colour thresholding technique (Figure 2.20). After thresholding, the segmented images were compared to the original image to ensure the segmented images were good representations of the actual tissue area (Bouxsein et al., 2010). Any area that was not segmented by the thresholds was manually added using the wand tool (Figure 2.21)

Following the thresholding, the percentage of RG and NB within ROI was measured (%RG and %NB); each tissue of RG and NB (mm^2) was divided by ROI (mm^2) and multiplied by 100 to generate the percentage value for each tissue (%). To calculate the percentage of mineralised tissue (%MT), %RG and %NB were added together.

2.4.2 *Radiomorphometric analysis*

Radiomorphometric analysis was performed in μCT and CBCT images. Firstly, grayscale was calibrated into known density using a set of hydroxyapatite discs as calibration standards. Calibrated images were then thresholded to segment RG and NB based on threshold obtained from radiographic standards. These process and steps will be described in detail in the following sections.

2.4.2.1 Preparation of calibration standards for grayscale calibration

μCT and CBCT produce radiographic images of grayscale. Calibration of grayscale into mineral density gHAp/cm^3 [the mass of hydroxyapatite (HAp) per unit volume] is required for quantitative analysis of bone tissue mineralisation (Zou et al., 2011; Bouxsein et al., 2010). We used radiographic standards created and used in a study by Schwass et al. (2009) to calibrate

grayscale in our μ CT and CBCT images. The standards consisted of three hydroxyapatite (HAp) discs with different known densities (low, medium, and high-density HAp) (Figure 2.22). Hydroxyapatite constitutes the main mineral component of bone and Endobon[®]. The details on how these discs were made and their density are described in Appendix IV.

2.4.2.1.1 Scan of the HAp discs with μ CT

The calibration standards (HAp discs) were scanned using the μ CT machine under the same setting used for the specimens. The discs were stacked vertically with an increasing order of HAp density. (Figure 2.23). The scanned raw image was reconstructed using Skyscan's NRecon software to produce a stack of cross-sectional images where each image slice consisted of 2000 x 2000 pixels with sixteen-bit grayscale.

The cross-sectional images were then opened in Image J to measure mean grayscale for each HAp disc. In image J, the images were opened as a stack. This allowed viewing the images in their cross-sections, which can then be scrolled up and down using a bar to view other images within the stack. A boundary of each disc was outlined using an oval tool as regions of interest (ROIs). This was performed on one image every 50~60 consecutive images. ROIs were then interpolated to produce a volume of interest (VOI). VOI representing each disc volume was determined, and the mean grayscale of each disc was calculated (Figure 2.24)

Acquired mean grayscales of the three HAp discs were then correlated with their total effective density. A scatter plot showed a linear relationship between the mean grayscale and the total density (Figure 2.25) (Huang et al., 2007; Zou et al., 2009). This scatter plot was applied to our μ CT images to convert grayscale into density (gHAp/cm^3).

2.4.2.1.2 Scan of the HAp discs with CBCT

The HAp discs were also scanned using CBCT in order to convert grayscale into mineral density in CBCT images. The stacked HAp discs were scanned in the CBCT under the same settings used for the specimens (Figure 2.23).

Following the scanning, the 3-D raw data of CBCT was exported from the Galaxis (Sirona Dental, USA) in DICOM format with following settings: highly dynamic (16bit), 0.1mm resolution voxel size. The exported stack of DICOM files were opened in the Osirix (32-bit version, Pixmeo, Switzerland). Excess radiographic voids were removed, and the remaining volume representing the discs was exported as RGB file.

The cross-sectional images were than opened in Image J to measure mean grayscale for each HAp disc. In image J, the images were opened as a stack. This allowed viewing the images in their cross-sections, which can then be scrolled up and down using a bar to view other images within the stack. A boundary of each disc was outlined using an oval tool as regions of interest (ROIs). This was performed on one image every 50~60 consecutive images. ROIs were then interpolated to produce a volume of interest (VOI). This VOI represents each disc volume, and the mean grayscale of each disc was calculated (Figure 2.26)

The acquired mean grayscale of the three HAp discs was then correlated with their total effective density. A scatter plot showed a linear relationship between the mean grayscale and the total density (Figure 2.27). This scatter plot was used to calibrate grayscale into mineral density in all CBCT images.

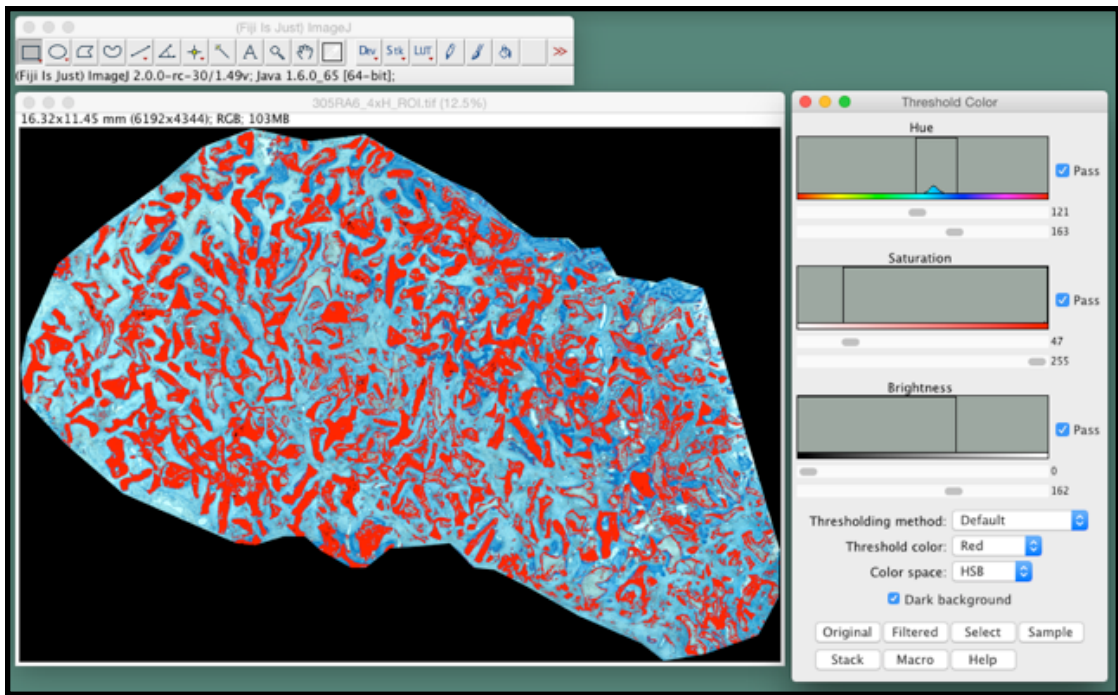


Figure 2.20 Colour thresholding of residual graft in a histological image. Hue, saturation and brightness bars in the threshold window were adjusted to select different tissues of interest (residual graft and new bone) within all histological images.

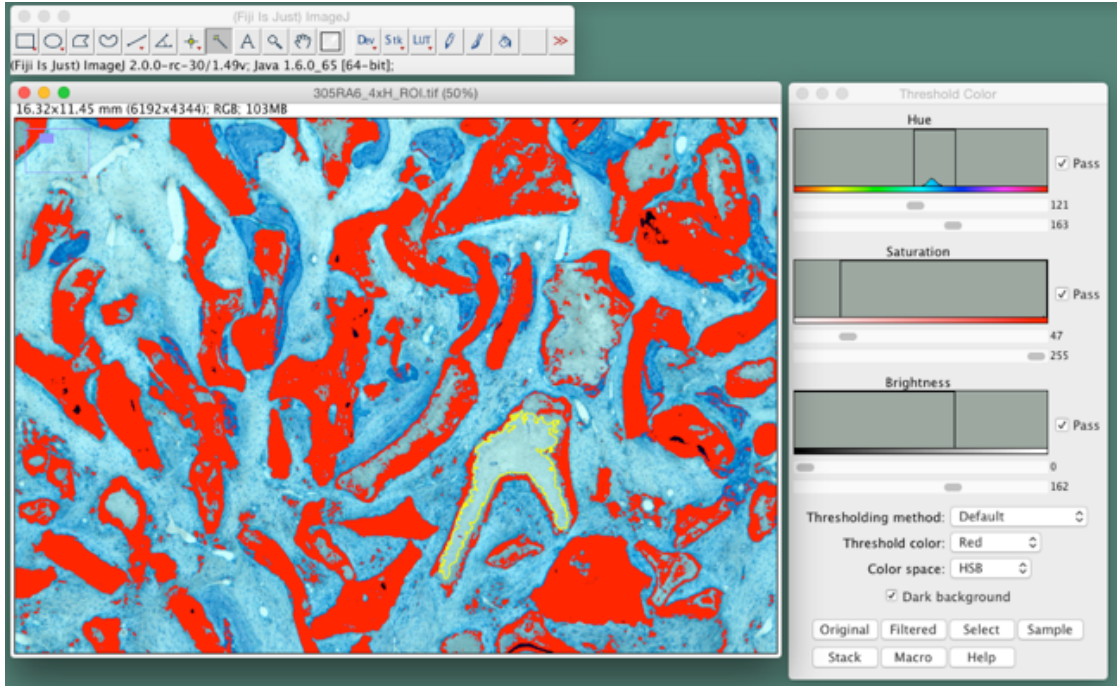


Figure 2.21 Any area that was not segmented using colour thresholding was manually selected using a wand (tracing) tool in Image J (shown in yellow outline).



Figure 2.22 3x Hydroxyapatite radiographic standards (courtesy of Dr Schwass).

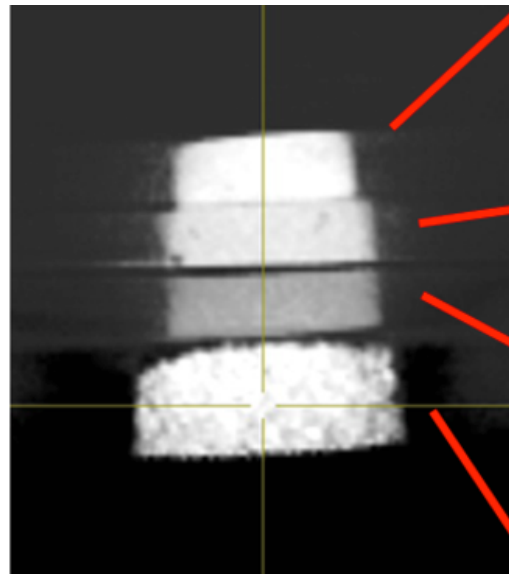
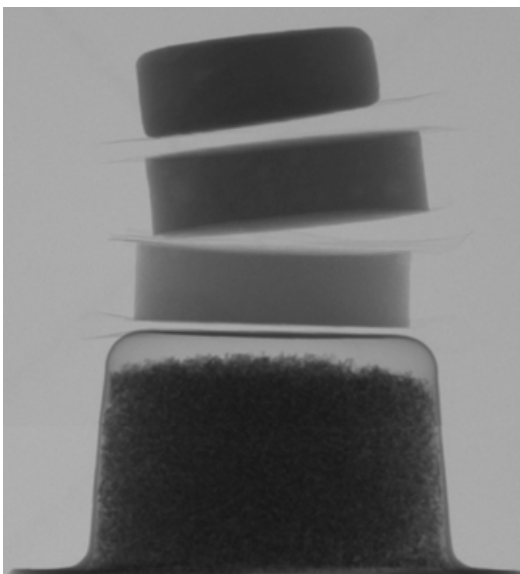


Figure 2.23 Radiographic standards of hydroxyapatite discs (x3) and an Endobon® sample mounted on platform (top), μ CT scan of the standards (bottom left), CBCT scan of the standards (bottom right).

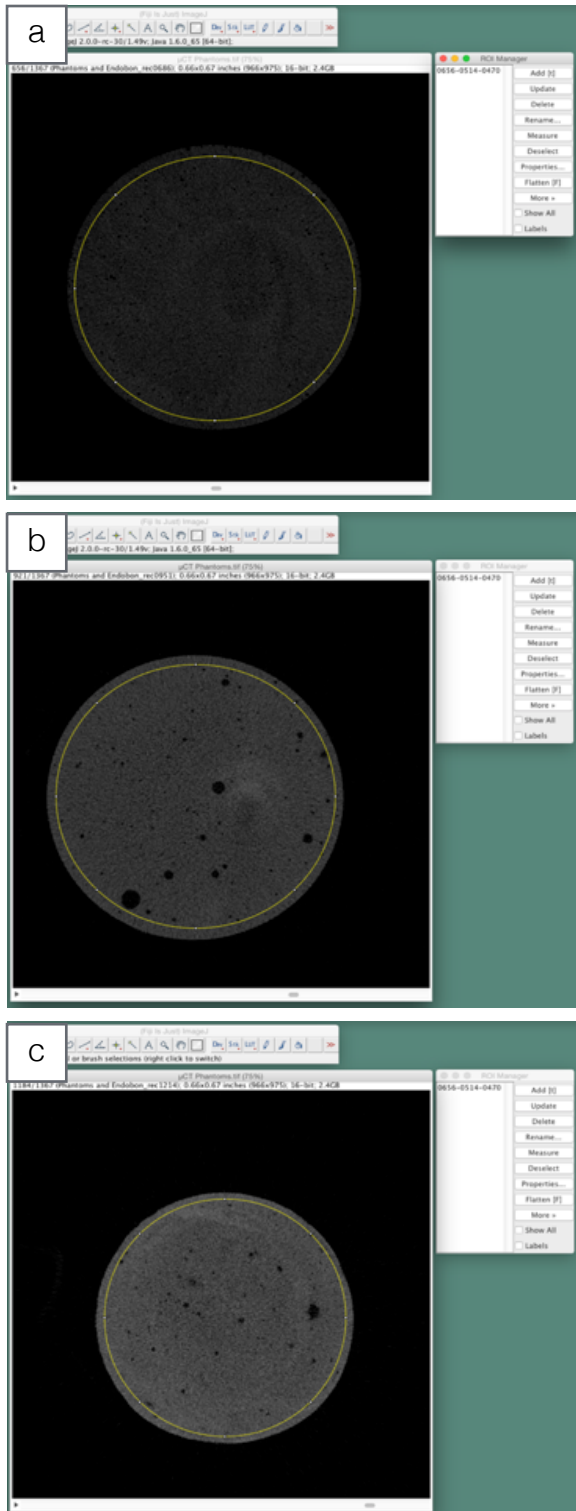


Figure 2.24 Cross sectional μ CT images of HAp (hydroxyapatite) discs with ROI (yellow outline), (a) Low density HAp, (b) Medium density HAp and (c) High density HAp. ROI was drawn on one image every 50~60 images and the ROIs were interpolated vertically throughout images to produce a volume of interest (VOI) representing each disc and the mean grayscale of each disc was calculated.

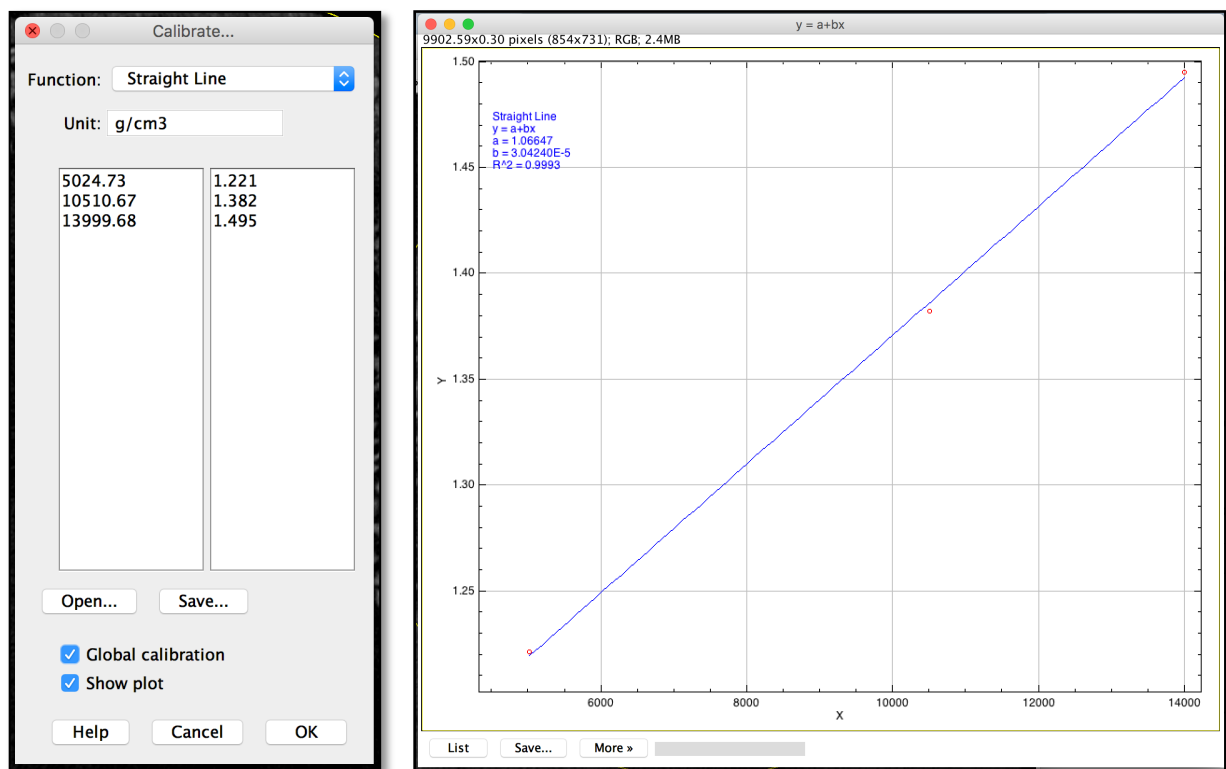


Figure 2.25 Grayscale calibration of μ CT images using HAp discs. Mean grayscale of HAp discs obtained were correlated with corresponding total effective density (g/cm³). A scatter plot shows a linear relationship between the grayscale (X-axis) and the density (Y-axis).

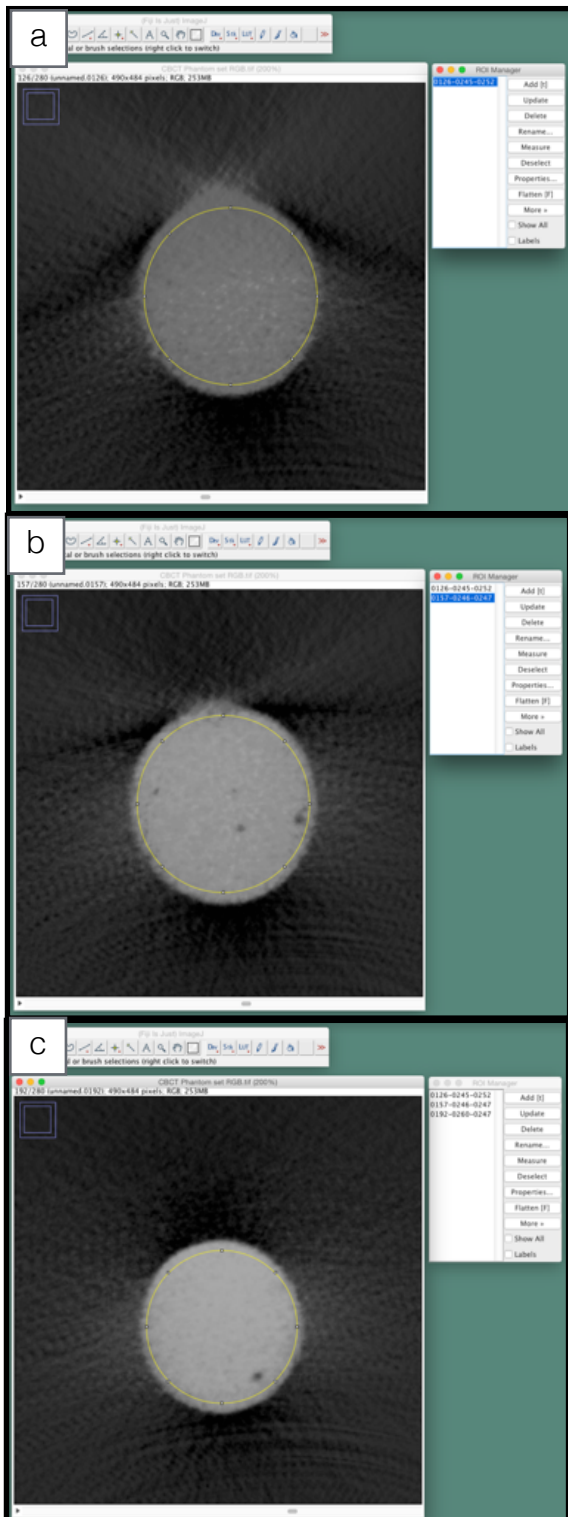


Figure 2.26 Cross sectional µCT images of HAp (hydroxyapatite) discs with ROI (yellow outline), (a) Low density HAp, (b) Medium density HAp and (c) High density HAp. ROI was drawn on one image every 50~60 images and the ROIs were interpolated vertically throughout images to produce a volume of interest (VOI) representing each disc and the mean grayscale of each disc was calculated.

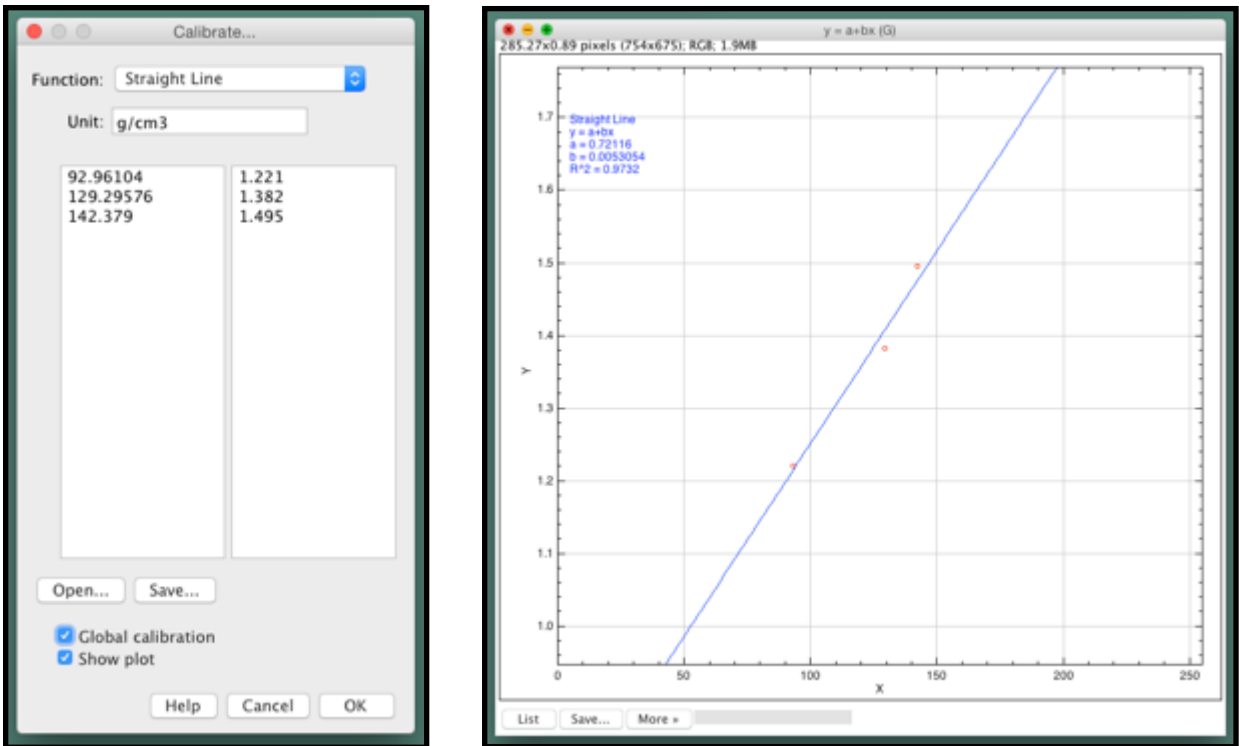


Figure 2.27 Grayscale calibration of CBCT images using HAp discs. Mean grayscale of HAp discs were correlated with corresponding total effective density (g/cm^3). A scatter plot shows a linear relationship between the grayscale (X-axis) and the density (Y-axis).

2.4.2.2 Thresholding of residual graft and new bone

Thresholding is a method to separate an area or tissue of interest within an image. In our study, radiographic standards were used to determine threshold and segment tissues of NB and RG in both μ CT and CBCT images.

2.4.2.2.1 *Endobon[®] standard*

The same Endobon[®] xenograft used for the animal surgery was packed in an emptied plastic prophylaxis paste plastic container. The prophylaxis paste in the container was emptied and cleaned and 1.8 g of Endobon[®] was packed into the container, which was then sealed with cellophane tape (Figure 2.28).

This Endobon[®] standard was scanned at the same time when the HAp discs were scanned in μ CT and CBCT (Figure 2.23). Following the scan, the raw image data of μ CT was reconstructed using Skyscan's NRecon software to produce a stack of reconstructed cross-sectional images displaying the Endobon[®] (figure 2.29). Each slice image consisted of 2000 x 2000 pixels with 16-bit grayscale. File sizes were approximately four megabytes per image. This reconstructed images were later used for thresholding of residual graft in μ CT images in ImageJ.

Similarly, scanned CBCT data of the Endobon[®] was exported from Galaxis (Sirona Dental, USA) in DICOM format with the following settings: highly dynamic (16-bit), 0.1 mm resolution voxel size. The exported data was then opened in Osirix (32-bit version, Pixmeo, Switzerland). Excess void volume was removed, and the remaining volume of the Endobon[®] standard was exported in a RGB format (Figure 2.29). This exported image set was used later for thresholding of residual graft in CBCT images in Image J.

2.4.2.2.2 Bone standard

Bone is a dynamic tissue that is characterised by inconsistent density depending on the degree of mineralisation. Even in the same cortical bone, the density may vary as the bone remodels over time. In our study, we did not include a radiographic standard for NB. Instead, the antral wall of the sinus was used as a radiographic standard for thresholding NB within μ CT and CBCT images (Figure 2.30)

2.4.2.3 μ CT

2.4.2.3.1 Grayscale calibration

The grayscale of the HAp discs obtained from 2.4.2.1.1 was correlated to the HAp density to calibrate grayscale in Image J. A scatter plot for the calibration of the discs showed a linear relationship between grayscale values and the total density (Figure 2.25) (Huang et al., 2007; Zou et al., 2009). This relationship was applied to all μ CT images in order to change grayscale into density (g/cm^3).

2.4.2.3.2 Automated thresholding

Thresholding RG and NB in the μ CT images was performed. Using Endobon[®] radiographic image obtained from 2.4.2.2.1, the upper and lower threshold levels were determined (Figure 2.31) The range was applied to the μ CT images to identify RG. To measure %RG, RG was divided by ROI and multiplied by 100.

To measure NB, the antral cortical bone of maxilla from within the same μ CT image was thresholded to identify NB within ROI (Figure 2.32). This resulted in the segmentation of NB within the grafted site, and the area was measured. To measure %NB, NB was divided by ROI and multiplied by 100.

We were also interested in measuring MT combining RG and NB. There was considerable overlap in radiodensity between RG and NB shown in grayscale histogram (1.60-2.71 gHAp/cm³ for RG and 1.50-1.70 gHAp/cm³ for NB). Therefore, threshold range for MT was represented by the lower threshold of NB and the upper threshold of RG (1.50-2.71 gHAp/cm³) (Figure 2.33). This threshold range was applied to our μ CT images to segment MT. %MT was calculated by dividing MT by ROI and multiplied by 100.

2.4.2.4 CBCT

2.4.2.4.1 *Grayscale calibration*

The grayscale of the HAp discs obtained from section 2.4.2.1.2. was correlated to the HAP density to calibrate grayscale in Image J. A scatter plot for the calibration of the discs showed a linear relationship between grayscale values and the total effective density (Huang et al., 2007; Zou et al., 2009). This calibration was applied to all 2-D CBCT images of the specimens to change grayscale to density value (g/cm³)

2.4.2.4.2 *Automated thresholding*

Thresholding RG and NB in the CBCT images was performed. Using Endobon® radiographic image obtained from 2.4.2.2.1, the upper and lower grayscale thresholds were determined. The range was applied to the CBCT images to identify RG (Figure 2.34). To quantify %RG, RG was divided by ROI (grafted site) and multiplied by 100.

To measure NB, the adjacent cortical bone of the sinus within the same CBCT image was used as a calibration standard to set threshold for NB. This resulted in the segmentation of NB within the grafted site, and the area was measured (Figure 2.35). To quantify %NB, NB was divided by the ROI and multiplied by 100.

MT was measured. A considerable overlap in radiodensity between RG and NB was noted (1.37-1.78 gHAp/cm³ for RG 1.31-1.61 gHAp/cm³ for NB). Therefore, threshold range for MT was represented by the lower threshold of NB and the upper threshold of RG (1.31-1.78 gHAp/cm³) (Figure 2.36). This threshold range was applied to our μ CT images to segment MT. %MT was calculated by dividing MT by ROI and multiplied by 100.

2.5 Statistical analysis

Statistical analysis was performed using Microsoft Excel (Microsoft Corp, USA). A one way paired t-test was performed to compare mean values of %RG, %NB, %MT of CBCT, μ CT, against histology for each and all animals. $P \leq 0.05$ was considered to be statistically significantly different.



Figure 2.28 1x Prophylaxis paste container (11mm high x 20mm diameter), Emptied, cleaned with water/Alcohol 100%, dried. Filled with 1.8g Endobon® granules, packed and top sealed with 2 layers of adhesive tape

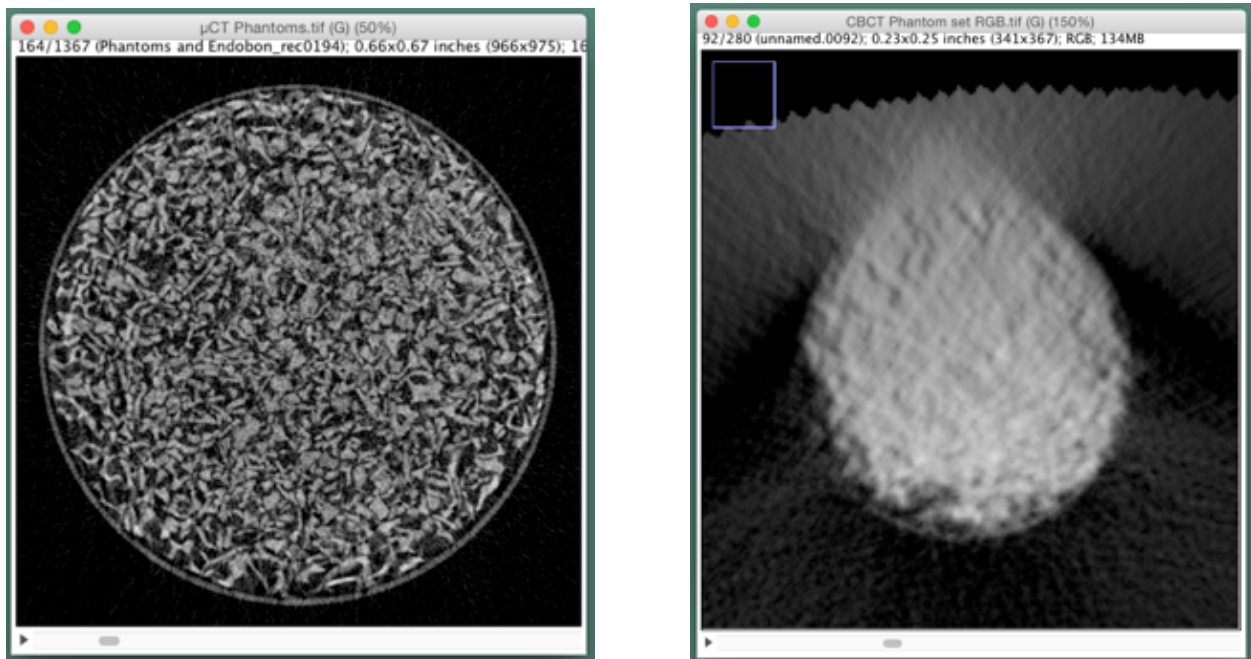


Figure 2.29 Reconstructed cross-sectional images of Endobon® in μCT (Left) and CBCT (Right) scan.

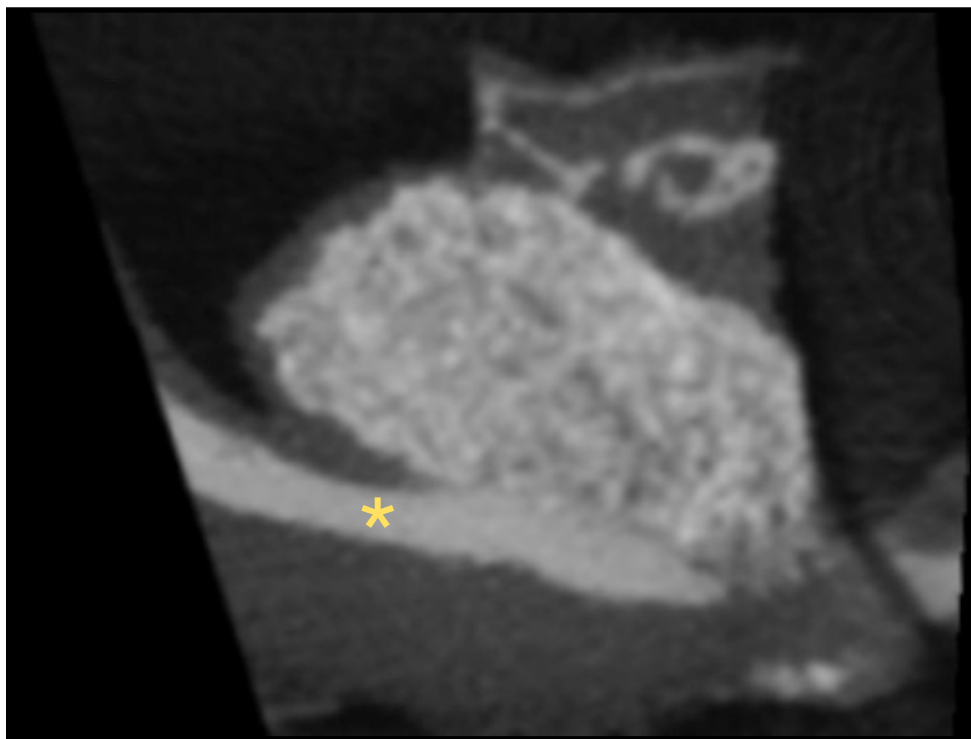


Figure 2.30 To threshold new bone in grafted sinus, the antral cortical wall (asterisk) was used as a radiographic standard in both μ CT (Top) and CBCT (Bottom) images.

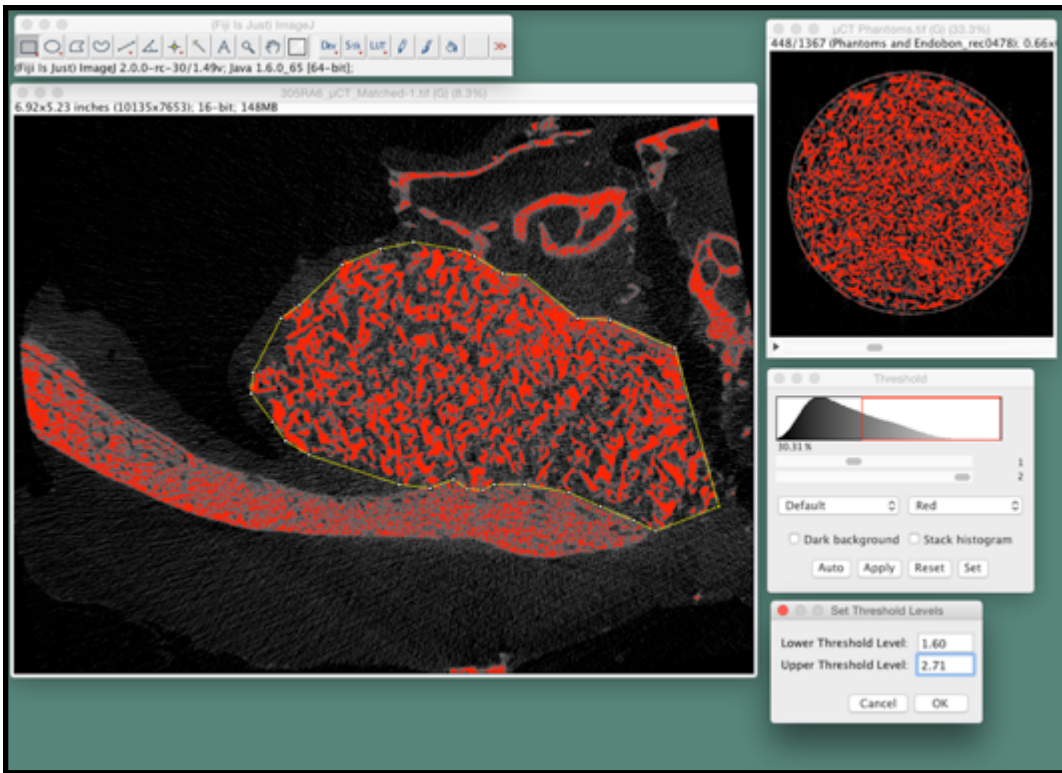


Figure 2.31 Thresholding residual graft using Endobon[®] scan (Upper right) as a standard (1.60-2.71 gHAp/cm³). This was applied to our µCT image (Left) to measure residual graft

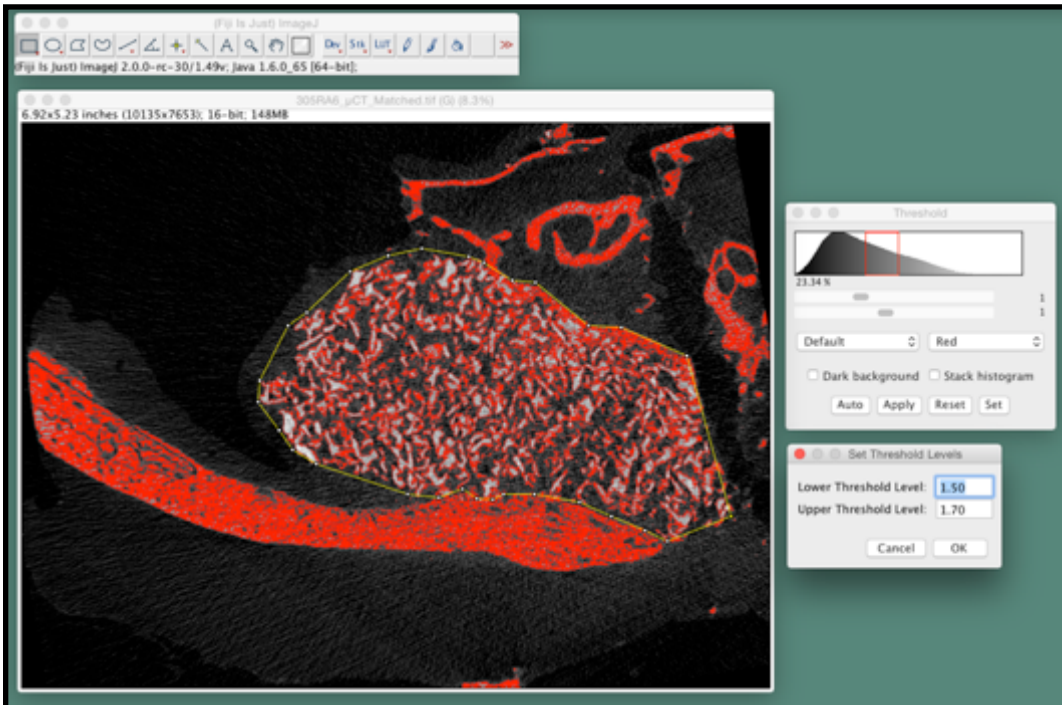


Figure 2.32 Thresholding new bone using the antral cortical bone as a standard (1.50-1.70 gHAp/cm³)

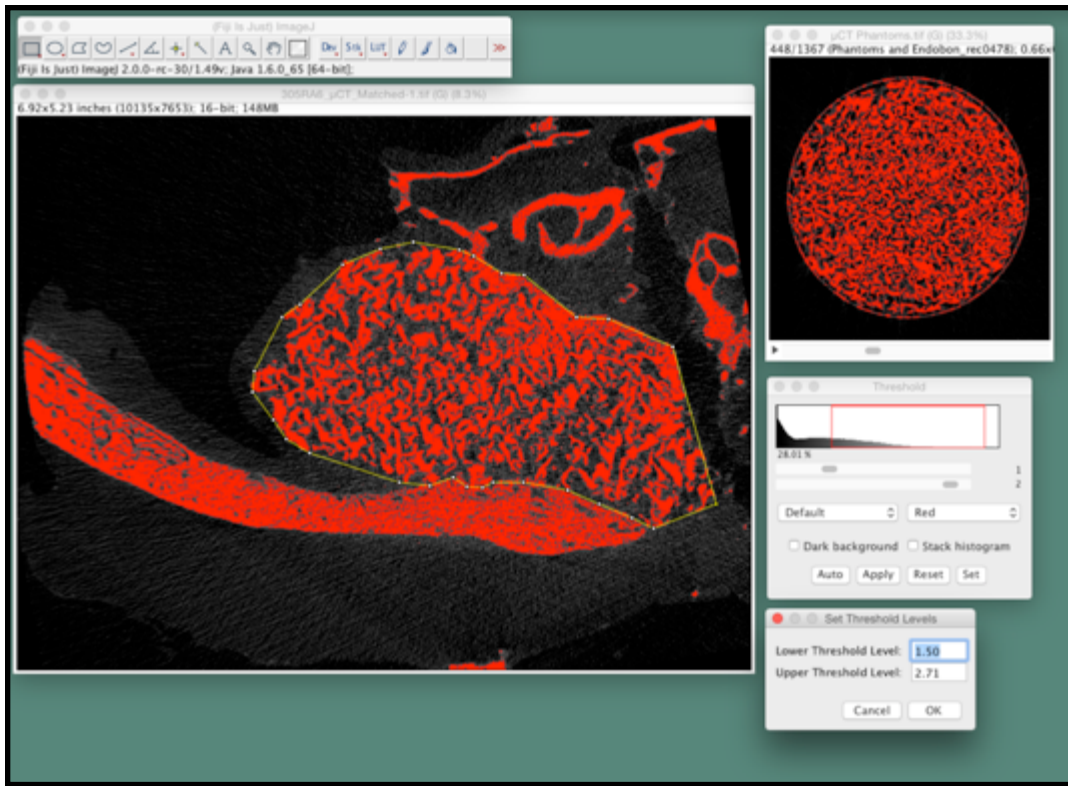


Figure 2.33 Thresholding mineralised tissue (Residual graft + new bone) by combining the threshold range of residual graft and bone ($1.50\text{-}2.71 \text{ gHAp/cm}^3$)

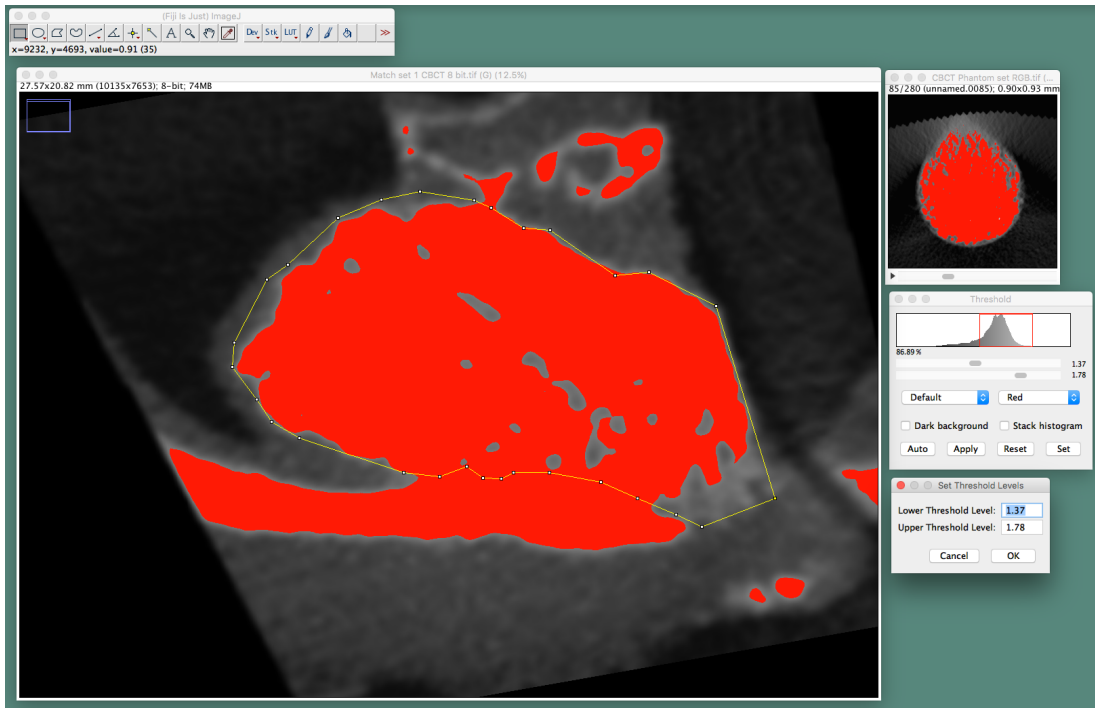


Figure 2.34 Thresholding residual graft using Endobon® scan (Upper right) as a standard (1.37-1.78 gHAp/cm³). This was applied to our CBCT image (Left) to measure residual graft.

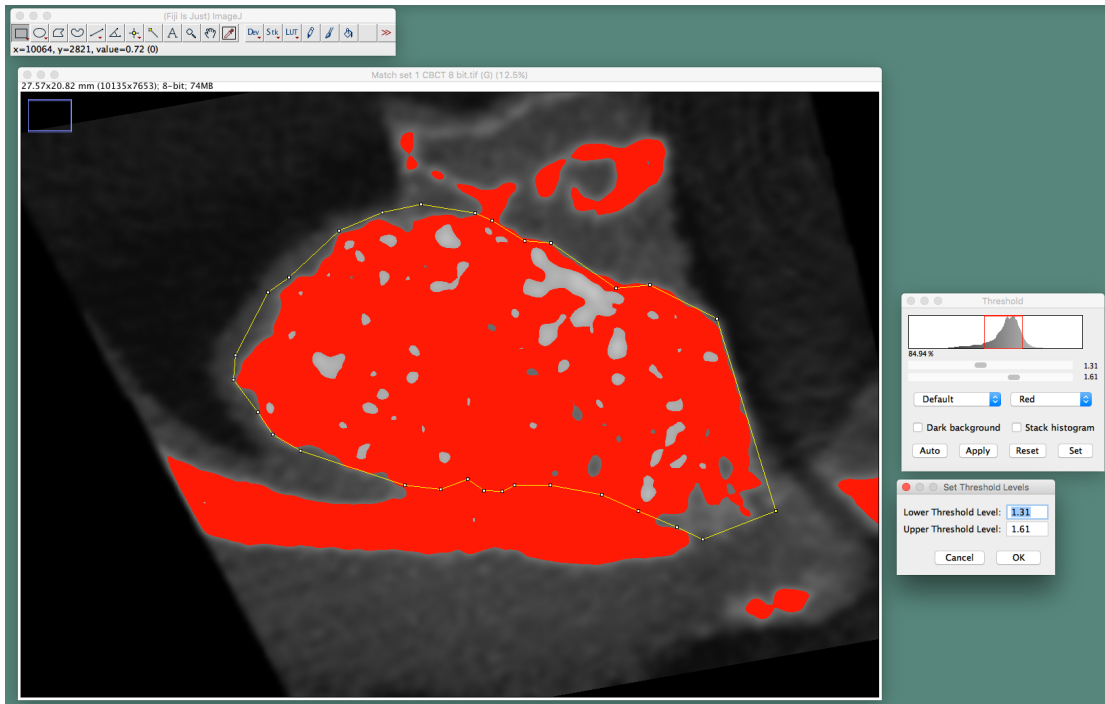


Figure 2.35 Thresholding new bone using the antral cortical bone as a standard (1.31-1.61 gHAp/cm³).

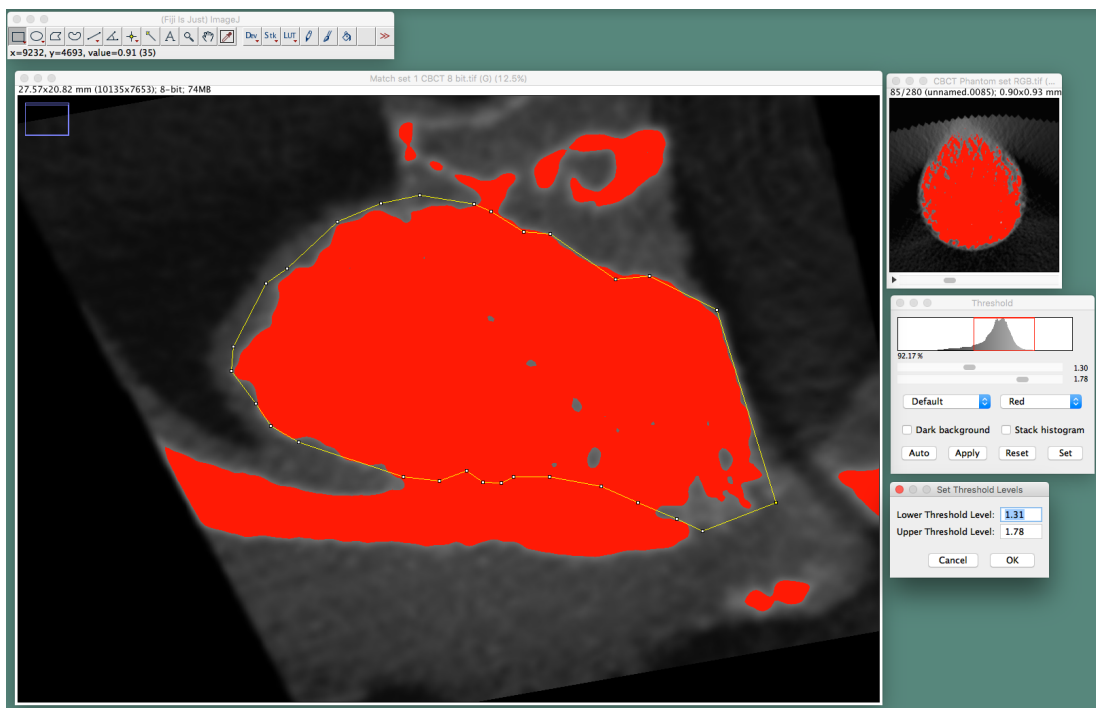


Figure 2.36 Thresholding mineralised tissue (Residual graft + new bone) by combining the threshold range of residual graft and bone ($1.31\text{--}1.78 \text{ gHAp/cm}^3$).

Chapter 3 Results

3.1 Post-operative recovery

No postoperative complications were encountered following the sinus floor elevation. All sites healed after sixteen weeks.

3.2 Radiographic examinations of resin-embedded specimens

The radiographs of resin-embedded specimen showed radio-opaque grafted sinus with a superimposed osteotomy site. An amalgam marker placed on the lower front side (i.e. anteroventral) of the antral wall was also observed (Figure 2.9).

3.3 Descriptive analysis of matched images of CBCT, μ CT, and histology

3.3.1 Morphology of grafted sinus

CBCT images displayed a smeared out, grainy image of the grafted sinus where residual graft islets were indistinguishable from the neighbouring connective tissue. In contrast, μ CT showed images of high contrast in which well-defined area of graft islets were recognised. μ CT images also demonstrated porosity within the cortical bone of the antral wall, which seems to match with that in histology. Histological images showed well-outlined tissue of residual graft, bone, and connective tissue that are distinct from each other by their morphology and the colour intensity (Figure 2.17)

3.3.2 Segmented image

For histological images in each specimen, the area occupied by newly formed bone (NB), residual bone graft (RG), mineralised tissue (MT) were identified using colour thresholding on a computer-based image analysis system, Image J.

Similarly, for μ CT and CBCT images, same tissue parameters in histology were measured using thresholding where the threshold for each tissue was determined using radiographic standards of Endobon® and the cortical bone of antral sinus wall.

3.3.2.1 *Residual graft*

Thresholded image of residual graft in histology, μ CT and CBCT were compared (Figure 3.1). In histological images, graft islets within the sinus were observed. μ CT thresholded what appears to be residual graft and the pattern of that thresholded area was very similar with that in histology. CBCT segmented a large mass within the sinus, which did not show any similarity to the segmented images of histology and μ CT (Figure 3.1)

3.3.2.2 *New bone*

Histology presented in-growth pattern of new bone from the sinus floor extending into the centre of the graft. μ CT recognised the floor of sinus as new bone, presenting a similar pattern of segmentation with histology. However, μ CT also segmented the periphery of residual graft as new bone. CBCT recognised the centre of the grafted sinus as residual graft exhibited as a large central mass within the sinus, which was conflicting with what was segmented in histology (Figure 3.2).

3.3.2.3 *Mineralised tissue (Residual graft + New bone)*

Histology revealed a thresholded image of residual graft and new bone clearly leaving the background image of connective tissue. The area of mineralized tissue indicated by μ CT demonstrated a similar pattern to histology where residual graft islets as well as new bone on the sinus floor were extracted. In CBCT, however, the area indicated as mineralized tissue involved the entire area of grafted sinus leaving almost no background tissue within ROI. This thresholded image of CBCT for mineralized tissue, once again was inconsistent with what was demonstrated in histology (Figure 3.3).

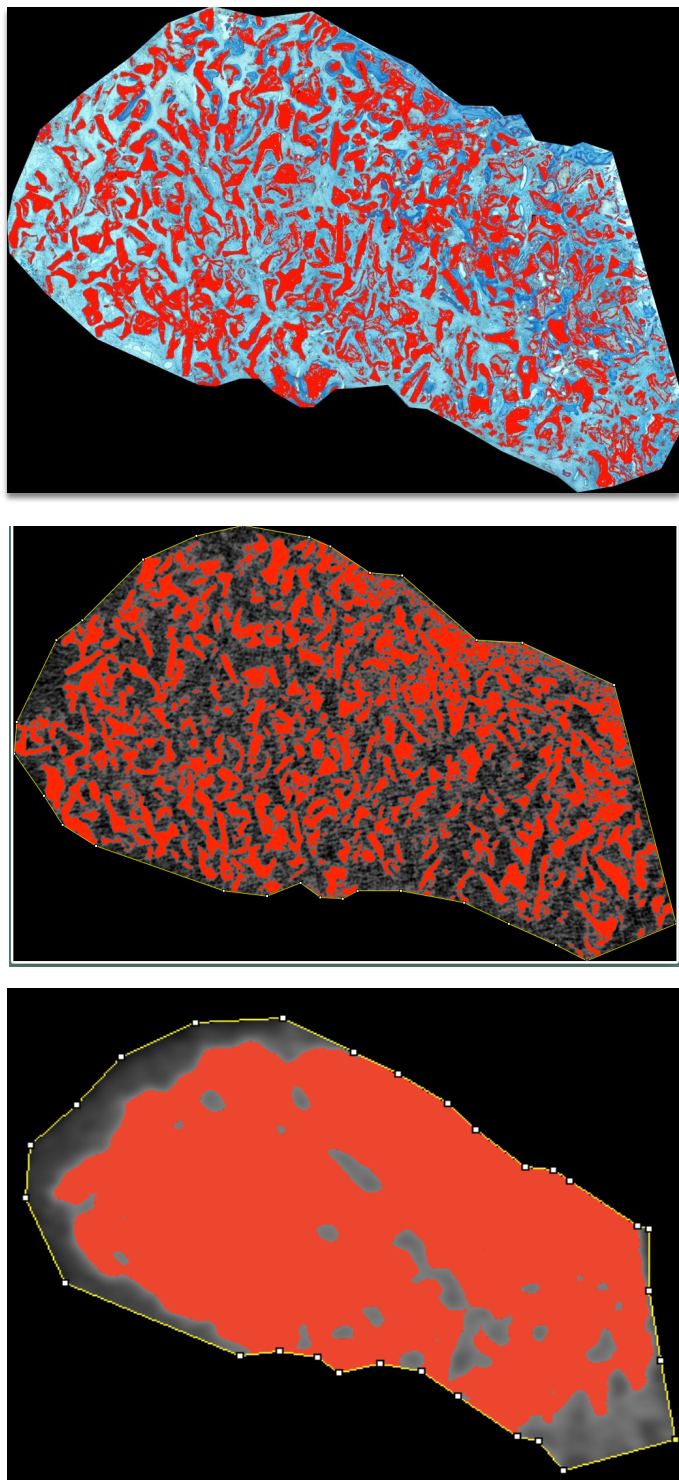


Figure 3.1 Thresholded image of residual graft in histology (top), μ CT (middle) and CBCT (bottom).

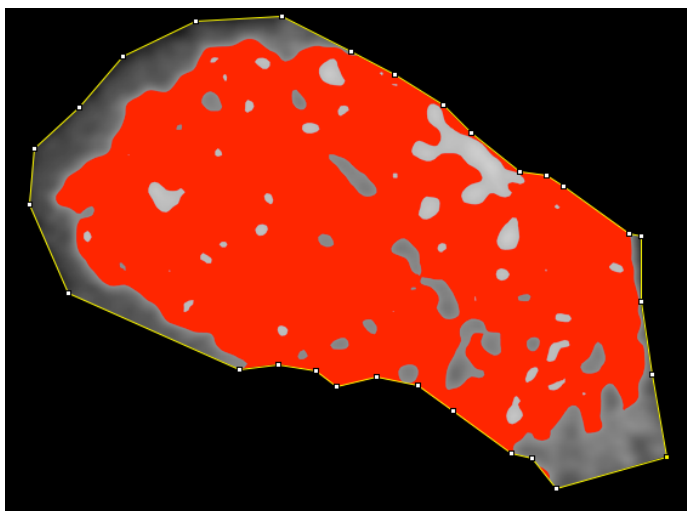
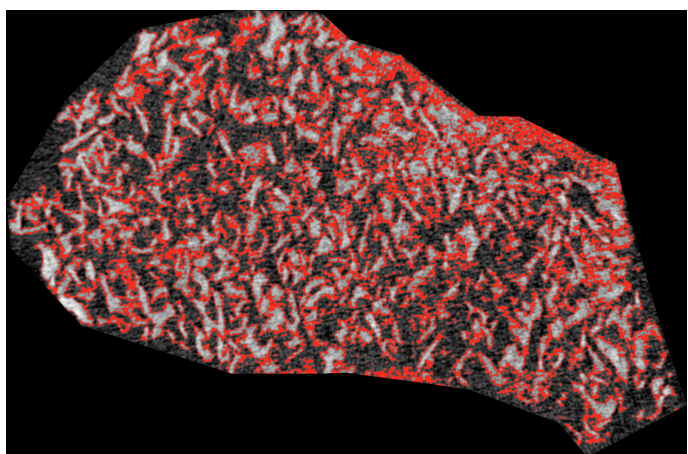
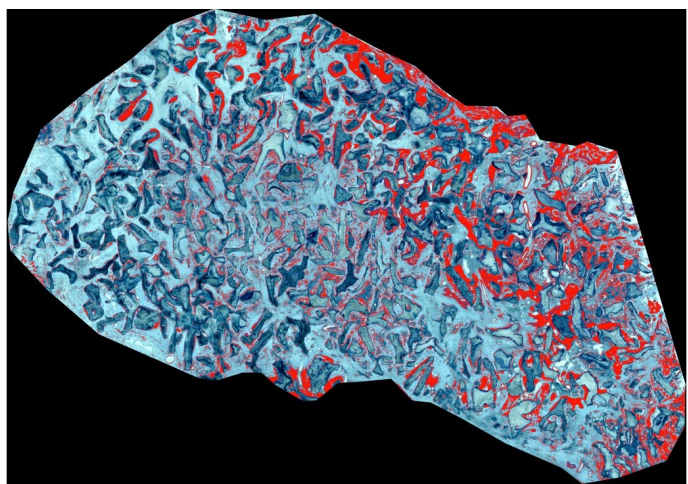


Figure 3.2 Thresholded image of new bone in histology (top), μ CT (middle) and CBCT (bottom).

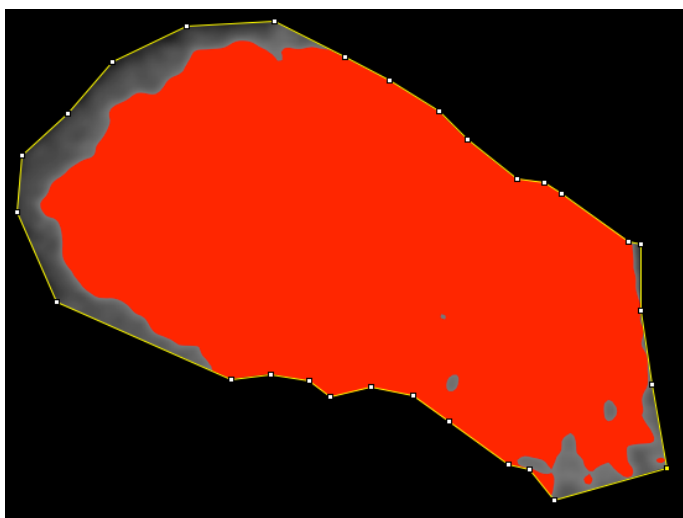
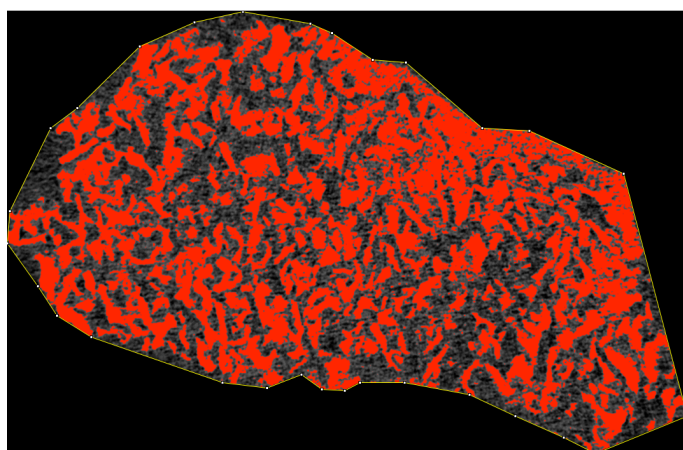
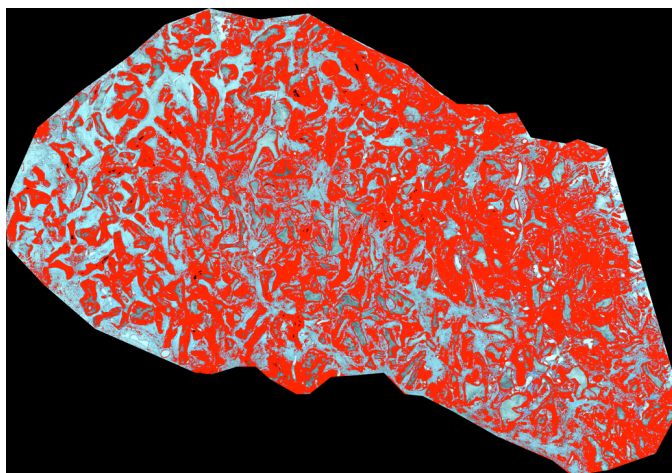


Figure 3.3 Thresholded image of mineralised tissue in histology (Top), μ CT (middle) and CBCT (bottom).

3.4 Quantitative analysis

One-way paired t-test was performed to compare the results of CBCT against μ CT and histology. P values ≤ 0.05 were accepted for statistical significance. The test was carried out for the overall mean results including all animals and also for mean results for each animal.

3.4.1 Overall mean and individual mean for different tissues in CBCT, μ CT and histology

3.4.1.1 *Residual graft*

The overall mean and the standard error (SE) for the percentage of residual graft (%RG) measured by CBCT, μ CT and histology are presented (Table 3.1 and Figure 3.5). The % RG \pm SE measured was $69.9 \pm 2.1\%$ for CBCT, $35.1 \pm 1.3\%$ for μ CT and $34.2 \pm 1.18\%$ for histology. % RG measured by CBCT was significantly greater from both histology and μ CT ($p \leq 0.05$), however, % RG measured by μ CT was not statistically significantly different from that measured by histology ($p = 0.307$).

The % RG measured by CBCT, μ CT and histology in each animal is presented (Table 3.2 and Figure 3.9). All animals exhibited a similar pattern of difference of % RG between CBCT, μ CT and histology. In all animals, %RG measured by CBCT was significantly greater than μ CT and histology ($p \leq 0.05$) (Table 3.2). The overall mean results showed that % RG measured by μ CT and histology were not significantly different ($p = 0.307$). However, in two animals (310L, 6003L) %RG measured by μ CT was significantly higher than %RG measured by histology ($p \leq 0.05$).

3.4.1.2 *New bone*

The overall mean and the standard error (SE) of the percentage of new bone (%NB) measured by CBCT, μ CT and histology are presented (Table 3.1, Figure 3.4). %NB \pm SE was $66 \pm 2.1\%$, $25.9 \pm 1.5\%$ and $9.5 \pm 1.1\%$ for CBCT, μ CT and histology, respectively. %NB measured by both CBCT and μ CT were statistically significantly greater than that measured by histology ($p \leq 0.05$). CBCT showed much greater value for new bone compared to μ CT ($p \leq 0.05$).

The mean and the standard deviation for the percentage of new bone (% NB) measured by CBCT, μ CT and histology in each animal are presented (Table 3.2 and Figure 3.8). All animals showed a similar trend in the difference of % NB measured by the three techniques. % NB measured by CBCT was the highest and this was followed by μ CT and histology. The results measured by all three techniques were statistically significantly different from each other ($p \leq 0.05$).

3.4.1.3 Mineralised tissue (New bone + residual graft)

The overall mean and the standard error for % mineralised tissue (MT, new bone + residual graft) measured by CBCT, μ CT and histology are presented (Table 3.1 and Figure 3.6). % MT \pm SE was 87.93 ± 0.87 % for CBCT, 48.92 ± 1.67 % for μ CT and 43.71 ± 1.87 % for histology. % MT measured by μ CT was similar to that measured by histology, however they were still statistically significantly different ($p = 0.0207$). CBCT showed significantly greater value of % MT compared to μ CT and histology ($p \leq 0.05$)

The % MT measured by CBCT, μ CT and histology in each animal are presented (Table 3.2 and Figure 3.10). All animal groups presented a similar trend in their results. % MT measured by CBCT was significantly greater than μ CT and histology in all animals ($p \leq 0.05$) (Table 3.2). The overall mean % MT in μ CT was similar to that in histology, however, the two values were significantly different ($p \leq 0.05$) (Table 3.1). Interestingly, two animals showed statistically no significant difference of % MT between μ CT and histology (animal 317L and 6003L with p value of 0.395 and 0.058, respectively) (Table 3.2).

Table 3.1 Overall mean results and standard error for the area occupied by different tissues measured by CBCT, μ CT and histology.

Tissue	Mean and standard error (%)			P value		
	CBCT	μ CT	Histology	Histology vs. CBCT	Histology vs. μ CT	μ CT vs. CBCT
Residual graft	69.9 ± 2.1	35.1 ± 1.3	34.2 ± 1.2	≤ 0.05	†NS	≤ 0.05
New bone	66.0 ± 1.5	25.9 ± 1.5	9.5 ± 1.1	≤ 0.05	≤ 0.05	≤ 0.05
#Mineralised tissue (Graft + Bone)	87.9 ± 0.9	48.9 ± 1.7	43.7 ± 1.9	≤ 0.05	≤ 0.05	≤ 0.05
*Connective tissue (CT)	12.1 ± 0.9	51.1 ± 1.7	56.3 ± 1.9	≤ 0.05	≤ 0.05	≤ 0.05

* % Connective tissue = $100 - \% \text{ mineralised tissue}$

† NS = not statistically significant

‡ % Mineralised tissue for μ CT and CBCT is not equal to % Residual graft + % New bone. % Mineralised tissue was measured using a combined threshold range for residual graft and new bone. % Mineralised tissue for histology was measured by adding % residual graft and % new bone.

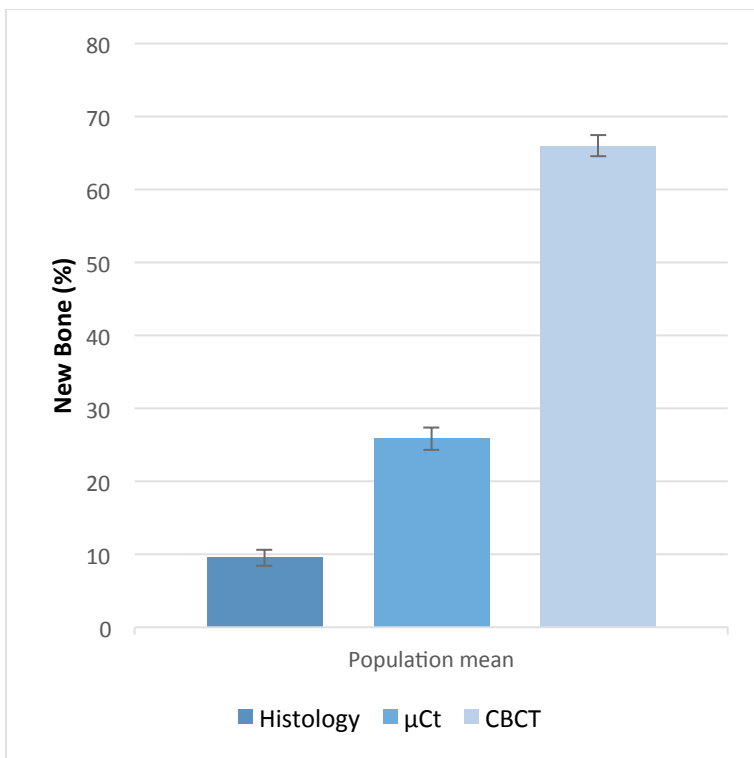


Figure 3.4 Overall mean of new bone in histology, μ CT and CBCT with the standard error.

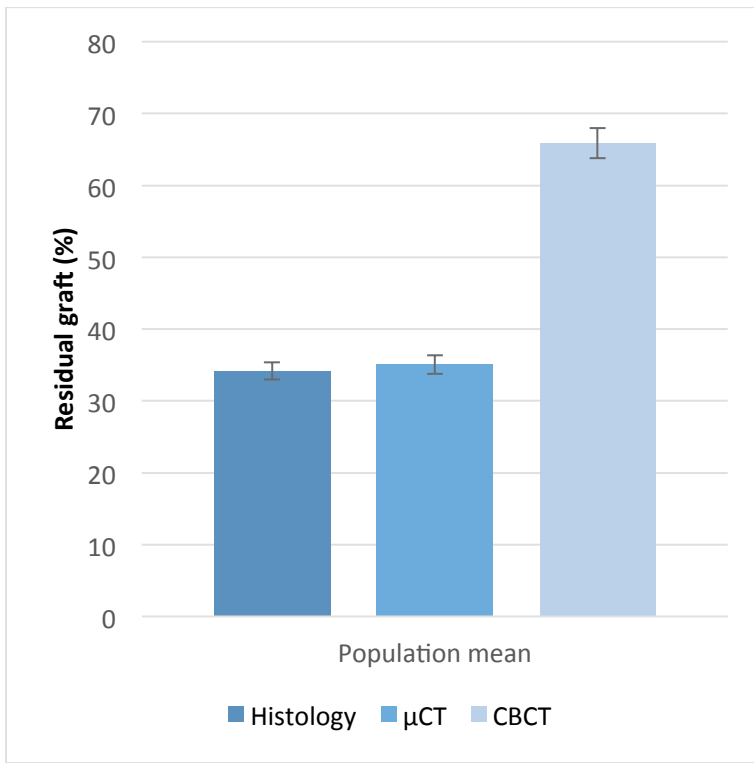


Figure 3.5 Overall mean of residual graft in histology, μ CT and CBCT with the standard error.

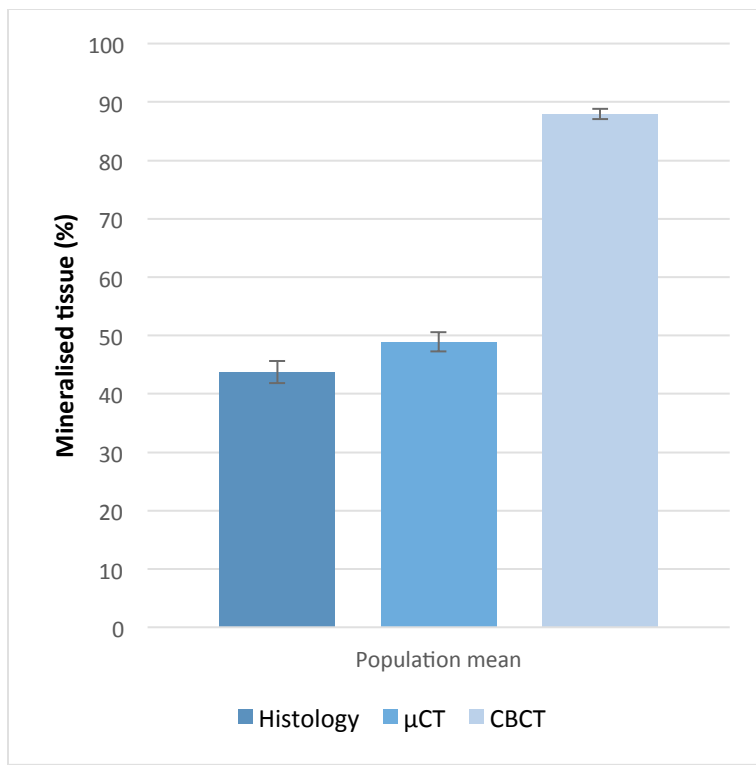


Figure 3.6 Overall mean of mineralised tissue (new bone + residual graft) in CBCT, μ CT and histology with the standard error.

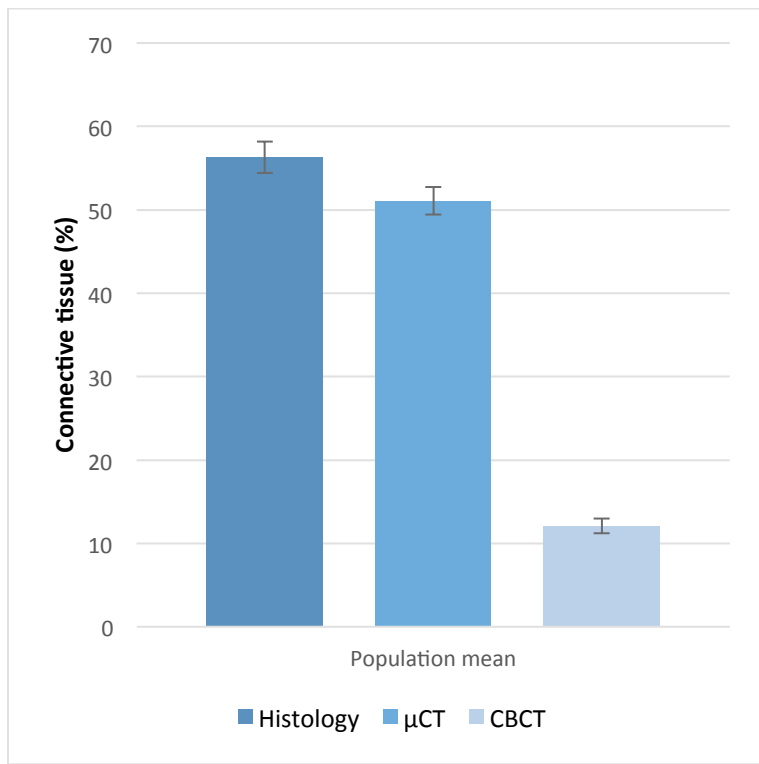


Figure 3.7 Overall mean of connective tissue in CBCT, μ CT and histology with the standard error.

Table 3.2 Sample mean and standard deviation for each tissue measured by different techniques.

Tissue	Mean and standard deviation (%)			P value		
	CBCT	μ CT	Histology	Histology vs CBCT	Histology vs μ CT	μ CT vs CBCT
Sheep ID: 305R						
Residual graft	73.8 ± 10.1	31.1 ± 2.2	33.3 ± 4.2	≤0.05	†NS	≤0.05
New bone	62.9 ± 7.6	23.5 ± 2.3	14.1 ± 3.3	≤0.05	≤0.05	≤0.05
‡Mineralised tissue (Graft + Bone)	87.7 ± 5.2	45.0 ± 3.7	47.4 ± 5.2	≤0.05	†NS	≤0.05
Connective tissue*	12.3 ± 5.2	55 ± 3.7	52.6 ± 5.2	≤0.05	†NS	≤0.05
Sheep ID: 310L						
Residual graft	73.2 ± 3.0	39.5 ± 1.7	34.8 ± 2.0	≤0.05	≤0.05	≤0.05
New bone	66.0 ± 4.3	28.7 ± 1.4	6.6 ± 1.9	≤0.05	≤0.05	≤0.05
‡Mineralised tissue (Graft + Bone)	91.0 ± 4.0	52.2 ± 2.2	41.4 ± 2.4	≤0.05	≤0.05	≤0.05
Connective tissue*	9.02 ± 4.0	47.8 ± 2.2	58.7 ± 2.4	≤0.05	≤0.05	≤0.05
Sheep ID: 316L						
Residual graft	69.3 ± 6.4	33.1 ± 1.3	35.8 ± 3.7	≤0.05	†NS	≤0.05
New bone	54.9 ± 5.0	38.8 ± 2.9	6.3 ± 2.9	≤0.05	≤0.05	≤0.05
‡Mineralised tissue (Graft + Bone)	89.4 ± 3.3	53.2 ± 2.4	42.1 ± 6.1	≤0.05	≤0.05	≤0.05
Connective tissue*	10.5 ± 3.3	46.8 ± 2.4	57.9 ± 6.1	≤0.05	≤0.05	≤0.05
Sheep ID: 317L						
Residual graft	70.1 ± 8.0	41.5 ± 2.45	38.1 ± 3.3	≤0.05	†NS	≤0.05
New bone	73.3 ± 3.2	30.9 ± 2.5	19.5 ± 6.0	≤0.05	≤0.05	≤0.05
‡Mineralised tissue (Graft + Bone)	90.1 ± 2.5	57.0 ± 2.62	57.6 ± 3.7	≤0.05	†NS	≤0.05
Connective tissue*	9.11 ± 2.49	43.0 ± 2.6	42.4 ± 3.7	≤0.05	†NS	≤0.05
Sheep ID: 320R						
Residual graft	44.5 ± 4.8	24.1 ± 1.9	22.9 ± 2.5	≤0.05	†NS	≤0.05
New bone	67.6 ± 4.6	1.29 ± 2.4	3.9 ± 3.7	≤0.05	≤0.05	≤0.05
‡Mineralised tissue (Graft + Bone)	82.1 ± 5.7	32.3 ± 3.6	26.9 ± 5.5	≤0.05	≤0.05	≤0.05
Connective tissue*	17.9 ± 5.7	67.7 ± 3.6	73.1 ± 5.5	≤0.05	≤0.05	≤0.05
Sheep ID: 6003L						
Residual graft	63.5 ± 3.9	47.4 ± 1.8	43.4 ± 3.0	≤0.05	≤0.05	≤0.05
New bone	76.7 ± 2.9	24.7 ± 1.5	7.8 ± 7.3	≤0.05	≤0.05	≤0.05
‡Mineralised tissue (Graft + Bone)	88.1 ± 4.0	60.4 ± 2.0	51.2 ± 10.3	≤0.05	†NS	≤0.05

Connective tissue*	11.9 ± 4.0	39.6 ± 2.0	48.8 ± 10.3	≤0.05	+NS	≤0.05
---------------------------	-------------------	-------------------	--------------------	--------------	------------	--------------

* % Connective tissue = 100 - % mineralised tissue

+ NS = Not statistically significant

† % Mineralised tissue for µCT and CBCT is not equal to % Residual graft + % New bone. % Mineralised tissue was measured using a combined threshold range for residual graft and new bone. % Mineralised tissue for histology was measured by adding % residual graft and % new bone.

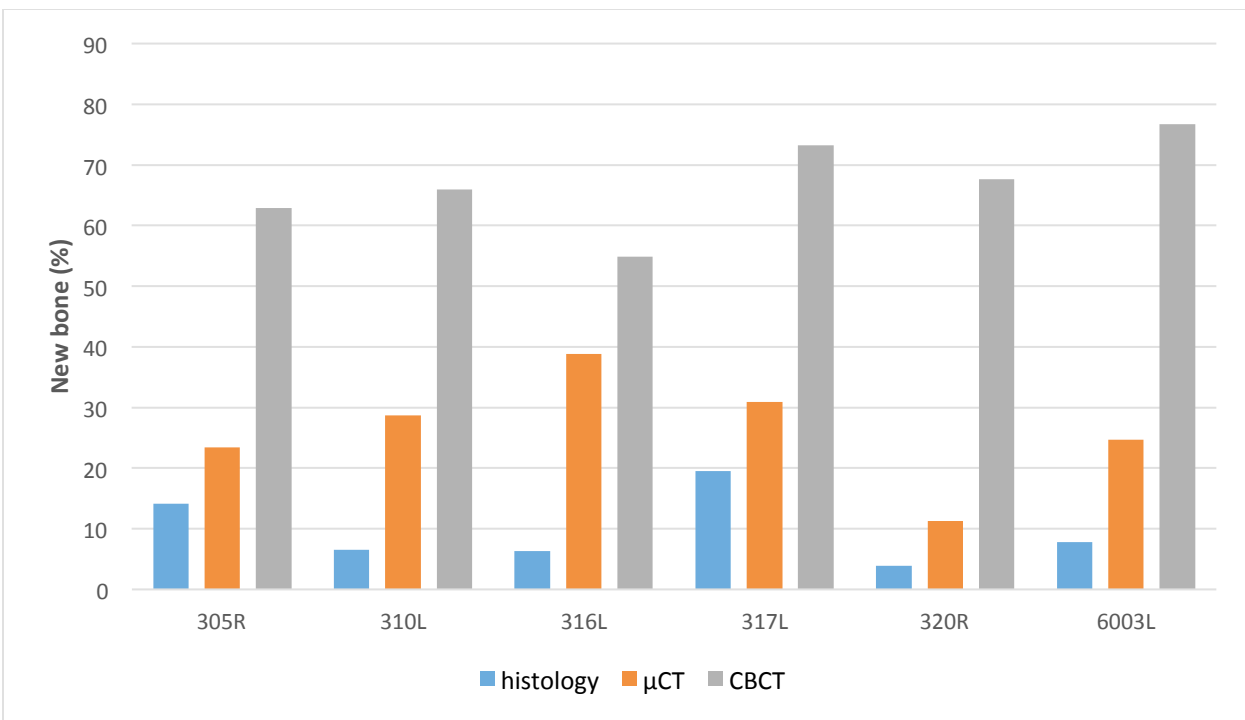


Figure 3.8 Mean % New bone measured by histology, μ CT and CBCT in all six animals.

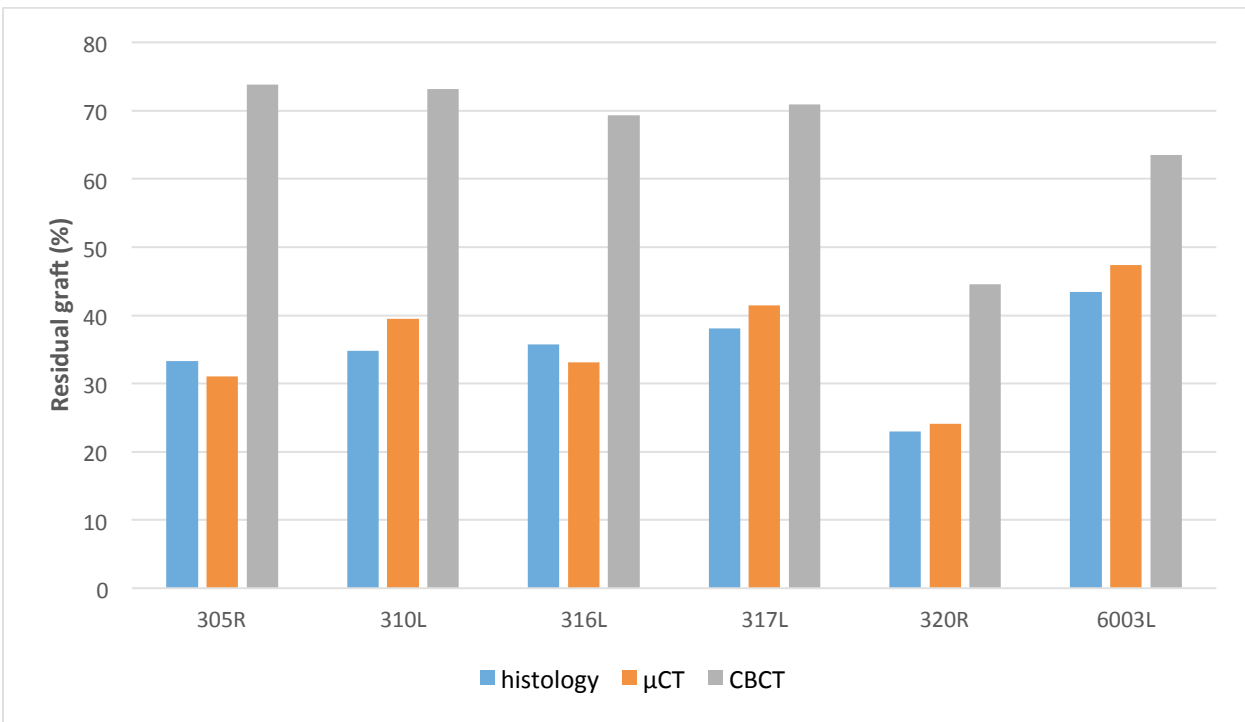


Figure 3.9 Mean % Residual graft measured by histology, μ CT and CBCT in all six animals.

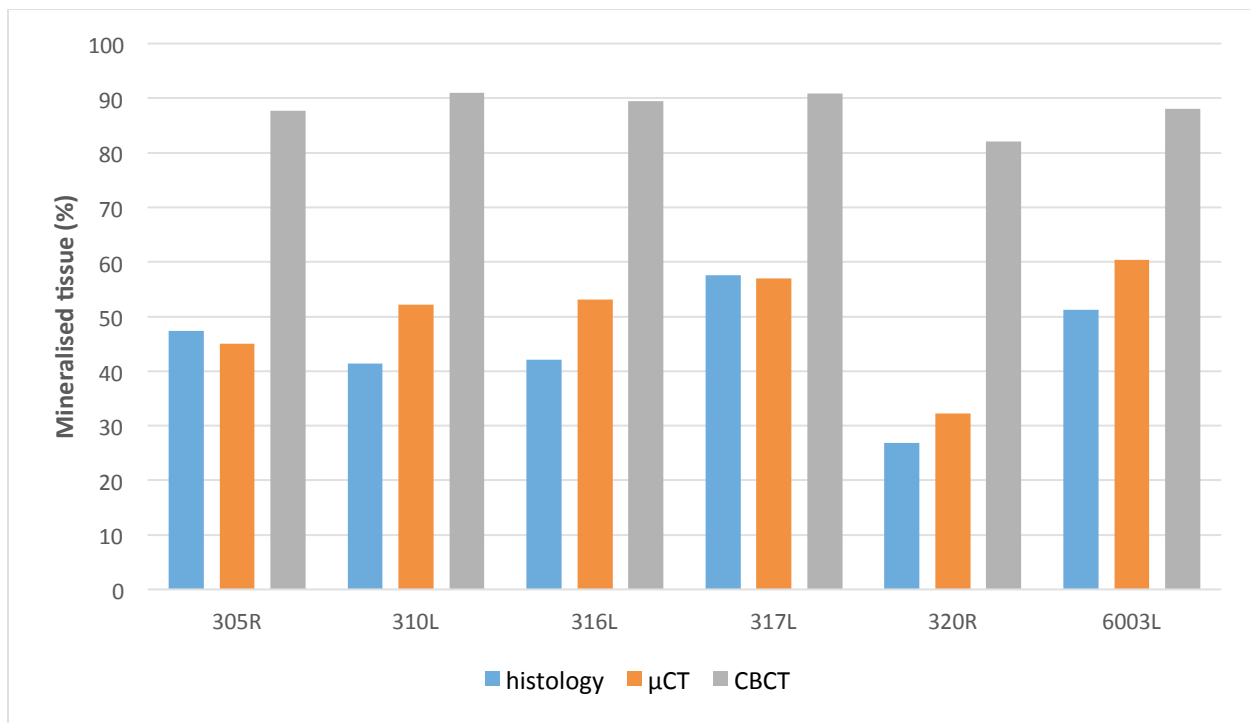


Figure 3.10 Mean % Mineralised tissue (% residual graft + % new bone) measured by histology, μ CT and CBCT from all six animals

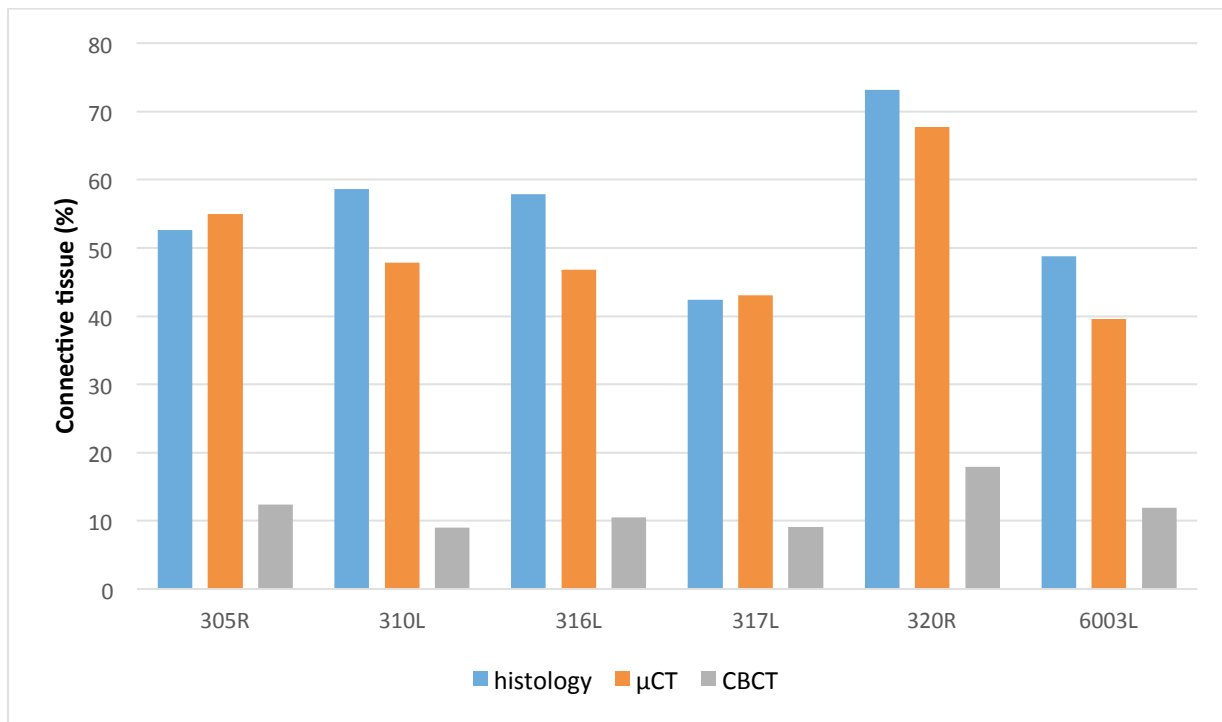


Figure 3.11 Mean % Connective tissue measured by histology, μ CT and CBCT from all six animals.

Chapter 4 Discussion

4.1 Introduction

The aim of this study was to assess the efficacy of CBCT to determine newly-formed bone in grafted sinuses. We assessed %NB, %RG and %MT in grafted sheep maxillary sinuses using CBCT, and compared the results against two reference techniques; histology and μ CT. The hypothesis was that CBCT would accurately determine newly-formed bone and residual graft in grafted sinuses, with a similar accuracy to two reference standards: histology and μ CT.

The statistical analysis, however, demonstrated that CBCT overestimated %NB, %RG and %MT compared to μ CT and histology. μ CT was able to estimate %RG similar to histology, but it overestimated %NB. μ CT slightly overestimated %MT in comparison to histology and the results between the two techniques were statistically significantly different.

As a part of our study, we also developed a new protocol involving how to orient and match 2-D radiographic images with histological images with the assistance of computer imaging software and the use of radiographic standards for grayscale calibration and thresholding.

4.2 CBCT

In the current study, CBCT overestimated %RG, %NB and %MT, compared to histology and μ CT.

Previous studies have documented the effectiveness of CBCT in both linear and volumetric measurements of mineralised tissues (Gribel et al., 2010; Benavides et al., 2012; Feichtinger et al., 2007). For example, Feichtinger et al. (2007) measured the volume of new bone following grafting in cleft lip cases using two-dimensional (2D) orthopantomogram (OPG) and CBCT. CBCT demonstrated a more reliable measure of the actual 3D dimension of grafted volume compared to OPG, the measurement of which was limited by 2D assessment. Similarly, Gribel et

al. (2010) documented a great correlation between CBCT and lateral cephalograms for craniometric measurements and concluded that CBCT can be a substitute for lateral cephalograms. A recent systematic review of Benavides et al. (2012) reported that linear and volumetric measurements by CBCT are accurate and useful.

The efficacy of CBCT for bone density measurement was also conducted in the field of endodontics. Several studies that documented CBCT have a greater probability in detecting apical periodontitis than other 2-D conventional intraoral radiographs and concluded CBCT can detect changes in bone density (Alayan et al., 2015; Velvart et al., 2001). However, this greater sensitivity of CBCT for the detection of apical periodontitis appears to contribute to its 3-D analysis at different planes, which made it easy to detect the presence of such lesions. Additionally, in order to detect periapical radiolucency, studies reported there should be more than a 50% loss of mineral loss (Bender and Seltzer, 1961a; b; Estrela et al., 2008) which is different from grafted sinus which is a compound of residual graft and new bone, the two mineralised tissues at different density. Currently, there is a limited amount of evidence on the accuracy of CBCT for density measurement including the measurement of healing within grafted sinus (Benavides et al., 2012).

In this study, we tested the efficacy of CBCT to quantify the amount of newly-formed bone within grafted sinus. 2-D virtual radiographic images of CBCT were compared against matched 2-D images of μ CT and histology, and %NB, %RG and %MT were measured. We found that, in virtually all specimens, CBCT overestimated all three tissue parameters compared to histology or μ CT.

The segmented images representing new bone, residual graft and mineralised tissue in CBCT exhibited a large undefined area that was different from the corresponding images in μ CT and histology (Figure 3.1, Figure 3.2 and Figure 3.3). This result of qualitative analysis appeared to be due to the low resolution and hence poor quality image produced by CBCT, which hindered segmentation of the true tissue area. In comparison to the same radiographic images of μ CT, CBCT images were smeared and grainy in appearance, with a poorly defined area of residual graft islets. In contrast, μ CT produced images with an excellent detail of graft granules,

distinguishable from the background soft tissue. A similar phenomena was observed and discussed in a paper by Yamashita-Mikami et al. (2013). The group radiographically assessed a human alveolar bone biopsy from the lower left first molar site using a conventional CT and μ CT. While μ CT captured good details of plate-like trabeculae extending from the lingual cortical bone, the same pattern was not identifiable in CBCT images due to its limited resolution.

The low resolution of CBCT images is explained by the large voxel size and short exposure time. While μ CT is a research radiographic tool that has significantly smaller voxel size compared to CBCT (up to $1\mu\text{m}$ versus $100\mu\text{m}$, respectively) having an average exposure time three to four hours (at least in this research), CBCT exposure time is approximately 15 to 20 seconds with a lower voxel size. Such differences result in low resolution and a high noise level of CBCT images and produces a significant error in segmentation of different tissues.

This influence of voxel size on the result of image segmentation was demonstrated (Waarsing et al., 2004a). A trabecular biopsy specimen of canine distal femora, embedded in MMA, was scanned with μ CT with the original system voxel size of $18\mu\text{m}$. This raw data was then altered to produce two extra datasets with a higher voxel size of 35 and $53\mu\text{m}$. These three μ CT images with different voxel sizes were thresholded and segmentation results were compared. The results revealed that, when the voxel size changed from $18\mu\text{m}$ to $35\mu\text{m}$, the parameters changed on average by 13%. When the voxel size was further increased to $53\mu\text{m}$, the performance of thresholding deteriorated significantly, resulting in changes greater than 30% in the segmentation outcome (Waassing et al., 2004a). This indicates that the voxel size is a critical factor that determines the outcome of segmentation. This may explain why CBCT resulted in overestimation of both residual graft and bone compared to both histology and μ CT in the current study.

Image noise was also shown to affect segmentation (Waassing et al., 2004b). If scanning time is shortened, there is more noise within the image. This is particularly true for CBCT, as this is a clinical imaging hardware that takes less than 20 seconds to complete the scan. An increase in noise level will result in over-segmentation with thresholding which partly seems to be the case with CBCT images in this research. In their study, two μ CT datasets with different

noise levels of medium and high were created by adding noise with an SD of 0.005 (medium) and 0.01 (high). These two data sets, along with the original dataset (considered as the low-noise reference), were globally segmented, and the results were compared. The results showed that the values in the medium-noise group were changed 6%, while values were changed by 7% when a high noise level was added (Waarsing et al., 2004b).

It should also be emphasised that the resolution of CBCT images was further affected by the use of the third-party image software OsiriX. Any DICOM files imported into OsiriX can only be exported into RGB format. This reduced the image resolution. Compared to the raw CBCT dataset, the same dataset exported from Osirix as a RGB format featured a significantly lower grayscale range (Figure 2.16). This affected segmentation for %NB, %RG and %MT where all three tissues were significantly overestimated compared to μ CT and histology.

To the author's knowledge, the current study is the first to employ CBCT to quantify newly formed bone, residual graft and overall mineralised tissue in grafted maxillary sinus and compared the results with μ CT and histology. The results of the study demonstrated that CBCT could not distinguish between residual graft and new bone due to inadequate resolution and image noise, resulting in an overestimation in quantifying both tissues.

4.3 Micro-computed tomography (μ CT)

Previous studies reported a moderate to high correlation between μ CT and histology for the assessment of trabecular bone architecture (Thomsen et al., 2005; Chappard et al., 2005; Ito et al., 1998; Zupan et al., 2013). Thomsen et al. (2005) analysed the trabecular structure of human tibia biopsies using histomorphometry and μ CT. A strong correlation between the two methods was observed, indicating that μ CT can be used as a substitute for conventional histology for the morphometric analysis of bone. Other previous studies also documented similar findings using trabecular bone biopsies obtained from various sites (Chappard et al., 2005; Ito et al., 1998; Zupan et al., 2013). Based on these previously documented reports, both histology and μ CT were employed as reference techniques to validate the accuracy of CBCT for bone morphometric analysis in this study.

However, this research demonstrated that, while μ CT estimated %RG similar to histology, it overestimated %NB.

The biggest reason why μ CT was unable to estimate %NB appears to be due to the similar radiodensity between residual graft and new bone. Both bone and residual graft (Endobon[®]) mainly consists of porous hydroxyapatite. A histogram analysis of grayscale revealed a considerable overlap of grayscale between the two tissues; this similar grayscale (hence, a similar radiodensity) affected segmentation results. Between new bone and residual graft, a segmentation of one tissue without the introduction of the other tissue was not possible by thresholding; while thresholding new bone, a part of residual graft was added resulting in overall increase in %NB. Conversely, a portion of new bone was introduced into residual graft resulting in an increase of %RG (Figure 4.1). This resulted in an increase in both %RG and %NB in μ CT compared to histology. However, because the ratio of residual graft to new bone was very high in all grafted sinuses (34.17% versus 9.54%), %NB was more affected by thresholding while %RG was less affected. As a result, the statistical analysis demonstrated %RG of μ CT was not statistically significantly different from histology while %NB was significantly different between μ CT and histology.

This challenge of thresholding each tissue of residual graft and new bone in grafted sinus was also reported in a study by Trisi et al. (2006). Three patients received maxillary sinus grafting using a bioactive glass graft (Biogran[®]) mixed with autogenous bone. Biopsied tissues after various healing periods were analysed using μ CT and histomorphometry. In thresholding of residual graft and new bone in μ CT, the authors experienced a similar radiodensity between bone and the graft, which complicated complete segmentation of one tissue from another. The fundamental process of thresholding is to be able to extract a particular area or tissue based on its different grayscale or pixel intensity from other neighbouring areas. The presence of bone and bone substitute (i.e., graft) sharing a similar radiodensity (i.e., grayscale) will compromise segmentation by thresholding as demonstrated in our study as well as in Trisi et al. (2006).

This is not a problem for morphometric analysis of anatomical sites composed of two tissues with completely different density. For example, trabecular bone consists of bone marrow and bone (Bonnet et al., 2009; Ito et al., 1998; Thomsen et al., 2005; Zupan et al., 2013). Bone and marrow are physiological tissues whose density is completely distinct from each other. This enables easy segmentation of each tissue by thresholding. In this regard, μ CT demonstrated a good correlation with histology for morphometric analysis of trabecular bone. For example, Müller et al. (1998) measured trabecular bone structure in bone biopsies using μ CT and compared them against 2-dimensional histology. The study found a good correlation between μ CT and histology, concluding that μ CT is a reliable alternative to conventional histology, offering non-destructive 3-dimensional measurement of trabecular structures. The study used μ CT to determine trabecular connectivity and volume and the thresholding procedure to segment trabecular bone from bone marrow. Segmentation of trabecular bone from bone marrow was simple, as the contrast between these two tissues was very high (approximately 10:1). This resulted in a uniform threshold, making the segmentation efficient and fast Müller et al. (1998).

Since the presence of residual graft complicated segmentation of new bone in this research, we decided to segment the area occupied by mineralised tissue (MT), defined as the area that is occupied by both residual graft and new bone. As mineralised tissue demonstrates a high contrast to background soft tissue, we anticipated that μ CT would be able to measure the area of mineralized tissue similar to that measured by histomorphometry.

The results demonstrated that μ CT overestimated %MT compared to histology (presented as %[SE]: 48.9 [1.7] vs 43.7 [1.9], respectively, $p \leq 0.05$). The statistical results showed %MT in μ CT is statistically different from histology. At an animal level, two animals demonstrated no statistically significant difference between μ CT and histology for %MT (317L and 6003L had p -value of 0.395, 0.058, respectively). If the statistical significance was set to 1% instead of 5% ($p \leq 0.01$), μ CT was not significantly different from histology for %MT ($p = 0.021$). This is quite similar in trend to the observations made by Trisi et al. (2006) who observed a good correlation between μ CT and histology for mineralised tissue. The study concluded μ CT could quantify the volume of mineralised tissue (bone + residual graft) but not the separate area of bone and

residual graft due to their similar radiographic density. We also observed that there is a strong correlation between μ CT and histology for %MT using Pearson's correlation analysis ($r= 0.767$).

It is important to note the correlation does not indicate two techniques will always result in a very similar outcome. A recent study by Dias et al. (2013) commented that Pearson correlation is based on an assumption of a linear relationship and a strong correlation between μ CT and histology does not make μ CT interchangeable with histology for bone analysis. In order to find the association between μ CT and histology for bone morphometric analysis, the study used mandibular bone biopsies obtained from 32 patients; jaw bone microarchitecture was assessed with μ CT and histology in parallel. Although the Pearson's correlation coefficient found a good agreement for BV/TV (bone volume density) between the two methods, constant systemic bias was observed. The authors concluded that μ CT and histology should not be used interchangeably for the analysis of bone density and jaw bone. Another study by Tamminen et al. (2011) observed a moderate agreement between histomorphometry and μ CT in the measurements of trabecular bone in iliac samples (Tamminen et al., 2011). They concluded histomorphometry remains the gold standard for the morphometric quantification of trabecular bone. Although two animals in the current study observed no statistically significant difference between μ CT and histology for %MT, it is important to note that %MT by μ CT and histology for the whole sample still demonstrated a significant difference which agreed with the findings of (Dias et al., 2013; Tamminen et al., 2011)).

4.3.1 *Morphometric analysis of grafted sinus*

Previous studies between μ CT and histology used bone biopsies obtained from various anatomical sites, e.g., the iliac bone and femur. These physiological bone biopsies are different in composition to healed, grafted maxillary sinus which was utilised in our research. There are two studies that have compared efficacy of μ CT and histology for analysis of grafted sinus (Kühl et al., 2010; Trisi et al., 2006).

In a study by Kühl et al. (2010), bone biopsies from grafted maxillary sinuses of humans were analysed using μ CT to determine whether μ CT is a suitable radiographic tool for

quantification of bone and residual graft in grafted sinus. The samples were obtained from five patients, who received different mixtures of autogenous bone and bone substitute with different healing periods. The distribution of new bone and residual graft was measured by means of volumetric and density measurements. Area for bone and graft were segmented based on grayscale histogram analysis, where two peaks in y-axis representing each tissue were distributed at different threshold ranges (x-axis). The researchers observed a good segmentation of the volume of bone and residual graft using thresholding based on the histogram and concluded that μ CT is a reliable radiographic tool for the analysis of 3-D architecture and the remodelling of grafted maxillary sinus. However, the findings of this study were limited by the absence of a reference technique (e.g., histology) to validate the accuracy of measurements obtained in μ CT.

Similarly, in a study by Trisi et al. (2006), biopsied human samples of grafted maxillary sinus were analysed with μ CT and compared against histomorphometric results. Three sinuses, grafted with a mixture of autogenous bone and bone substitute (Biogran[®]), were biopsied after 5, 6 and 15 months. The samples were analysed by μ CT and histomorphometry to determine total volume/total bone volume (TV/TBV, which represents the total volume of bone plus residual graft in the matrix), bone volume/total volume (BV/TV, which represents the total volume of bone in the matrix), and graft volume/total volume (GV/TV, which represents the total volume of graft in the matrix). μ CT measurements were calculated from 400 reconstructed sections, while histomorphometry was performed from three sections per sample. The results showed that the TV/TBV measured by μ CT and histomorphometry were similar, but BV/TV was always higher in histomorphometry. GV/TV was shown to be lower in histomorphometry compared to μ CT.

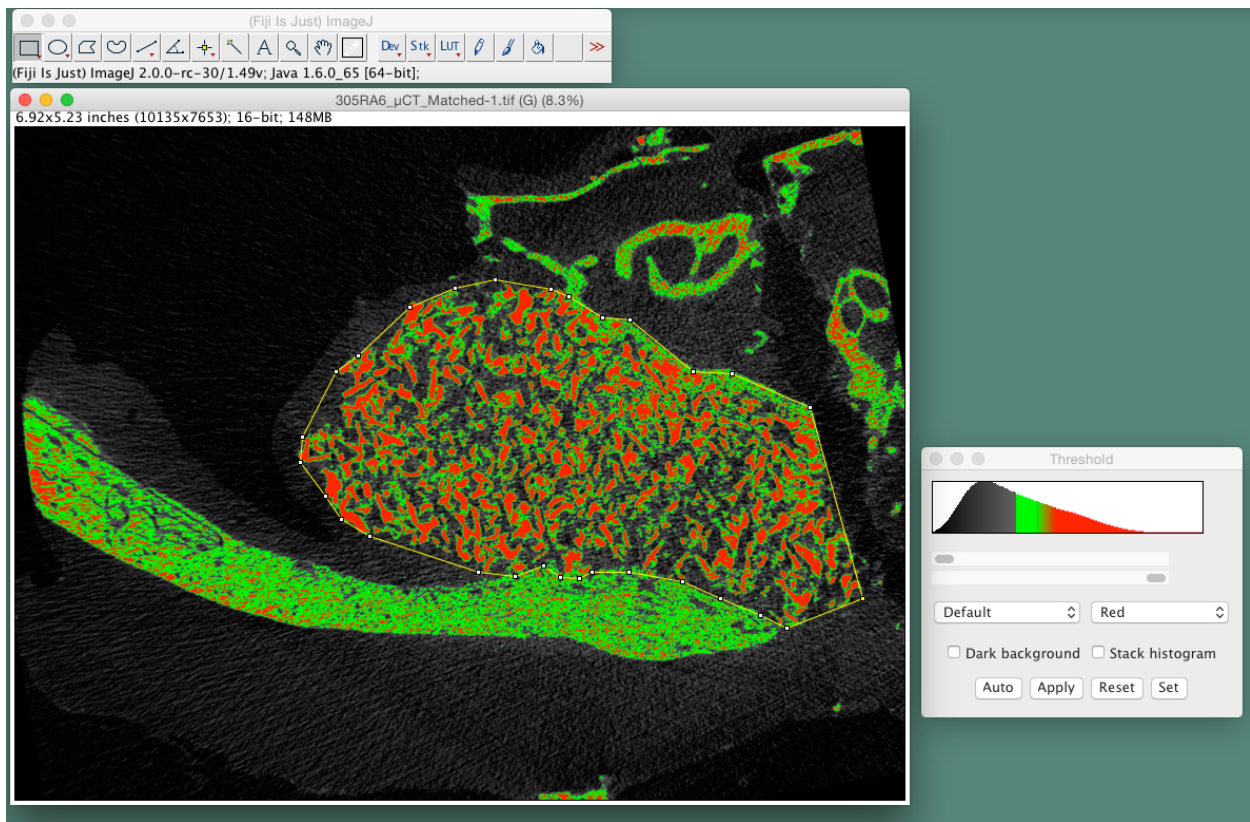


Figure 4.1 Thresholded μ CT image of grafted sinus. Green colour indicates threshold area for new bone and residual graft is shown as red colour. Due to a considerable overlap in grayscale between bone and graft, complete separation of two tissues was not possible using thresholding. Note the antral sinus wall, which is composed of both red and green colours. Due to the overlap in the grayscale range between graft and bone, some areas of antral bone thresholded as residual graft in red colour. Likewise, within the grafted sinus, the periphery of each graft islet is thresholded as new bone in green colour due to its similar radiodensity to residual graft (red). The threshold histogram (right) shows how new bone and residual graft overlap in their grayscale range.

4.4 Radiomorphometric analysis

4.4.1 *The use of radiographic standards*

Previous studies determined grayscale for residual graft and new bone by histogram analysis. In a study by (Kühl et al., 2010), grayscale thresholds for new bone and residual graft were obtained from grayscale histogram, where two peaks indicating both bone and graft were marked to set thresholds and segment each tissue within the total volume of grafted sinus. The study did not compare the results of μ CT to any other standards, and thus it is questionable whether μ CT is an accurate tool for bone and graft measurement. In the same manner, the same method was used in a study by Trisi et al. (2006). The grayscale histogram was analysed to identify threshold values for NB and RG. They used an intermediate grayscale between the two peaks of the materials (i.e., NB and RG) to segment each tissue from each other.

In our research, the radiographic image of an Endobon[®] sample and the cortical bone of the lateral sinus wall were used as radiographic standards for residual graft and new bone, respectively. Bone is a living tissue with a density that can change depending on the degree of mineralisation. The utility of cortical bone of the sinus wall to standardise threshold for bone might cause inherent errors (Kühl et al., 2010). In our study, histological images showed that after sixteen weeks of healing, the majority of new bone tissue shown in the grafted sinus samples were woven bone. Woven bone is an immature, unstructured bone that is less dense than lamellar bone. Therefore, the use of cortical bone as a radiographic standard to threshold new bone in our study was a potential source of bias. This may have resulted in a similar grayscale range between residual graft and bone that complicated the segmentation results of %NB and %RG.

4.4.2 Global threshold and partial volume effect

The research utilised the global threshold method to segment new bone, residual graft and overall mineralised tissue in the images of CBCT and μ CT. This method involved determination of a grayscale range, outside of which all grayscale will be marked as background tissue. This enables segmentation of a particular tissue of interest out of other tissues. Previous studies were able to find a moderate to good correlation between μ CT and histomorphometry for trabecular bone analysis using this global threshold (Thomsen et al., 2005; Chappard et al., 2005; Uchiyama et al., 1997).

The quality of segmented image using global thresholding in this research was affected by the partial volume effect. The partial volume effect is defined as the loss of intensity or grayscale of regions due to the resolution of the imaging system. This results in a “smear-out” phenomenon on radiographic images with less demarcated boundaries of tissue compartments. This was apparent in CBCT images where due to its low resolution, the overall image of islands of graft particles was washed out and presented as a gradient pattern of black and white (CBCT images in Figure 2.29, Figure 2.30).

Waarsing et al. (2004a, 2004b) introduced a new segmentation algorithm that uses local threshold instead of global threshold. This method can overcome the partial volume effect of the radiographic images and provide a greater accuracy of segmentation results compared to the global threshold. Compared to the global threshold, where segmentation depends on a selected single range of grayscale, local threshold assesses grayscale of voxels at the interface between the two tissues, where the smear-out effect is prominent within the radiographic image. The local threshold technique mitigates the smear-out voxels and thus increase the accuracy to the level comparable to histomorphometry.

In Waassing et al. (2004b) compared the local and global threshold methods to determine to determine bone architecture using the same μ CT images. These two measurements were also compared to the conventional histomorphometry to ascertain which method provides values most similar to histomorphometry. Both global and local thresholds were applied to an image to

quantify trabecular bone from the background image of non-bone. Quantitative analysis showed that while the local threshold method results in an image with the difference between -0.4 and 0.6% compared to histology, global threshold resulted in a difference that varied between -1 and 1%. The resultant segmented image demonstrated that the global threshold method resulted in the overestimation of bone outside of the core sample.

A couple of studies that used this local threshold method demonstrated that μ CT and histomorphometry are significantly different in their results for trabecular bone analysis (Tammisen et al., 2011; Dias et al., 2013). This is in contrast to other previous studies and this research that utilised the global threshold for morphometric analysis between μ CT and histomorphometry (Thomsen et al., 2005; Chappard et al., 2005; Uchiyama et al., 1997). Tammisen et al. (2011) adapted this local threshold approach of (Waarsing et al., 2004b). They observed only moderate agreement between histomorphometry and μ CT in the measurements of trabecular bone in iliac samples and concluded histomorphometry as the continued gold standard for morphometry of the trabecular bone (Tammisen et al., 2011). A study by (Dias et al., 2013) used mandibular bone biopsies obtained from 32 patients; the 3D assessment of a jaw bone microarchitecture was performed in parallel to μ CT and histology. Using Pearson's correlation, the study found poor agreement between the measures obtained by histomorphometry and μ CT. They concluded that μ CT and histomorphometry should not be interchangeably used for a jawbone analysis.

4.5 Parameters

Most previous publications comparing μ CT and histology for morphometric analysis of trabecular bone reported their results using parameters that included bone volume fraction (BV/TV), bone-surface-to-volume (BS/TV), trabecular number (Tb.N), trabecular thickness (Tb.Th), and trabecular separation (Tb.Sp).

The decision on which morphometric parameters should be reported is largely dependent on the research question (Bouxsein et al., 2010). The objective of our research was to determine how well CBCT can determine newly-formed bone within the grafted sinus. Grafted maxillary sinus consists of a mixture of new bone, residual graft, and connective tissue that is different from trabecular bone. Also, while earlier studies compared 3-D morphometric analysis of μ CT against indirect three-dimensional measure of histomorphometry with stereological analysis, our study focused on comparing matched 2-D images between the different techniques. Therefore, to meet the objective of our research, the results were reported using parameters including %NB, %RG and %MT.

Previous studies using μ CT to analyse the remodelling of grafted maxillary sinus used similar parameters as ours (Kürl et al., 2010). Kürl and colleagues performed a direct 3-D (three-dimensional) assessment of biopsied grafted sinus using μ CT scan. The parameters they used included the total volume of interest (TV), the volume of graft material (VS), the volume of bone (BV), and the volume of grafting material in relation to the total mineralised tissue volume (VS/[VS + BV]). Apart from being a 3D assessment, the parameters used in Kürl et al. (2010) and our research were very similar. Our study compared 2-D images; therefore, we used percentage value based on area instead of volume in all our parameters.

4.6 Animal study

Sheep was chosen as an animal model for the research. Sheep have already widely been used as animal models in research related to bone, including in dental implant research (Duncan, 2005; Vlaminck et al., 2008), periodontitis and periodontal defect studies (Baharuddin, 2010; Duncan et al., 2003), and maxillary sinus augmentation (Duncan, 2005; Haas et al., 1998; Haas et al., 2001). However, to the author's knowledge, this was the first study that used sheep as an animal model to compare the quantitative analysis of bone architecture of grafted maxillary sinus using μ CT and histology. Many previous studies compared μ CT and histology for a morphometric analysis of trabecular bone used human bone biopsies (e.g., the iliac bone and femur) to understand the changes of trabecular bone pattern in patients with bone disorders (e.g., osteoporosis). Only a few studies have utilised animal models for the quantitative analysis of bone architecture; for example, in a study by (Bonnet et al., 2009), the tibial trabecular bones of female Wistar rats were used to assess trabecular bone architecture using μ CT devices (Skyscan and Scanco) and histomorphometry.

Sheep have a body-to-weight ratio and a bone turnover rate similar to human beings. However, sheep have a different rate of healing compared to humans. Clinically, in human patients, a period of five to six months of healing is provided following sinus floor elevation, prior to implant placement. Duncan (2005) compared the healing rates of sheep and human beings. The study found that a period of five to six months of healing after sinus floor elevation in humans is equal to sixteen weeks of healing in sheep. Therefore, our specimens in this study were retrieved and examined at sixteen weeks to simulate the same period of healing in human subjects, which was deemed appropriate.

One of the main differences observed in the healing of grafted maxillary sinus in sheep is the lack of osteogenic potential from elevated sinus membrane. It has been reported in both in vitro and in vivo experiments that the Schneiderian membrane in human subjects has an osteogenic potential that can play the important role in the augmentation procedure (Srouji et al., 2009). However, the current research observed that in-growth of new bone in grafted sheep sinus

originates from the floor of the sinus towards the centre of the graft, but no bone in-growth was observed near the elevated sinus membrane (Figure 3.2).

This histological finding is in agreement with previous studies, which also observed bone in-growth originating from the floor of the sinus and the antral wall but not from the elevated sinus membrane (Alayan et al., 2015; Duncan, 2005; Haas et al., 1998; Haas et al., 2001). Variations in the pattern of remodelling have been observed depending on the type of graft material placed and the healing period. Alayan et al. (2015) examined remodelling in two different types of graft material, including a mixture of iliac graft and Bio-Oss® (50:50 ratio) and bioactive glass at eight, twelve, and sixteen weeks following sinus floor elevation. Histological analysis showed that the amount of new bone formation is proportional to the length of the healing period. The in-growth of new bone was observed from the floor of the sinus; however, no bone in-growth was observed near the elevated sinus membrane. The authors concluded that the sinus membrane lacks osteogenic potential in sheep, and new bone mainly originated from the bony walls of the sinus. A similar finding was also documented by Haas et al. (1998), where new bone formation was observed from the antral wall of the sinus but not from the sinus membrane.

4.7 Influence of resin embedding on the quality of radiographic images

The specimens in the current study were scanned with CBCT and µCT before the resin-embedding procedure. Since resin-embedded specimens are easy to handle and help to align the specimens either with the vertical or horizontal axis on the scanner platform, previously other studies carried out µCT scan of bone biopsies in resin (Thomsen et al., 2005). However, any resin materials or any medium added to the specimens could alter the attenuation of x-ray beam passing through the specimens, which could alter the quality of the radiographic images (Nazarian et al., 2008; Bousxtein et al., 2010). This influence of embedding medium on the x-ray attenuation coefficient and the quality of radiographic images was also pointed out by other authors (Nazarian et al., 2008; Park et al., 2005; Sennerby et al., 2001). Sennerby et al. (2001) examined µCT tomographic images of mini implants embedded in resin. The image displayed

radiopacity due to the presence of resin, which decreased the quality of the images. Therefore, in our study, non-embedded specimens were radiographically scanned.

Therefore, in this research, instead of resin-embedding prior to radiographic scans, the specimens were wrapped with a thin plastic wrap during μ CT scans while the plastic wrap was not used during CBCT scan. The purpose of the wrap was to prevent the dehydration of the specimens during scan.

4.8 Histomorphometric analysis: methodology

In this research, a semi-automated segmentation method was used to identify the area of different tissues in the digitised histological images. Thresholding was performed to segment the area of new bone and residual graft according to the differences in pixel intensity. The segmented images were compared to the originals to ensure that the segmented tissue image was a good representation of the actual structure (Bouslein et al., 2010). Variation in the uptake of stain between homogenous tissues was observed. This resulted in some of the tissues being unaccounted for after the thresholding, requiring manual selection of these tissues using the wand tool in Image J. The resultant segmented tissues were measured and expressed as area percentages within the ROI.

Different methods for the evaluation of histological sections were reported previously in the literature. The majority of prior studies investigating bone graft materials utilised computer-assisted histomorphometric analysis to select and measure the tissue proportions (Alayan et al., 2015; Heberer et al., 2008; Heberer et al., 2011). This method requires a selection of areas occupied by the tissue of interest, manually. The area occupied by the particular tissue can then be calculated by the computer. This technique can be time-consuming and labour intensive, as each tissue area must be delineated manually using selecting tools.

Another commonly used method is point-counting stereology. A grid system is superimposed on the actual or projected histological image to count the presence or absence of a particular tissue of interest within the grid. The percentage of area occupied by different types of

tissues may then be calculated. Compared to computer-assisted analysis, this technique is simple and quick.

The efficacy of the two techniques has been compared to ascertain whether they correlate to each other in their histomorphometric analysis. For example, Duncan (2005) compared the bone to implant contact percentages (%BIC) measured by the stereology analysis and the computer-assisted analysis. The author observed significant differences between the techniques. The result in %BIC using stereology was significantly higher than the computer-assisted analysis. Another earlier study (Leichter et al., 1998) also noted that a consistently higher percentage of bone was identified using stereology when compared to a computer-assisted histomorphometric analysis of surgically created defects in the furcation of mandibular second premolars in sheep. To carry out computer-assisted histomorphometric analysis, the authors measured the area of bone manually using the polygon tool in the Image J software. The authors reported the issues of distortion of the image during processing, limited pixel capture ability of the camera, and restricted image magnification in the computer-assisted analysis technique. The stereology technique was the preferred option as the process was easier, faster, and less expensive; less preparation was required as well.

The computer-assisted semi-automated segmentation technique is a common procedure in analysing medical magnetic resonance images and microscopic images (Al-Attar et al., 2006; Bae and Tai, 2009; Imelińska et al., 2000). Compared to the manual selection of the computed assisted histomorphometric analysis, thresholding technique is used to segment the tissue of interest based on the pixel contrast from neighbouring tissues. It has been suggested that the use of a semi-automated approach in a large dataset would greatly reduce the effects of intra-reader and inter-reader variability, as compared to manual segmentations (Swanson et al., 2010). At the same time, compared to the manual method, this technique is time-efficient. The studies comparing the semi-automated segmentation to the point counting stereology showed good correlation between the two methods (Amenábar et al., 2006; Amira et al., 2008; Montgomery et al., 2007). In a study by Amenábar et al. (2006), rat tongues were histologically examined using point counting stereology and semi-automated segmentation in parallel. Paired-t test results

showed that the two methods are not significantly different from each other, showing good correlation.

Both the point counting stereology and the semi-automated segmentation method appear to be reliable methods for histomorphometry. The accuracy of stereology is dependent on the size of the grid system. To provide a minimum level of confidence of 95% in a large image, however, a huge number of grid points must be evaluated. On the other hand, semi-automated segmentation relies on the quality of the digitised image, which will be analysed by computer software. High-resolution images captured at a high magnification are critical. Also, a care must be taken with the illumination and focus of the lenses, which should be constant throughout the entire image. The choice of staining method, which provides great contrast between tissues of interest and neighbouring tissues, is also important. Furthermore, image analysis software that can handle a large image dataset must be available. Variability in the experimental settings of these factors may have resulted in different observations.

The point counting stereology can also be applied to radiographic images in order to measure area or volume of a tissue of interest. In the research, for CBCT and μ CT, segmentation by thresholding was used to determine %NB, %RG and %MT. The utility of point counting stereology is only effective if the tissue of interest is clearly distinguishable from other adjacent tissues by the difference in pixel intensity. However, identifying new bone and residual graft in radiographic images of μ CT and CBCT is difficult. The two tissues exhibited similar grayscale and hence they are represented as areas with a similar level of shadows on radiographic images (Figure 2.30). Therefore, the utility of point counting stereology would have not improved the segmentation results of %NB and %RG in this research.

The point counting stereology is useful if the tissue of interest within radiographic images exhibits clearly demarcated boundaries from adjacent tissues. For example, in a study by Emirzeoglu et al. (2007), the volume of paranasal sinuses shown in CT scans were measured using the point counting stereology. The use of point stereology was possible as the area of sinus (which is soft tissue) was clearly demarcated by boundaries of dense bone tissues. Therefore, the point counting stereology can be useful in radiographic images but only if the naked eye can

distinguish the area of interest from other adjacent tissues, at a similar level to histological images.

4.9 Clinical implications

Maxillary sinus floor elevation is a surgical procedure that increases the quantity of bone in posterior maxilla prior to implant placement. In a two-stage surgical protocol, the grafted sinus is left to heal, allowing formation of new bone, which is directly related to implant success. At the moment, there is no clinical tool to assess new bone formation in the grafted sinus, and clinicians must infer the amount of new bone formation based on observations made in animal studies and human *in vivo* biopsy studies.

CBCT has already been validated as a useful clinical tool for linear and volumetric measurements. Our study set out to ascertain whether CBCT determines the quantity of new bone within the grafted sinus by detecting changes in radiodensity. However, the observation showed that low resolution of CBCT does not allow differentiation between the residual graft and new bone and hence cannot make any prediction on graft healing. This also holds true for μ CT, as it overestimated the quantity of newly formed bone compared to histology.

Nevertheless, the resolution of CBCT is expected to increase over time, and this study forms a basis for future studies comparing between CBCT, μ CT and histology. However, the resolution that is necessary to determine bone healing in grafted sinus is still questionable. A part of the research was to compare μ CT and histology for assessment of new bone and residual graft in the grafted sinus. Despite having a voxel size of $17.35\mu\text{m}$, which is significantly smaller than CBCT voxel size of $100\mu\text{m}$, this research finding demonstrated μ CT could not accurately determine %NB, %RG and %MT within the grafted sinuses. This result was partly due to some major flaws in the research design; a radiographic standard for new bone was inappropriate as cortical bone of the lateral sinus wall was used and a similar radiodensity between the graft and new bone did not allow segmentation of one tissue from another.

To minimise the confounding variable of similar radiodensity between graft and bone, overall mineralised tissue (MT) was measured in CBCT and μ CT. However, both radiographic techniques significantly overestimated %MT compared to histology but the %MT difference between μ CT and histology was relatively small, possibly indicating μ CT may be able to estimate mineralized tissue. This may indicate that, in order to quantify at least overall mineralised tissue within the grafted sinus, CBCT should increase its resolution to a similar level to μ CT that was used in the research. However, whether this can be achieved without increasing radiation dose cannot be answered. Also, as the statistical analysis of this research demonstrated significant difference between μ CT and histology in all tissue parameters, even at μ CT level of resolution, CBCT may not be able to quantify newly formed bone or overall mineralised tissue. It is also important to point out that CBCT images in the research lost resolution when exported from Osirix software. Raw format of CBCT images were converted into RGB format, which significantly reduced the resolution of images. This affected the observations made in CBCT in the current research. Future studies should be carefully designed to minimise any methodological errors first in order to determine the critical resolution at which new bone and residual graft can be measured.

Even if CBCT was found to estimate %NB, %RG and %MT in an animal model, the use of CBCT in clinical settings may be different from experimental settings. The presence of other soft tissues (e.g., external skin and fat) may alter the quality of radiographic images obtained in clinical trials. Mimicking these soft tissues in experimental settings using an external medium may provide a better replication of clinical situations; however, the influence of such a medium on the x-ray attenuation coefficient and the quality of the radiographic image and subsequent image analysis must be taken into account carefully. In addition, any micro-movement of the patient during CBCT scan, the type of bone or bone substitute placed within the sinus, the presence of any metal restorations or implants near the sinus and the system settings offered by different CBCT machines may change the quality of the CBCT image. A firm conclusion on the validity of CBCT for radiographic assessment of bone formation in the sinus should be on hold until further studies using different types of graft materials at various sites and using various brands of CBCT machines are published.

It is also important to note that, compared to our CBCT device, other CBCT devices manufactured by different companies may yield different outcomes under the same experiment settings, as they may have a higher or lower resolution. Therefore, the findings of this study are limited to the Galileos CBCT device.

4.10 Confounding factors and other issues with the investigation

4.10.1 Experimental design

To our knowledge, this was the first study comparing CBCT and μ CT against histology to ascertain the accuracy of radiographic images in determining bone formation in grafted sinus of sheep based on density measurements. There was a steep learning curve in developing a method of comparative image analysis between the techniques, including the identification of matching 2-D images, image calibration, thresholding, and others.

The samples were scanned with CBCT and μ CT as raw, non-embedded specimens because resin embedding may change the nature of the x-ray beam, resulting in distortion or modification of the final radiographic data. However, the specimens were oriented arbitrarily during our CBCT and μ CT scan, as alignment of raw specimens to either vertical or horizontal axis on radiographic scanner platform was not easy. This later on resulted in the difficulty in matching 2-D images between the techniques. The matched images between CBCT, μ CT and histology were similar but never identical.

A previous study by Thomsen et al. (2005) performed resin embedding of samples prior to their μ CT scan so that the samples can be oriented to align the vertical axis during μ CT scan, and this made it easier to determine the direction of cutting for histology. This technique was not utilised in this research. Future studies may consider the use of specimen holders or embedding in an external medium that yields a minimum attenuation of the x-ray beam.

4.10.2 Discarded animals

In this study, four out of ten animals (two out of zero healing group (baseline) and two out of sixteen-week healing group) were excluded from analysis. This was due to a procedure

error where improper radiographic scan settings were used for these animals. Also, in the remaining six animals, four histological slides had to be excluded, leaving only 34 histological slides used for analysis. This was due to the inadequate experience of the researcher for the study where histological slides were polished excessively, leaving some tissue areas void. These procedural errors could be improved on future research if the operator performs a trial phase where an appropriate setting for radiographic scans is identified. Also, for polishing, the final thickness for histological images can be increased in order to minimise the risk of excessive tissue loss. Alternatively, instead of manual polishing, the use of an automatic polisher with a standardised load pressure onto polishing paper would minimise the risk of loss of tissue contents and can acquire even thickness of histological sections throughout samples.

4.10.3 Examiner blindness and reproducibility of techniques

The comparative analysis of all three techniques in this study, including CBCT, μ CT, and histology were carried out by a single examiner. This may have resulted in selection bias, where selection of threshold for bone and residual graft in the radiographic images may have deliberately adjusted to generate results that are similar to the histomorphometric analysis. Having a separate examiner for histomorphometric analysis who is blinded from radiomorphometric analysis would have eliminated the selection bias.

Thresholding used for bone and residual graft was based on manual selection of thresholds using radiographic standards of Endobon® and cortical bone of the lateral sinus of the sinus in the research. This manual adjustment of thresholding is often not standardized and the reproducibility is often limited. Image J provides a set of thresholding algorithms that can standardise thresholding methods if utilised appropriately. However, no single algorithm was able to segment the radiographic standards (i.e., scan of Endobon® for residual graft and cortical bone of the sinus for new bone) in both CBCT and μ CT images. Therefore, selection of thresholds for the research was carried out manually by a visual inspection on a computed monitor until radiographic standards were separated from the background image (Figure 2.31, Figure 2.32). This manual approach is highly subjective and may carry a large standard deviation. Repeatability in both intra- and inter-examiners may be difficult to achieve.

Future studies may require a pilot study where an algorithm for thresholding for residual graft and new bone within grafted sinuses is determined. Alternatively, blinded examiners of more than one can be employed for repeated measurements in order to determine both intra- and inter-examiner variability and this should be reported in the results section of research. Statistical analysis such as the Wilcoxon signed-rank test can be applied to determine if there are any differences between the two repeated measurements (Tamminen et al., 2011). In the study, moderate agreement was observed between histomorphometry and μ CT in the measurements of trabecular bone in iliac samples (Tamminen et al., 2011).

4.10.4 Lack of a control group

A control group that consists of grafted sinus samples with a zero-week healing period was not included in the research. Samples of a control group could have been utilised to set thresholds for Endobon®, which then can be used to segment residual graft in samples with 16-week healing period.

Also, radiomorphometric analysis to quantify %RG in the control sample would have been an interest in this research. The control sample partly simulates an environment where residual graft has failed to consolidate and been fibrous encapsulated. Radiomorphometric analysis of the control sample compound of graft material and blood clot also produces a high contrast between the two tissues and the efficacy of CBCT and μ CT to quantify %RG in such control sites may provide a better understanding on the efficacy of the radiographic tools to assess mineralised tissue.

4.10.5 Samples from another experimental research

All samples used in the research were obtained from another large animal study where histologic analysis of different sources of graft materials placed in sheep maxillary sinus was carried out. Therefore, parts of this research design (e.g., animal selection, a choice of graft material) were dependent on the design of the other research.

4.10.6 Image scale

In this research, the image scale between the radiographic images and histological image were matched prior to their morphometric analysis of different tissues. CBCT and μ CT images were not used as reference images to set scale for corresponding 2-D histological images. Instead, 2-D μ CT and CBCT images were scaled to match 2-D histological images. Resin-embedding for histological preparation resulted in tissue distortion and shrinkage and this was also apparent in the 2-D histological images. Therefore, matching the scale of the histological images to the radiographic images may have partly eliminated the distortion and shrinkage occurred in histological images as the radiographic images were not distorted.

4.11 Recommendations for future research

4.11.1 3-D analysis

The biggest advantage of CBCT and μ CT over histomorphometry in the scope of experimental studies is the 3-D evaluation of the mineralised tissues. Future studies should carry out 3-D analysis of μ CT and CBCT and then compared with histomorphometry with stereological analysis.

4.11.2 Non-grafted sinus / use of other bone substitute

The use of Endobon[®], which has a similar radiodensity to bone, hindered proper segmentation between bone and graft. This, therefore, modified the observations made in this study. Future studies should involve the use of different sources of graft materials that feature a different radiodensity from new bone so the accuracy of CBCT in the thresholding of such graft material from bone can be assessed properly. In case of utilising animal sinuses, two different sources of grafting material can be placed on both left and right hand sinuses. This produces a larger sample size to analyse and allows a comparison of healing of different sources of grafting materials and how this different pattern or extent of consolidation may influence the radiographic analysis of μ CT and CBCT for new bone and residual graft.

4.11.3 Investigation in other periodontal and peri-implant sites

The application of CBCT for the determination of bone healing should not be limited to grafted sinus sites. Other applications such as bone remodelling following guided tissue regeneration; guided bone regeneration should also be studied with carefully designed experimental settings. Furthermore, the use of CBCT to determine peri-implant bone density can be assessed; however, the beam hardening effect produced by metal implants should be pointed out (Park et al., 2010).

4.11.4 Use of other imaging software

Not all image software programs function identically. Different imaging software feature different algorithms, which, to a certain extent, can downgrade the quality of the image during analysis. Our study used Osirix to reslice the DICOM data of CBCT, which resulted in a significant loss in the quality of the image as demonstrated by the changes in the range of grayscale within the image. Imaging software that can retain the original quality of the image should be used for future studies. Galileos CBCT comes with its own software called Sidexis that can render CBCT DICOM files into 3-D volume image for dental treatment planning. However, the software is not a research platform where the export of 2-D sliced images from the 3-D CBCT volume or reoriented 3-D CBCT volume is not possible. The DICOM files can only be exported as a set of untouched, raw files. Therefore, we employed OsiriX which not only allows visualisation of 3-D CBCT images, but it allows reslice of 3-D volume into 2-D image stacks and saving them as a separate file. However, the software does not allow quantitative analysis by segmenting different tissues based on grayscale and therefore, another image software, Image J had to be used for analysis of different tissue parameters. Also, the major problem with OsiriX was that when a 2-D image is exported, OsiriX changes the image format from the raw tiff file to RGB hindering the resolution of the raw images.

There are numerous third party programmes available for image processing. The utility of software that is a research platform allowing visualisation, segmentation and quantitative analysis is probably ideal for radiomorphometry in μ CT and CBCT and should be used in future studies. For example, a programme called 3D-Slicer is a free open-source software that can be

used as a research tool for quantitative analysis of radiographic images. It not only allows visualisation of CBCT DICOM files but within the software, segmentation based on pixel intensity (i.e., grayscale) and quantitative analysis can also be carried out (Fedorov et al., 2012). It is currently used in medical fields, particularly in in vivo research concerning cancers, as it demonstrated its efficacy to segment glioblastoma (brain tumour) (Kikinis and Pieper, 2011).

Chapter 5 Conclusion

CBCT lacks the resolution to determine the newly formed bone in the grafted sinus and overestimated both the new bone and the residual graft significantly compared to histology.

This study employed two reference methods for the quantitative analysis of bone including histology and μ CT. The research demonstrated μ CT should not be used interchangeably with histology to estimate newly formed bone and only showed similar results for the residual graft with histology. When both the new bone and the residual graft were measured together (mineralised tissue), μ CT overestimated its result compared to histology.

Histomorphometry appears to remain as the preferred reference method for assessing new bone. Further studies focusing on 3D analysis with a refined method to segment residual graft and new bone should be carried out to validate the efficacy of CBCT or μ CT for determination of new bone within the grafted sinus, which is an important step prior to implant placement.

Chapter 6 Appendix

6.1 Appendix I: Ethical approval and sheep sinus surgery

6.1.1 Ethical approval

Ethical approval for the study was obtained from an animal experimental work by the University of Otago Animal Ethics Committee (AEC# 50-08 and 65-11) and funded by New Zealand Dental Association Research Foundation, Fuller Scholarship, Zürich Institute for Chemical and Bioengineering, and Zürich University Centre for Dental Medicine.

6.1.2 Experimental animals

Ten cross-bred ewes, all two years old, were selected from flocks sourced by the AgResearch Invermay Breeding Station. Two animals were selected representing a zero-week (baseline) healing period (euthanised immediately after the surgery) whereas the remaining eight animals were chosen for sixteen-week healing periods.

6.1.3 A choice of graft material

Sterile, sealed package of Endobon® (Particle size 0.5-1.0mm, Xenograft granules volume 2.0ml, Biomet 3i, USA) was used as a sinus graft material during sinus elevation procedures. A new vial was opened for each animal.

6.1.4 Surgical protocol

All sheep surgeries were performed in the facilities of the Animal Research Centre, Hercus Building, Otago University Medical School.

6.1.4.1 Antibiotics and General Anaesthesia

An antibiotic was administered subcutaneously (Strepsin 5ml) one hour prior to the surgery. General anaesthesia was induced by thiopentone, which was administered intravenously via the cephalic vein (20mg /kg until effect). The animals were then intubated by a veterinarian, and anaesthesia was maintained by a mixture of halothane (1-2%) and nitrous oxide/oxygen (1:2). Rumen was compressed, and a stomach tube was inserted and the contents allowed to drain into the plastic bucket on the floor.

6.1.4.2 Surgical procedure

Ten sheep had a single (left or right) maxillary sinus randomly allocated grafted with bovine xenograft (Endobon®, Biomet 3i). We used a surgical procedure described by Duncan et al. (2005), which is a modified version of a technique developed by Haas and co-workers (Haas et al., 1998)

The surgery was carried out extraorally. The side of the sheep's face was shaved with a mechanical trimmer to remove the hair. The surgical site was anaesthetised with a Mepivacaine HCl (Xylocaine® 1:20,000 plus adrenaline) (Figure 6.1). Adrenaline in the anaesthetic cartridge allowed haemorrhagic control of the surgical site during the surgery. A 5 cm long paramedian sagittal skin incision was made using an electrosurgical unit (NeoMed 3000a ESU, Solid State Electrosurgery Unit, USA) in a 'cut' mode. The exposed masseter muscle was dissected, and the underlying bony wall was exposed. To maintain visualisation of the site, any haemorrhagic arterioles were clamped with haemostat. A circular bony window approximately 1 cm in diameter was created using a Satalec Piezotome™ (Figure 6.2, (b)). Sterile saline was used as a cooling agent during the use of the Piezotome™ device. The resultant circular bony plate was gently detached from the underlying Schneiderian membrane (SM) and then removed and discarded. The exposed Schneiderian membrane was dissected from inside of buccal bony wall and elevated supero-medially with blunt sinus dissectors (Osstem, Korea).

A graft of Endobon® was mixed with approximately 1 ml of blood acquired from the surgical field. The mixture was then packed into the resultant sinus space (Figure 6.2, (c)). Care was taken not to perforate the SM during the packing. The site was then covered with Bio-Gide (Geistlich, Switzerland), and the wound was closed (Figure 6.2, (d)). The deep muscle layers were sutured with resorbable 1-0 Vicryl™ (Ethicon™, Inc., USA) and externally with 4-0 Vicryl™. Once the wound was closed and sutured, a postoperative long-acting anaesthetic Bupivacaine HCL 5 mcg/ml (Marcaine®) was administered.

6.1.5 Postoperative pain and infection control

Antibiotics (Trimethoprim) anti-inflammatory medications (Carprofen) were administered (See table below for further details). No animal was observed to suffer any short or long-term complications after the surgery.

6.1.6 Euthanasia and perfusion protocol

The sheep were euthanized under general anaesthesia and perfused through the carotid arteries using 10% neutral buffered formalin (NBF) (BioLab Ltd., New Zealand). There were two animals that were euthanized immediately after the surgery whereas eight animals were euthanized following 16-week healing periods. General anaesthesia was induced by intravenous (IV) thiopentone; 20mg per kilogram was administered systemically via the cephalic vein. This was maintained with halothane (1~2%) and nitrous oxide/oxygen (ratio 1:2). The animal was laid on a trolley table in a supine position with its neck slightly overextended. The hairs on the neck were shaved using a mechanical trimmer. A transcutaneous incision of approximately 10cm was made followed by the dissection of the underlying muscles to expose the carotid artery. The arteries were cannulated bilaterally using 14G x 2" indwelling catheters (Optiva™, Smiths Medical, UK). The catheters were ligated to prevent displacement of the cannula. An anaesthetic overdose was administered, and the animals were moved to the post-mortem room. The cannulated carotid artery was connected to a one litre sterile saline bag of 0.9% normal saline (Baxter Healthcare Pty Ltd, Australia) with 1.5ml of 5000 IU heparin. The external jugular veins were severed to allow the free drainage of blood. A further two litres of 10% neutral buffered formalin (NBF) (BioLab Ltd., New Zealand) was introduced via the same route.

Table 6.1 Medications used during the sheep surgery.

Medication	Route	Dose
Thiopentone	Intravenous	20mg/kg
Halothane	Inhalation	1-2% (to effect)
Nitrous Oxide	Inhalation	1:2 (to effect)
Trimethoprim	Intramuscular	1ml/15kg
Carprofen	Intramuscular	5ml once/day for 3 days
Mepivacaine HCL (1:20,000 adrenaline)	Local infiltration	2x2.2ml cartridges around surgical site prior to surgery
Bupivacaine HCL (1:200,000 adrenaline)	Local infiltration	.5ml around surgical site post-operatively

6.1.7 *Harvesting*

Following the death of the animals, maxilla was resected en block and harvested. The mandible was disarticulated and removed to allow easy access to the maxilla. Soft tissues including overlying skin, nose, and cartilaginous regions anterior to the grafted sinus site were removed using a large scalpel. The grafted sinus was located by identifying scarring at the site of

the healing antral bone. A hack was then used to separate the maxilla from the skull, distal to the last standing molar. The block was sectioned through the midline with the hack and the two halves labelled. Retrieved specimens were immediately immersed in a 10% neutral buffered formalin (NBF) solution in a sealed container. After 48 hours, the specimens were transferred to a solution of 20% ethanol and held at 4°C until required.

6.2 Appendix I

6.2.1 *Chemical reagents used*

Distilled Water, (purified via reverse osmosis unit, RiOsTM unit, Millipore Intertech, USA)

Xylene, C₆H₄(CH₃)₂, (Ajax Finechem Pty Ltd, New Zealand)

Ethanol, C₂H₅OH, (High grade, Absolute Ethanol, Thermo Fisher Scientific, USA)

Haematoxylin, (Surgipath®, Gill II Hematoxylin, Leica Microsystems, USA)

10% Natural Buffered Formalin (NBF), (BioLab Ltd, New Zealand)

Methyl methacrylate 99% (MMA), (Sigma Aldrich, USA)

10% Ethylenediamine tetraacetic acid (EDTA) solution, (supplied by Histology Unit, University of Otago, New Zealand)

Scotts water, (supplied by Histology Unit, University of Otago, New Zealand)

6.2.2 *Equipment used*

Piezosurgery® 3 unit, (Mectron, Genoa, Italy)

Piezosurgery® Insert EX1, EX2 and EX3, (Mectron, Genoa, Italy)

Tegra-Pol, polishing machine, (Struers, Ballerup, Denmark)

Silicon Carbide Paper, Grades 180-4000 (Struers, Ballerup, Denmark)

Accutom, cutting machine, (Struers, Ballerup Denmark)

Incubating/shaking machine, (Multitron®, Infors HT, Switzerland RiOsTM wall mounted water distillation unit, (Millipore Intertech, USA)

Olympus AX70 upright compound microscope, (Olympus Optical co. ltd, Japan)

Montaging software Volocity 5.2.0, (Improvision, MA, USA)

Montaging software Autopano Pro 2.5.2, (Kolor, USA)

Osirix 32-bit version (Pixmeo, Switzerland)

Image J software version 1.47q, (NIH, USA)



Figure 6.1 The surgical site for maxillary sinus elevation in sheep.

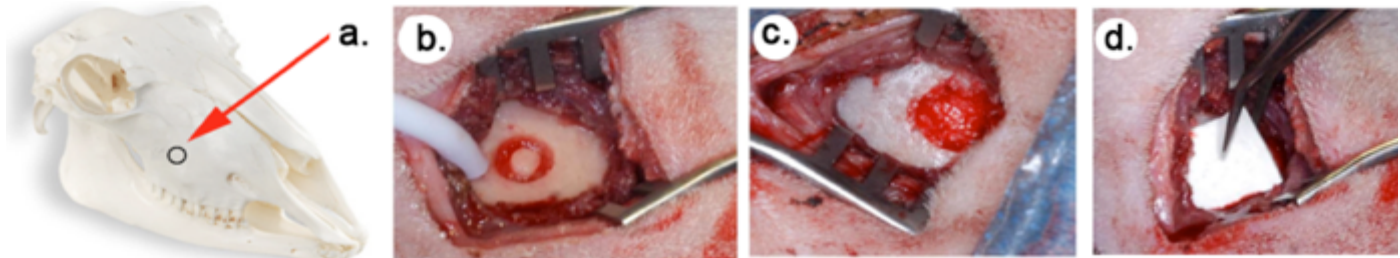


Figure 6.2 The steps in the surgical procedure: (a) the surgical site for maxillary sinus floor elevation in sheep, (b) Preparation of a circular osteotomy on cortical bone of sinus (c) Placement of bone graft following the elevation of sinus membrane (d) Placement of Endobon® (Smith, 2011).

6.3 Appendix III

6.3.1 Ingredients for resin embedding

Methyl methacrylate, (M55909, Sigma Aldrich, USA)

Benzoyl peroxide, (517909, Sigma Aldrich, USA)

Dibutylphthalate, (524980, Sigma Aldrich, USA)

Xylene, (Ajax Finechem Pty Ltd, New Zealand)

Method for MMA I

4 parts Methyl methacrylate

1% Benzoyl peroxide

1 Part Dibutylphthalate

Method for MMA II

4 parts Methyl methacrylate

0.5% Benzoyl peroxide

1 part Dibutylphthalate

Method for MMA III

4 parts Methyl methacrylate

1% Benzoyl peroxide

1 part Dibutylphthalate

6.3.2 Resin embedding protocol

Transfer specimens to ethanol in cassettes with label.

Place specimens in 20% ethanol for 4 days, change solution after 2 days.

Place specimens in 40% ethanol and then 75% ethanol for 2 days each.

Place specimens in 95% ethanol for 4 days, change solution after 2 days.

Place specimens in 100% ethanol for 6 days, change solution every 2 days.

Immerse specimens in xylene for 4 days in fume cupboard on rotating platform, change solution after 2 days

Wash specimens in methyl methacrylate MMA monomer Transfer specimens to MMAI for 2 days in fume cupboard on rotating platform.

Fill glass jars to one third depth with MMAIII, and place in plastic light-proof container part-filled with water. Leave undisturbed until set.

Immerse specimens in MMAII for 2 days in fume cupboard on rotating platform. Place specimens in glass jars with pre-set bases and cover with MMAIII.

Place glass jars in water bath in light-proof container, at room temperature. Leave undisturbed until set.

6.3.3 Staining with MacNeal's Tetrachrome/Toluidine Blue solution

Solution A (supplied by Histology Unit, University of Otago, New Zealand)

0.5g Methylene blue

0.8g Azur II

0.1g Methyl violet 2B

250ml Methanol

250ml Glycerol

Mix together. Stir with magnetic stirrer

Leave for 12 hours at 50°C then 3 days at 37°C.

Solution B (supplied by Histology Unit, University of Otago, New Zealand)

Toluidine blue in 100ml distilled water +1.0g borax.

Combine 10ml Solution A and 5ml Solution B.

Stir and make up to 100ml using distilled water.

Staining protocol

Place slides in 20% ethanol in Coplin jar.

Place in ultrasonic bath for 5 minutes.

Replace ethanol with 0.1% formic acid for 5 minutes in ultrasonic bath.

Wash with tap water.

Cover section on slide with diluted combination of Solution A+B for 5 minutes.

Rinse with distilled water for 5 minutes before air-drying.

6.4 Appendix IV: Radiographic Calibration Standards (Phantoms) for Micro-CT (Schwass et al., 2009)

To make low- and medium-density HAP discs, pure HAP powder was weighed, mixed with known volumes of resin (Delton, Dentsply Professional, USA), and then mixed vigorously for five minutes until it became homogeneous. The HAP-resin mixture was then placed into a polished cylindrical stainless steel mold (Smileline, Courtelary, Switzerland) and cured with a 390-515nm wavelength blue light (BluePhase LED curing light; Ivoclar Vivadent, Schaan, Liechtenstein). For the high-density HAP

disc, a sintered HAP (1200°C , 90 min) disc of known mass was placed under a vacuum, and dental resin was allowed to infiltrate into the disc over 2-3 hours. The disc was then retrieved and light cured. The discs were weighed, and their dimensions were measured to determine mineral and effective total densities.

All discs made using commercially pure 99.9% hydroxyapatite (HAP)

Resin composition

- Predominantly bisphenol A glycidyl methacrylate (BIS-GMA)
- Low viscosity monomers
- Triethylene glycol dimethacrylate
- Barium alumino fluroboro silicate glass
- Sodium fluoride
- Camphoroquinone photo initiator
- Stabiliser

Resin product

Delton LC Pit and Fissure Sealant (Dentsply DeTrey GmbH, Konstanz, Germany)

Low density disc

Light cured mix of resin + HAp

Medium density disc

Light cured mix of resin + HAp

High density disc

Sintered HAP (1200°C , 90 min.), then resin infiltrated under vacuum and light cured

Table 6.2 Calibration standards densities.

Low density (g/cm ³) +/- 0.005		Medium density (g/cm ³) +/- 0.005		High density (g/cm ³) +/- 0.005	
HAP concentration	Total effective density	HAP concentration	Total effective density	HAP concentration	Total effective density
0.139	1.211	0.515	1.394	0.781	1.481

References

- Aghaloo TL, Moy PK (2006). Which hard tissue augmentation techniques are the most successful in furnishing bony support for implant placement? *The International Journal of Oral & Maxillofacial Implants* 22(49-70).
- Al-Attar SA, Pollex RL, Robinson JF, Miskie BA, Walcarus R, Rutt BK *et al.* (2006). Semi-automated segmentation and quantification of adipose tissue in calf and thigh by MRI: a preliminary study in patients with monogenic metabolic syndrome. *BMC Medical Imaging* 6(1):11.
- Alayan J, Vaquette C, Saifzadeh S, Hutmacher D, Ivanovski S (2015). A histomorphometric assessment of collagen - stabilized anorganic bovine bone mineral in maxillary sinus augmentation—a randomized controlled trial in sheep. *Clinical Oral Implants Research*.
- Albrektsson T, Zarb G, Worthington P, Eriksson A (1986). The long-term efficacy of currently used dental implants: a review and proposed criteria of success. *The International Journal of Oral & Maxillofacial Implants* 1(1):11-25.
- Albrektsson T, Johansson C (2001). Osteoinduction, osteoconduction and osseointegration. *European Spine Journal* 10(2):S96-S101.
- Amenábar JM, Martins GB, Cherubini K, Figueiredo MAZ (2006). Comparison between semi-automated segmentation and manual point-counting methods for quantitative analysis of histological sections. *Journal of Oral Science* 48(3):139-143.
- Amira A, Chandrasekaran S, Montgomery DW, Uzun IS (2008). A segmentation concept for positron emission tomography imaging using multiresolution analysis. *Neurocomputing* 71(10):1954-1965.
- Anderegg CR, Alexander DC, Friedman M (1999). A bioactive glass particulate in the treatment of molar furcation invasions. *Journal of Periodontology* 70(4):384-387.
- Anitua E, Orive G, Aguirre JJ, Andía I (2008). Five-year clinical evaluation of short dental implants placed in posterior areas: a retrospective study. *Journal of Periodontology* 79(1):42-48.
- Annibali S, Cristalli M, Dell'Aquila D, Bignozzi I, La Monaca G, Pilloni A (2012). Short dental implants a systematic review. *Journal of Dental Research* 91(1):25-32.

Aparicio C, Perales P, Rangert B (2001). Tilted implants as an alternative to maxillary sinus grafting: a clinical, radiologic, and periotest study. *Clinical Implant Dentistry and Related Research* 3(1):39-49.

Araújo MG, Lindhe J (2005). Dimensional ridge alterations following tooth extraction. An experimental study in the dog. *Journal of clinical periodontology* 32(2):212-218.

Artzi Z, Weinreb M, Givol N, Rohrer MD, Nemcovsky CE, Prasad HS *et al.* (2003). Biomaterial resorption rate and healing site morphology of inorganic bovine bone and beta-tricalcium phosphate in the canine: a 24-month longitudinal histologic study and morphometric analysis. *The International Journal of Oral & Maxillofacial Implants* 19(3):357-368.

Aukhil I (2000). Biology of wound healing. *Periodontology 2000* 22(1):44-50.

Bae E, Tai X-C (2009). Graph cut optimization for the piecewise constant level set method applied to multiphase image segmentation. In: Scale space and variational methods in computer vision: Springer, pp. 1-13.

Baharuddin N (2010). Expression of RANKL, RANK and OPG in surgically created periodontal defects in a sheep model. *Dunedin: Otago*.

Bauer TW, Muschler GF (2000). Bone graft materials: an overview of the basic science. *Clinical Orthopaedics and Related Research* 371(10-27).

Beirne OR (2000). A review of survival rates for implants placed in grafted maxillary sinuses using meta-analysis.

Bell JF (1939). Notes on the uses of methyl methacrylate" lucite" in a geological laboratory. *Economic Geology* 34(7):804-811.

Benavides E, Rios HF, Ganz SD, An C-H, Resnik R, Reardon GT *et al.* (2012). Use of cone beam computed tomography in implant dentistry: the International Congress of Oral Implantologists consensus report. *Implant Dentistry* 21(2):78-86.

Bender I, Seltzer S (1961a). Roentgenographic and direct observation of experimental lesions in bone: II. *The Journal of the American Dental Association* 62(6):708-716.

Bender I, Seltzer S (1961b). Roentgenographic and direct observation of experimental lesions in bone: I. *The Journal of the American Dental Association* 62(2):152-160.

Bergh J, Bruggenkate CM, Disch FJ, Tuinzing DB (2000). Anatomical aspects of sinus floor elevations. *Clinical oral implants research* 11(3):256-265.

Bonnet N, Laroche N, Vico L, Dolleans E, Courteix D, Benhamou CL (2009). Assessment of trabecular bone microarchitecture by two different x-ray microcomputed tomographs: a comparative study of the rat distal tibia using Skyscan and Scanco devices. *Medical physics* 36(4):1286-1297.

Bouxsein ML, Boyd SK, Christiansen BA, Guldberg RE, Jepsen KJ, Müller R (2010). Guidelines for assessment of bone microstructure in rodents using micro-computed tomography. *Journal of Bone and Mineral Research* 25(7):1468-1486.

BOYNE PJ (1980). Grafting of maxillary sinus floor with autogenous marrow and bone. *J Oral Surg* 38(613-616).

Bruggenkate CM, Bergh J (1998). Maxillary sinus floor elevation: a valuable pre - prosthetic procedure. *Periodontology 2000* 17(1):176-182.

Busenlechner D, Huber CD, Vasak C, Dobsak A, Gruber R, Watzek G (2009). Sinus augmentation analysis revised: the gradient of graft consolidation. *Clinical Oral Implants Research* 20(10):1078-1083.

Cancian D, Hochuli-Vieira E, Marcantonio R, Marcantonio Jr E (1998). Use of BioGran and Calcitite in bone defects: histologic study in monkeys (*Cebus apella*). *The International Journal of Oral & Maxillofacial Implants* 14(6):859-864.

Cancian D, Hochuli-Vieira E, Marcantonio R, Garcia JI (2003). Utilization of autogenous bone, bioactive glasses, and calcium phosphate cement in surgical mandibular bone defects in *Cebus apella* monkeys. *The International Journal of Oral & Maxillofacial Implants* 19(1):73-79.

Celeste AJ, Iannazzi JA, Taylor RC, Hewick RM, Rosen V, Wang EA *et al.* (1990). Identification of transforming growth factor beta family members present in bone-inductive protein purified from bovine bone. *Proceedings of the National Academy of Sciences* 87(24):9843-9847.

Chanavaz M (1989). Maxillary sinus: anatomy, physiology, surgery, and bone grafting related to implantology--eleven years of surgical experience (1979-1990). *The Journal of Oral Implantology* 16(3):199-209.

Chappard D, Retailleau - Gaborit N, Legrand E, Baslé MF, Audran M (2005). Comparison insight bone measurements by histomorphometry and μ CT. *Journal of Bone and Mineral Research* 20(7):1177-1184.

Chaushu G, Vered M, Mardinger O, Nissan J (2010). Histomorphometric analysis after maxillary sinus floor augmentation using cancellous bone-block allograft. *Journal of Periodontology* 81(8):1147-1152.

Chen T-W, Chang H-S, Leung K-W, Lai Y-L, Kao S-Y (2007). Implant placement immediately after the lateral approach of the trap door window procedure to create a maxillary sinus lift without bone grafting: a 2-year retrospective evaluation of 47 implants in 33 patients. *Journal of Oral and Maxillofacial Surgery* 65(11):2324-2328.

Chueh H-S, Tsai W-K, Fu H-M, Chen J-C (2006). Evaluation of the quantitative capability of a home-made cone-beam micro computed tomography system. *Computerized Medical Imaging and Graphics* 30(6):349-355.

Cordaro L, Bosshardt DD, Palattella P, Rao W, Serino G, Chiapasco M (2008). Maxillary sinus grafting with Bio - Oss® or Straumann® Bone Ceramic: histomorphometric results from a randomized controlled multicenter clinical trial. *Clinical Oral Implants Research* 19(8):796-803.

Cypher TJ, Grossman JP (1996). Biological principles of bone graft healing. *The Journal of Foot and Ankle Surgery* 35(5):413-417.

Dalle Carbonare L, Valenti M, Bertoldo F, Zanatta M, Zenari S, Realdi G *et al.* (2005). Bone microarchitecture evaluated by histomorphometry. *Micron* 36(7):609-616.

Davies J (1997). Mechanisms of endosseous integration. *The International Journal of Prosthodontics* 11(5):391-401.

Davies JE (2003). Understanding peri-implant endosseous healing. *Journal of Dental Education* 67(8):932-949.

De Vos W, Casselman J, Swennen G (2009). Cone-beam computerized tomography (CBCT) imaging of the oral and maxillofacial region: a systematic review of the literature. *International Journal of Oral and Maxillofacial Surgery* 38(6):609-625.

Del Fabbro M, Testori T, Francetti L, Weinstein R (2005). Systematic review of survival rates for implants placed in the grafted maxillary sinus. *The Journal of Prosthetic Dentistry* 94(3):266.

Del Fabbro M, Rosano G, Taschieri S (2008). Implant survival rates after maxillary sinus augmentation. *European Journal of Oral Sciences* 116(6):497-506.

Dias DR, Leles CR, Batista AC, Lindh C, Ribeiro - Rotta RF (2013). Agreement between Histomorphometry and Microcomputed Tomography to Assess Bone Microarchitecture of Dental Implant Sites. *Clinical Implant Dentistry and Related Research*.

Dimitriou R, Tsiridis E, Giannoudis PV (2005). Current concepts of molecular aspects of bone healing. *Injury* 36(12):1392-1404.

dos Santos Corpas L, Jacobs R, Quirynen M, Huang Y, Naert I, Duyck J (2011). Peri - implant bone tissue assessment by comparing the outcome of intra - oral radiograph and cone beam computed tomography analyses to the histological standard. *Clinical Oral Implants Research* 22(5):492-499.

Duncan W, Persson GR, Sims T, Braham P, Pack A, Page R (2003). Ovine periodontitis as a potential model for periodontal studies. *Journal of clinical periodontology* 30(1):63-72.

Duncan WJ (2005). Sheep mandibular animal models for dental implantology research, PhD Thesis. Dunedin: University of Otago.

Duncan WJ, Lee MH, Dovban AS, Hendra N, Ershadi S, Rumende H (2008). Anodization increases early integration of Osstem implants in sheep femurs. *Annals of the Royal Australasian College of Dental Surgeons* 19(152-156).

Ehrhart N, Kraft S, Conover D, Rosier RN, Schwarz EM (2008). Quantification of massive allograft healing with dynamic contrast enhanced-MRI and cone beam-CT: a pilot study. *Clinical Orthopaedics and Related Research* 466(8):1897-1904.

Einhorn TA (1998). The cell and molecular biology of fracture healing. *Clinical Orthopaedics and Related Research* 355(S7-S21).

Emirzeoglu M, Sahin B, Bilgic S, Celebi M, Uzun A (2007). Volumetric evaluation of the paranasal sinuses in normal subjects using computer tomography images: a stereological study. *Auris Nasus Larynx* 34(2):191-195.

Erben RG (1997). Embedding of bone samples in methylmethacrylate: an improved method suitable for bone histomorphometry, histochemistry, and immunohistochemistry. *Journal of Histochemistry & Cytochemistry* 45(2):307-313.

Estaca E, Cabezas J, Usón J, Sánchez - Margallo F, Morell E, Latorre R (2008). Maxillary sinus - floor elevation: an animal model. *Clinical Oral Implants Research* 19(10):1044-1048.

Estrela C, Bueno MR, Leles CR, Azevedo B, Azevedo JR (2008). Accuracy of cone beam computed tomography and panoramic and periapical radiography for detection of apical periodontitis. *Journal of Endodontics* 34(3):273-279.

Fedorov A, Beichel R, Kalpathy-Cramer J, Finet J, Fillion-Robin J-C, Pujol S *et al.* (2012). 3D Slicer as an image computing platform for the Quantitative Imaging Network. *Magnetic Resonance Imaging* 30(9):1323-1341.

Feichtinger M, Mossböck R, Kärcher H (2007). Assessment of bone resorption after secondary alveolar bone grafting using three-dimensional computed tomography: a three-year study. *The Cleft Palate-Craniofacial Journal* 44(2):142-148.

Feldkamp LA, Goldstein SA, Parfitt MA, Jesion G, Kleerekoper M (1989). The direct examination of three - dimensional bone architecture in vitro by computed tomography. *Journal of Bone and Mineral Research* 4(1):3-11.

Fenner M, Vairaktaris E, Fischer K, Schlegel KA, Neukam FW, Nkenke E (2009). Influence of residual alveolar bone height on osseointegration of implants in the maxilla: a pilot study. *Clinical Oral Implants Research* 20(6):555-559.

Fleischmann D, Boas FE (2011). Computed tomography—old ideas and new technology. *European Radiology* 21(3):510-517.

Fonseca RJ, Barber HD, Powers MP, Frost DE (2013). Oral and Maxillofacial Trauma: Elsevier Health Sciences.

Froum SJ, Wallace SS, Elian N, Cho SC, Tarnow DP (2006). Comparison of mineralized cancellous bone allograft (Puros) and anorganic bovine bone matrix (Bio-Oss) for sinus augmentation: histomorphometry at 26 to 32 weeks after grafting. *The International Journal of Periodontics & Restorative Dentistry* 26(6):543-551.

Gosau M, Rink D, Driemel O, Draenert F (2009). Maxillary sinus anatomy: a cadaveric study with clinical implications. *The Anatomical Record* 292(3):352-354.

Gribel BF, Gribel MN, Frazão DC, McNamara Jr JA, Manzi FR (2011). Accuracy and reliability of craniometric measurements on lateral cephalometry and 3D measurements on CBCT scans. *The Angle Orthodontist* 81(1):26-35.

Griffin TJ, Cheung WS (2004). The use of short, wide implants in posterior areas with reduced bone height: a retrospective investigation. *The Journal of Prosthetic Dentistry* 92(2):139-144.

Grunder U (2001). Immediate functional loading of immediate implants in edentulous arches: two-year results. *The International Journal of Periodontics & Restorative Dentistry* 21(6):545-551.

Haas AN, De Castro GD, Moreno T, Susin C, Albandar JM, Oppermann RV *et al.* (2008). Azithromycin as an adjunctive treatment of aggressive periodontitis: 12 - months randomized clinical trial. *Journal of Clinical Periodontology* 35(8):696-704.

Haas R, Donath K, Födinger M, Watzek G (1998). Bovine hydroxyapatite for maxillary sinus grafting: comparative histomorphometric findings in sheep. *Clinical Oral Implants Research* 9(2):117-122.

Haas R, Baron M, Donath K, Zechner W, Watzek G (2001). Porous hydroxyapatite for grafting the maxillary sinus: a comparative histomorphometric study in sheep. *The International Journal of Oral & Maxillofacial Implants* 17(3):337-346.

Hallman M, Sennerby L, Lundgren S (2002). A clinical and histologic evaluation of implant integration in the posterior maxilla after sinus floor augmentation with autogenous bone, bovine hydroxyapatite, or a 20: 80 mixture. *International Journal of Oral and Maxillofacial Implants* 17(5):635-643.

Heberer S, Al - Chawaf B, Hildebrand D, Nelson JJ, Nelson K (2008). Histomorphometric analysis of extraction sockets augmented with Bio - Oss Collagen after a 6 - week healing period: A prospective study. *Clinical Oral Implants Research* 19(12):1219-1225.

Heberer S, Al-Chawaf B, Jablonski C, Nelson JJ, Lage H, Nelson K (2011). Healing of ungrafted and grafted extraction sockets after 12 weeks: a prospective clinical study. *The International Journal of Oral & Maxillofacial Implants* 26(2):385.

Hernandez - Verdun D, Quintana C, Masson C, Gautier T, Arnoult J (1991). Cryofixation, cryosubstitution, cryo - embedding for visualizing of nuclear ultrastructure and for immunodetection HeLa cells. *Biology of the Cell* 72(1 - 2):121-132.

Hildebrand T, Laib A, Müller R, Dequeker J, Rüegsegger P (1999). Direct three - dimensional morphometric analysis of human cancellous bone: microstructural data from spine, femur, iliac crest, and calcaneus. *Journal of Bone and Mineral Research* 14(7):1167-1174.

Hing K, Best S, Bonfield W (1999). Characterization of porous hydroxyapatite. *Journal of Materials Science: Materials in Medicine* 10(3):135-145.

Hing KA, Best SM, Tanner KE, Bonfield W, Revell PA (2004). Mediation of bone ingrowth in porous hydroxyapatite bone graft substitutes. *Journal of Biomedical Materials Research Part A* 68(1):187-200.

Hising P, Bolin A, Branting C (2000). Reconstruction of severely resorbed alveolar ridge crests with dental implants using a bovine bone mineral for augmentation. *The International Journal of Oral & Maxillofacial Implants* 16(1):90-97.

Holberg C, Steinhäuser S, Geis P, Rudzki-Janson I (2005). Cone-beam computed tomography in orthodontics: benefits and limitations. *Journal of Orofacial Orthopedics/Fortschritte der Kieferorthopädie* 66(6):434-444.

Hsieh J Computed tomography: principles, design, artifacts, and recent advances 2009: SPIE Bellingham, WA.

Imelińska C, Downes M, Yuan W (2000). Semi-automated color segmentation of anatomical tissue. *Computerized Medical Imaging and Graphics* 24(3):173-180.

Ito M, Nakamura T, Matsumoto T, Tsurusaki K, Hayashi K (1998). Analysis of trabecular microarchitecture of human iliac bone using microcomputed tomography in patients with hip arthrosis with or without vertebral fracture. *Bone* 23(2):163-169.

Jemt T, Lekholm U (1994). Implant treatment in edentulous maxillae: a 5-year follow-up report on patients with different degrees of jaw resorption. *The International Journal of Oral & Maxillofacial implants* 10(3):303-311.

Jensen O, Shulman L, Block M, Iacono V (1997). Report of the sinus consensus conference of 1996. *The International Journal of Oral & Maxillofacial Implants* 13(11-45).

Jensen OT, Kuhlke L, Bedard J-F, White D (2006). Alveolar segmental sandwich osteotomy for anterior maxillary vertical augmentation prior to implant placement. *Journal of Oral and Maxillofacial Surgery* 64(2):290-296.

Kan JY, Rungcharassaeng K, Kim J, Lozada JL, Goodacre CJ (2002). Factors affecting the survival of implants placed in grafted maxillary sinuses: a clinical report. *The Journal of Prosthetic Dentistry* 87(5):485-489.

Kikinis R, Pieper S 3D Slicer as a tool for interactive brain tumor segmentation. Engineering in Medicine and Biology Society, EMBC, 2011 Annual International Conference of the IEEE2011: IEEE.

Kühl S, Götz H, Hansen T, Kreisler M, Behneke A, Heil U *et al.* (2010). Three-dimensional analysis of bone formation after maxillary sinus augmentation by means of microcomputed tomography: a pilot study. *The International Journal of Oral & Maxillofacial Implants* 25(5):930.

Lascala C, Panella J, Marques M (2014). Analysis of the accuracy of linear measurements obtained by cone beam computed tomography (CBCT-NewTom). *Dentomaxillofacial Radiology*.

Lei L, PEI F-x, TU C-q, ZHOU Z-k, LI Q-h (2008). Immunological study on the transplantation of an improved deproteinized heterogeneous bone scaffold material in tissue engineering. *Chinese Journal of Traumatology (English Edition)* 11(3):141-147.

Leichter JW, Pack ARC, Kardos TB (1998). A comparison of stereological and computer - assisted histomorphometric analysis as tools for histological quantification in regenerative studies. *Journal of Periodontal Research* 33(2):99-104.

Löe H (1959). Bone Tissue Formation A Morphological and Histochemical Study. *Acta odontologica Scandinavica* 17(3):312-427.

Lundgren S, Nyström E, Nilson H, Gunne J, Lindhagen O (1997). Bone grafting to the maxillary sinuses, nasal floor and anterior maxilla in the atrophic edentulous maxilla: a two-stage technique. *International Journal of Oral and Maxillofacial Surgery* 26(6):428-434.

Lundgren S, Anderson S, Gualini F, Sennerby L (2004). Bone reformation with sinus membrane elevation: a new surgical technique for maxillary sinus floor augmentation. *Clinical Implant Dentistry and Related Research* 6(3):165-173.

Macbeth R (1971). Caldwell, Luc, and their operation. *The Laryngoscope* 81(10):1652-1657.

Majzoub Z, Berengo M, Giardino R, Nicoli Aldini N, Cordioli G (1999). Role of intramarrow penetration in osseous repair: A pilot study in the rabbit calvaria. *Journal of Periodontology* 70(12):1501-1510.

Martinez A, Franco J, Saiz E, Guitian F (2010). Maxillary sinus floor augmentation on humans: Packing simulations and 8months histomorphometric comparative study of anorganic bone matrix and β -tricalcium phosphate particles as grafting materials. *Materials Science and Engineering: C* 30(5):763-769.

Martini L, Fini M, Giavaresi G, Giardino R (2001). Sheep model in orthopedic research: a literature review. *Comparative Medicine* 51(4):292-299.

Masoudifard M, Shojaei B, Vajhi AR (2008). Radiographic Anatomy of the Head of Sheep. *Iranian Journal of Veterinary Surgery* 3(4):41-48.

Matheny KE, Duncavage JA (2003). Contemporary indications for the Caldwell-Luc procedure. *Current Opinion in Otolaryngology & Head and Neck Surgery* 11(1):23-26.

Mawhinney W, Ellis H (1983). A technique for plastic embedding of mineralised bone. *Journal of Clinical Pathology* 36(10):1197-1199.

Mazess RB, Barden HS, Bisek JP, Hanson J (1990). Dual-energy x-ray absorptiometry for total-body and regional bone-mineral and soft-tissue composition. *The American Journal of Clinical Nutrition* 51(6):1106-1112.

Meredith N (1997). Assessment of implant stability as a prognostic determinant. *The International Journal of Prosthodontics* 11(5):491-501.

Misch CE, Dietsh F (1993). Bone-grafting materials in implant dentistry. *Implant Dentistry* 2(3):158-166.

Misch CE, Steigenga J, Barboza E, Misch-Dietsh F, Cianciola LJ, Kazor C (2006). Short dental implants in posterior partial edentulism: a multicenter retrospective 6-year case series study. *Journal of Periodontology* 77(8):1340-1347.

Montgomery DW, Amira A, Zaidi H (2007). Fully automated segmentation of oncological PET volumes using a combined multiscale and statistical model. *Medical Physics* 34(2):722-736.

Morand M, Irinakis T (2007). The challenge of implant therapy in the posterior maxilla: providing a rationale for the use of short implants. *Journal of Oral Implantology* 33(5):257-266.

Moy PK, Lundgren S, Holmes RE (1993). Maxillary sinus augmentation: histomorphometric analysis of graft materials for maxillary sinus floor augmentation. *Journal of Oral and Maxillofacial Surgery* 51(8):857-862.

Müller R, Koller B, Hildebrand T, Laib A, Gianolini S, Rüegsegger P (1996). Resolution dependency of microstructural properties of cancellous bone based on three-dimensional microtomography. *Technology and health care: official journal of the European Society for Engineering and Medicine* 4(1):113-119.

Müller R, Van Campenhout H, Van Damme B, Van der Perre G, Dequeker J, Hildebrand T et al. (1998). Morphometric analysis of human bone biopsies: a quantitative structural comparison of histological sections and micro-computed tomography. *Bone* 23(1):59-66.

Nafei A, Danielsen C, Linde F, Hvid I (2000). Properties of growing trabecular ovine bone Part I: mechanical and physical properties. *Journal of Bone & Joint Surgery, British Volume* 82(6):910-920.

Nazarian A, Snyder BD, Zurakowski D, Müller R (2008). Quantitative micro-computed tomography: a non-invasive method to assess equivalent bone mineral density. *Bone* 43(2):302-311.

Nisand D, Picard N, Rocchietta I (2015). Short implants compared to implants in vertically augmented bone: a systematic review. *Clinical Oral Implants Research* 26(S11):170-179.

Oberoi S, Chigurupati R, Gill P, Hoffman WY, Vargervik K (2009). Volumetric assessment of secondary alveolar bone grafting using cone beam computed tomography. *The Cleft Palate-Craniofacial Journal* 46(5):503-511.

Olson JW, Dent CD, Morris HF, Ochi S (2000). Long-term assessment (5 to 71 months) of endosseous dental implants placed in the augmented maxillary sinus. *Annals of Periodontology* 5(1):152-156.

Ostman P, Hellman M, Wendelhag I, Sennerby L (2005). Resonance frequency analysis measurements of implants at placement surgery. *The International Journal of Prosthodontics* 19(1):77-83; discussion 84.

Palma VC, Magro - Filho O, Oliveria D, Américo J, Lundgren S, Salata LA et al. (2006). Bone reformation and implant integration following maxillary sinus membrane elevation: an experimental study in primates. *Clinical Implant Dentistry and Related Research* 8(1):11-24.

Park C, Swain M, Duncan W (2010). Micro-computerised tomography optimisation for the measurement of bone mineral density around titanium dental implants. *Journal of Biomechanical Science and Engineering* 5(1):2-10.

Park YS, Yi KY, Lee IS, Jung YC (2005). Correlation between microtomography and histomorphometry for assessment of implant osseointegration. *Clinical Oral Implants Research* 16(2):156-160.

Pearce AI, Richards RG, Milz S, Schneider E, Pearce SG (2007). Animal models for implant biomaterial research in bone: a review. *Eur Cell Mater* 13(1):1-10.

Piattelli M, Favero GA, Scarano A, Orsini G, Piattelli A (1999). Bone reactions to anorganic bovine bone (Bio-Oss) used in sinus augmentation procedures: a histologic long-term report of 20 cases in humans. *International Journal of Oral and Maxillofacial Implants* 14(6):835-840.

Pietrokovski J, Massler M (1967). Alveolar ridge resorption following tooth extraction. *The Journal of Prosthetic Dentistry* 17(1):21-27.

Porter JA, von Fraunhofer JA (2004). Success or failure of dental implants? A literature review with treatment considerations. *General Dentistry* 53(6):423-432; quiz 433, 446.

Postnov A, Vinogradov A, Van Dyck D, Saveliev S, De Clerck N (2003). Quantitative analysis of bone mineral content by X-ray microtomography. *Physiological Measurement* 24(1):165.

Ramírez - Fernández M, Calvo - Guirado JL, Delgado - Ruiz RA, Maté - Sánchez del Val JE, Vicente - Ortega V, Meseguer - Olmos L (2011). Bone response to hydroxyapatites with open porosity of animal origin (porcine [OsteoBiol® mp3] and bovine [Endobon®]): a radiological and histomorphometric study. *Clinical Oral Implants Research* 22(7):767-773.

Rasmusson L, Meredith N, Cho I-H, Sennerby L (1999). The influence of simultaneous versus delayed placement on the stability of titanium implants in onlay bone grafts. *International Journal of Oral & Maxillofacial Surgery* 28(3):224-231.

Reikerås O, Shegarfi H, Naper C, Reinholt FP, Rolstad B (2008). Impact of MHC mismatch and freezing on bone graft incorporation: an experimental study in rats. *Journal of Orthopaedic Research* 26(7):925-931.

Ritter F (1978). Surgical procedures on the paranasal sinuses: the frontal sinus. *The paranasal sinuses: surgery and technique*, 2nd ed St Louis: Mosby 136(45).

Rodriguez A, Anastassov GE, Lee H, Buchbinder D, Wettan H (2003). Maxillary sinus augmentation with deproteinized bovine bone and platelet rich plasma with simultaneous insertion of endosseous implants. *Journal of Oral and Maxillofacial Surgery* 61(2):157-163.

Scarfe WC, Farman AG, Sukovic P (2006). Clinical applications of cone-beam computed tomography in dental practice. *Journal-Canadian Dental Association* 72(1):75.

Schlegel KA, Fichtner G, Schultze-Mosgau S, Wiltfang J (2002). Histologic findings in sinus augmentation with autogenous bone chips versus a bovine bone substitute. *The International Journal of Oral & Maxillofacial Implants* 18(1):53-58.

Schmidlin PR, Muller J, Bindl A, Imfeld T (2008). Sinus floor elevation using an osteotome technique without grafting materials or membranes. *The International Journal of Periodontics & Restorative Dentistry* 28(4):401.

Schouten C, Meijer GJ, van den Beucken JJJP, Spauwen PHM, Jansen JA (2009). The quantitative assessment of peri-implant bone responses using histomorphometry and micro-computed tomography. *Biomaterials* 30(27):4539-4549.

Schummer A, Nickel R, Sack WO (1979). viscera of the domestic animals: P. Parey; Springer-Verlag.

Schwass D, Swain M, Purton D, Leichter J (2009). A system of calibrating microtomography for use in caries research. *Caries research* 43(4):314-321.

Sennerby L, Wennerberg A, Pasop F (2001). A new microtomographic technique for non - invasive evaluation of the bone structure around implants. *Clinical Oral Implants Research* 12(1):91-94.

Sharan A, Madjar D (2008). Maxillary sinus pneumatization following extractions: a radiographic study. *International Journal of Oral and Maxillofacial Implants* 23(1):48-55.

Shegarfi H, Reikeras O (2009). Review article: Bone transplantation and immune response. *Journal of Orthopaedic Surgery* 17(2).

Sheikh Z, Sima C, Glogauer M (2015). Bone Replacement Materials and Techniques Used for Achieving Vertical Alveolar Bone Augmentation. *Materials* 8(6):2953-2993.

Smith MM (2011). Healing of grafts of BioOss® and MoaBone® in a sheep maxillary sinus model, University of Otago.

Sohn D-S, Lee J-s, Ahn M-r, Shin H-I (2008). New bone formation in the maxillary sinus without bone grafts. *Implant Dentistry* 17(3):321-331.

Sohn D-S, Kim W-S, An K-M, Song K-J, Lee J-M, Mun Y-S (2010). Comparative histomorphometric analysis of maxillary sinus augmentation with and without bone grafting in rabbit. *Implant Dentistry* 19(3):259-270.

Srinivasan M, Vazquez L, Rieder P, Moraguez O, Bernard JP, Belser UC (2014). Survival rates of short (6 mm) micro - rough surface implants: a review of literature and meta - analysis. *Clinical Oral Implants Research* 25(5):539-545.

Srouji S, Kizhner T, David DB, Riminucci M, Bianco P, Livne E (2009). The Schneiderian membrane contains osteoprogenitor cells: in vivo and in vitro study. *Calcified Tissue International* 84(2):138-145.

Stamberger H (1986). Endoscopic endonasal surgery-concepts in treatment of recurring rhinosinusitis. Part II. Surgical technique. *Otolaryngol Head Neck Surg* 94(147-156).

Stavropoulos A, Wenzel A (2007). Accuracy of cone beam dental CT, intraoral digital and conventional film radiography for the detection of periapical lesions. An ex vivo study in pig jaws. *Clinical Oral Investigations* 11(1):101-106.

Suba Z, Takács D, Gyulai-Gaál S, Kovács K, Velich N, Szigeti K et al. (2004). [Alveolar bone regeneration stimulated by a combination of platelet-rich plasma and Cerasorb graft in Beagle dogs. Histological and histomorphometric studies]. *Fogorvosi szemle* 97(4):143-149.

Sullivan-Brown J, Bisher ME, Burdine RD (2011). Embedding, serial sectioning and staining of zebrafish embryos using JB-4 resin. *Nature Protocols* 6(1):46-55.

Summers RB (1994). A new concept in maxillary implant surgery: the osteotome technique. *Compendium (Newtown, Pa)* 15(2):152, 154-156, 158 passim; quiz 162.

Sun X, Zhang Z, Wang S, Gittens S, Jiang X, Chou LL (2008). Maxillary sinus floor elevation using a tissue - engineered bone complex with OsteoBone™ and bMSCs in rabbits. *Clinical Oral Implants Research* 19(8):804-813.

Swanson M, Prescott J, Best T, Powell K, Jackson R, Haq F et al. (2010). Semi-automated segmentation to assess the lateral meniscus in normal and osteoarthritic knees. *Osteoarthritis and Cartilage* 18(3):344-353.

Tallgren A (1972). The continuing reduction of the residual alveolar ridges in complete denture wearers: a mixed-longitudinal study covering 25 years. *The Journal of Prosthetic Dentistry* 27(2):120-132.

Tamminen IS, Isaksson H, Aula AS, Honkanen E, Jurvelin JS, Kröger H (2011). Reproducibility and agreement of micro-CT and histomorphometry in human trabecular bone with different metabolic status. *Journal of Bone and Mineral Metabolism* 29(4):442-448.

Tatum Jr H (1986). Maxillary and sinus implant reconstructions. *Dental clinics of North America* 30(2):207-229.

Tatum O Maxillary sinus grafting for endosseous implants. Annual Meeting of the Alabama Implant Study Group1977.

Thomsen JS, Ebbesen E, Mosekilde L (2000). A new method of comprehensive static histomorphometry applied on human lumbar vertebral cancellous bone. *Bone* 27(1):129-138.

Thomsen JS, Laib A, Koller B, Prohaska S, Mosekilde L, Gowin W (2005). Stereological measures of trabecular bone structure: comparison of 3D micro computed tomography with 2D histological sections in human proximal tibial bone biopsies. *Journal of Microscopy* 218(2):171-179.

Tinsley D, Watson C, Ogden A (1999). A survey of UK centres on implant failures. *Journal of Oral Rehabilitation* 26(1):14-18.

Tofe A, Watson B, Bowerman M (1991). Solution and cell mediated resorption of grafting materials. *Journal of Oral Implantology* 17(345).

Tolman DE (1994). Reconstructive procedures with endosseous implants in grafted bone: a review of the literature. *The International journal of oral & maxillofacial implants* 10(3):275-294.

Trisi P, Rebaudi A, Calvari F, Lazzara RJ (2006). Sinus graft with biogran, autogenous bone, and PRP: a report of three cases with histology and micro-CT. *The International journal of periodontics & restorative dentistry* 26(2):113-125.

Tyndall DA, Rathore S (2008). Cone-beam CT diagnostic applications: caries, periodontal bone assessment, and endodontic applications. *Dental Clinics of North America* 52(4):825-841.

Uchiyama T, Tanizawa T, Muramatsu H, Endo N, Takahashi H, Hara T (1997a). A morphometric comparison of trabecular structure of human ilium between microcomputed tomography and conventional histomorphometry. *Calcified Tissue International* 61(6):493-498.

Uchiyama T, Tanizawa T, Muramatsu H, Endo N, Takahashi HE, Hara T (1997b). A morphometric comparison of trabecular structure of human ilium between microcomputed tomography and conventional histomorphometry. *Calcified Tissue International* 61(6):493-498.

Valbonetti L, Berardinelli P, Scarano A, Piattelli A, Mattioli M, Barboni B *et al.* (2015). Translational Value of Sheep as Animal Model to Study Sinus Augmentation. *Journal of Craniofacial Surgery* 26(3):737-740.

Van de Casteele E, Van Dyck D, Sijbers J, Raman E The effect of beam hardening on resolution in X-ray microtomography. *Medical Imaging 2004: International Society for Optics and Photonics*.

Van der Weijden F, Dell'Acqua F, Slot DE (2009). Alveolar bone dimensional changes of post - extraction sockets in humans: a systematic review. *Journal of Clinical Periodontology* 36(12):1048-1058.

Van Oosterwyck H, Duyck J, Sloten JV, Perre GV, Jansen J, Wevers M et al. (2000). The use of microfocus computerized tomography as a new technique for characterizing bone tissue around oral implants. *Journal of Oral Implantology* 26(1):5-12.

Vandeweghe S, Coelho PG, Vanhove C, Wennerberg A, Jimbo R (2013). Utilizing micro - computed tomography to evaluate bone structure surrounding dental implants: A comparison with histomorphometry. *Journal of Biomedical Materials Research Part B: Applied Biomaterials* 101(7):1259-1266.

Velvart P, Hecker H, Tillinger G (2001). Detection of the apical lesion and the mandibular canal in conventional radiography and computed tomography. *Oral Surgery, Oral Medicine, Oral Pathology, Oral Radiology, and Endodontology* 92(6):682-688.

Vlaminck L, Gorski T, Huys L, Saunders J, Schacht E, Gasthuys F (2008). Immediate postextraction implant placement in sheep's mandibles: A pilot study. *Implant Dentistry* 17(4):439-450.

Waarsing J, Day J, Van der Linden J, Ederveen A, Spanjers C, De Clerck N et al. (2004a). Detecting and tracking local changes in the tibiae of individual rats: a novel method to analyse longitudinal in vivo micro-CT data. *Bone* 34(1):163-169.

Waarsing JH, Day JS, Weinans H (2004b). An improved segmentation method for in vivo μ CT imaging. *Journal of bone and Mineral Research* 19(10):1640-1650.

Wallace SS, Froum SJ (2003). Effect of maxillary sinus augmentation on the survival of endosseous dental implants. A systematic review. *Annals of Periodontology* 8(1):328-343.

Widmark G, Andersson B, Ivanoff C-J (1997). Mandibular bone graft in the anterior maxilla for single-tooth implants: presentation of a surgical method. *International Journal of Oral and Maxillofacial Surgery* 26(2):106-109.

Willie BM, Bloebaum RD, Bireley WR, Bachus KN, Hofmann AA (2004). Determining relevance of a weight - bearing ovine model for bone ingrowth assessment. *Journal of Biomedical Materials Research Part A* 69(3):567-576.

Wolf E, Röser K, Hahn M, Welkerling H, Delling G (1992). Enzyme and immunohistochemistry on undecalcified bone and bone marrow biopsies after embedding in plastic: a new embedding method for routine application. *Virchows Archiv A* 420(1):17-24.

Wright DK, Manos MM (1990). Sample preparation from paraffin-embedded tissues. *PCR protocols: a guide to methods and applications* 19(153-159).

Xu H, Shimizu Y, Onodera K, Ooya K (2005). Long-term outcome of augmentation of the maxillary sinus using deproteinised bone particles experimental study in rabbits. *British Journal of Oral and Maxillofacial Surgery* 43(1):40-45.

Yamashita-Mikami E, Tanaka M, Sakurai N, Yamada K, Ohshima H, Nomura S *et al.* (2013). Microstructural Observation with MicroCT and Histological Analysis of Human Alveolar Bone Biopsy from a Planned Implant Site: A Case Report. *The Open Dentistry Journal* 7(47).

Zijderveld SA, Zerbo IR, Van Den Bergh J, Schulten E, ten Bruggenkate CM (2004). Maxillary sinus floor augmentation using a beta-tricalcium phosphate (Cerasorb) alone compared to autogenous bone grafts. *The International Journal of Oral & Maxillofacial Implants* 20(3):432-440.

Zou W, Hunter N, Swain M (2011). Application of polychromatic μ CT for mineral density determination. *Journal of Dental Research* 90(1):18-30.

Zupan J, van't Hof RJ, Vindišar F, Haring G, Trebše R, Komadina R *et al.* (2013). Osteoarthritic versus osteoporotic bone and intra - skeletal variations in normal bone: Evaluation with μ CT and bone histomorphometry. *Journal of Orthopaedic Research* 31(7):1059-1066.